Long-term Dynamics and Stabilization of Intertidal flats

A system approach

Maan, Cynthia

Citation (APA)
Maan, C. (2019). *Long-term Dynamics and Stabilization of Intertidal flats: A system approach*. [Dissertation (TU Delft), Delft University of Technology]. https://doi.org/10.4233/uuid:cbb5e163-eac7-44b8-b336-deb94106cfce

Important note
To cite this publication, please use the final published version (if applicable).
Please check the document version above.

LONG-TERM DYNAMICS & STABILIZATION OF INTERTIDAL FLATS

A SYSTEM APPROACH

Long-term dynamics & stabilization of intertidal flats

A system approach

Proefschrift

ter verkrijging van de graad van doctor
aan de Technische Universiteit Delft,
op gezag van de Rector Magnificus prof. dr. ir. T.H.J.J. van der Hagen,
voorzitter van het College voor Promoties,
in het openbaar te verdedigen op woensdag 13 maart om 15:00 uur

door

Debora Cynthia Maan

Master of Science in Physics & Climate Science, Utrecht, Nederland
geboren te Leidschendam, Nederland.

We can't impose our will on a system. We can listen to what the system tells us, and discover how it's properties and our values can work together to bring forth something much better than could ever be produced by our will alone.

Donella Meadows

CONTENTS

SUMMARY

Decreasing sediment availability, in combination with sea level rise and human fixation of the coastline, results in losses of the intertidal environment (lying in-between the mean low water and mean high water spring tide). This means a loss of biodiversity and an increased coastal vulnerability to extreme events and sea level rise. Therefore it is of utmost importance to understand the dynamics of the intertidal wetlands; their response to sea level rise and to different types of human interferences. The better we understand the processes that underlie the evolution of the intertidal system, the more effectively we can manipulate the system, to stimulate its rise and maintain its elevation relative to mean sea level.

The long-term morphodynamics is difficult to understand due to the interdependencies of the underlying processes; the morphology is shaped by the hydrodynamic forces, while it influences these forces at the same time. Due to the feedback loops, the components are strongly entangled and the whole system cannot be reduced to the sum of its parts and solved by the traditional reductionist method.

In this thesis, system theory and system analysis are applied to get towards an understanding of 'the intertidal morphodynamical system'. This is the philosophy that states arise that are understandable and possible to determine exactly, despite the many interactions between the variables and the apparent complexity of systems. To describe these states, I follow a top-down approach, where I learn from the observed system behavior. Hence, the observation of conserved properties leads to the important question: 'why are they conserved?' The answer to this question can reveal much of the system's dynamics.

I investigated the intertidal system by a systematical analysis of long-term numerical simulations. Two types of intertidal systems are considered: (1) gentle intertidal flats on which cross-shore tidal currents dominate (at least in the lower (sub)tidal domain, where the wave impact is relatively small), and (2) narrow fringing intertidal flats in the close vicinity of a tidal channel, on which long-shore tidal currents and wind waves dominate over the cross-shore tidal currents. The simulations show that these systems behave totally different: Tidal flats on which the cross-shore tidal current dominates shift in the cross-shore direction and are rarely in morphodynamic equilibrium. When the cross-shore tidal current loses its dominance, on the other hand, stationary equilibrium states can develop. These evolutions can be explained by the characteristic feedback loops between the hydrodynamic forces and the bathymetry.

When cross-shore tidal currents dominate, negative feedback loops between the bed levels and the erosion fluxes stabilize the profile slope and shape within the first decades of evolution. Namely: On the lower (sub)tidal flat, an increase (decrease) in the local bed level leads to smaller (larger) water depths and larger (smaller) tidal flow velocities (in combination with conserved discharges). Hence, net accretion (erosion) automatically leads to an increase (decrease) in the gross erosion rates. This feedback loop steers

towards a local balance between the deposition and erosion flux on much of the tidal flat. Despite the balances between the vertical fluxes, a horizontal net transport generally remains. Namely, a stabilizing feedback loop does not exist on the upper flat. Hence, the tidal hydrodynamic energy remains low on the upper flat and sediment continuously settles there. This also means that the balances on the seaward sections are permanently disturbed by the changes of the upper shore. This results in seaward progradation with a conserved cross-sectional profile, which I call the 'lagrangian equilibrium state'.

Also in the presence of wind waves (acting together with *cross-shore* tidal currents), migrating states (i.e. long-term coastal progradation or retreat) develop. This tendency indicates a persistent imbalance on the upper flat in combination with the tide-related feedback loop described in the previous paragraph (which explains the horizontal shift). Because maximum wave-induced bed shear stresses occur close to the tidal front, i.e. in very shallow waters, any section within the intertidal domain will experience maximum wave-induced bed shear stresses, independent of the precise bed elevation. Hence, a strong stabilizing feedback loop between the wave-induced bed shear stress and the bed level is not present. Depending on the specific wave climate and sediment supply, the upper shore is accretive or erosive, resulting in respectively seaward progradation or landward retreat.

Based on the knowledge that the system converges to a 'lagrangian equilibrium state', system variables can be expressed in terms of independent driving factors. Quantitative relationships are derived between the progradation speed of migrating flats and the suspended sediment concentration in the adjacent waters, wave-induced erosion and sea level rise. These show that the speed increases stronger than linearly with the concentration in the adjacent deep waters (channels). Sea level rise and erosion by wind waves, on the other hand, affect the progradation speed in a linear fashion. In this thesis it is shown that a critical sediment concentration level exists below which a system shifts from progradation to retreat and this value is calculated for the Yangtze Estuary. For this estuary, it is estimated that at least ~ 30% of the sediment concentration in 1990 is needed to keep up with the projected rate of sea level rise till 2100.

The other type of considered intertidal systems are fringing intertidal flats under influence of along-shore tidal currents (in combination with cross-shore tidal currents and wind waves). Fringing flats exist along the fringes of bays or estuaries, at sites that are locally shielded from the strong along-shore tidal currents in the adjacent channels (so that the along-shore current is reduced in the cross-shore direction). On the lower flat, the cross-shore currents are negligible, as in contrast with the wide (open coast) tidal flats considered in the previous paragraphs. My results indicate that even small wind waves (5-10cm) can have an important stabilizing effect on the long-term morphodynamics of the fringing intertidal flats. Maximum wave-induced bed shear stresses were found in shallow waters (at the tidal fronts) and these decrease with increasing water depth. This relationship results in a strong stabilizing morphodynamic feedback loop in the subtidal domain, where the minimum water depth strongly decreases (increases) with a increasing (decreasing) bed level. After stabilization of the subtidal region, an additional stabilizing feedback loop gets important on the intertidal flat. Namely, landward of the stable section, an increase (decrease) in the local bed level leads to an increase (decrease) in the cross-sectional slope -in the offshore direction- and thereby to an increase

(decrease) in the relative importance of wave shoaling versus wave dissipation. These processes result in the development of a stationary equilibrium state. The equilibrium state is characterized by a shoreward increasing wave-induced bed shear stress, which counteracts the tidal energy gradient (which, in turn, is hardly affected by the intertidal bathymetry). Closer to the shore, where the along-shore current becomes negligible, the wave-induced erosion (and maximum bed shear stress) is approximately homogeneous on the equilibrium bathymetry. Such a homogeneous maximum wave-induced bed shear stress (exerted by small wind waves in shallow waters) is related with a linear cross-shore equilibrium profile. On a straight line, the effects of wave shoaling and wave dissipation at the tidal fronts (where the wave impact peaks) are homogeneous. This result differs from the concave equilibrium profiles for larger incoming wind waves as derived analytically by *Friedrichs & Aubrey* (1996).

SAMENVATTING

Tijdens hun verre vluchten over land en over zee stoppen veel trekvogels op het wad om zich (tijdens laagwater) te goed te doen aan een rijke collectie van vis en schaaldieren. Deze modder- en zandplaten, ook wel intergetijdengebieden genoemd, komen wereldwijd voor langs kusten en in riviermondingen. Daar vormen zij bijzondere natuurgebieden die onmisbaar zijn voor de ecologie in hun wijde omgeving. Van economisch belang is verder de rol die zij vervullen in de kustverdediging, bijvoorbeeld doordat golven erop breken en hun energie verliezen voordat ze inslag maken op de achterliggende dijken.

Ondanks de internationale regelgeving die moet toezien op het behoud van het wad (voorbeelden zijn de 'Ramsar Convention for the protection of migratory birds' en de 'European Natura2000 legislation'), is erosie van het intergetijdengebied een bekend verschijnsel. Ingenieursprojecten, die worden uitgevoerd voor de scheepvaart of ter bescherming van de kust, hebben onbedoeld vaak een desastreus effect op deze gevoelige natuurgebieden. Een van de redenen waarom het ons niet goed lukt om het wad te beschermen, is dat we de processen die ten grondslag liggen aan de kustdynamiek niet goed genoeg begrijpen. De moeilijkheid zit hem in de onderlinge afhankelijkheid van de processen die een rol spelen: de bodemligging wordt gevormd door de krachten van het water op de bodem, maar beïnvloedt tegelijkertijd dezelfde krachten. Deze onderlinge afhankelijkheid van variabelen maakt het systeem moeilijk te doorgronden.

In dit proefschrift wordt het systeemdenken en de systeemanalyse toegepast op de dynamiek van intergetijdengebieden om deze beter te begrijpen. Dit is de filosofie dat zich toestanden voordoen die te begrijpen zijn en exact bepaald kunnen worden, ondanks de vele onderlinge afhankelijkheden tussen de variabelen en de complexiteit van een systeem. Om deze toestanden te beschrijven, volg ik een 'top-down' benadering, waarbij ik uitga van het waargenomen systeemgedrag en daarvan probeer te leren. Het herkennen van behouden eigenschappen leidt tot de belangrijke vraag: 'waarom zijn deze behouden?'. Het antwoord op deze vraag kan veel van de systeemdynamiek onthullen.

Ik bekijk het intergetijdensysteem door middel van een systematische analyse op numerieke simulaties over de lange termijn (decennia tot eeuwen). Twee soorten systemen, die verschillen in de dominante stromingsrichting, worden bekeken: (1) intergetijdengebieden met de dominante stromingsrichting loodrecht op de kust (d.w.z. loodrecht op de dieptelijnen), en (2) intergetijdengebieden in de onmiddellijke nabijheid van een getijdengeul. De dominante stromingsrichting is hier parallel aan de kust (d.w.z. parallel aan de dieptelijnen). De simulaties laten zien dat deze systemen zich totaal anders gedragen: kusten met een dominante transversale stroming (d.w.z. loodrecht op de dieptelijnen) schuiven in deze richting op met een behouden dwarsprofiel en zijn zelden in een morfodynamisch evenwicht. Wanneer de dominante stromingsrichting parallel is aan de kust, kunnen wel stationaire evenwichtstoestanden ontstaan. Deze verschillende

gedragingen kunnen worden verklaard door de karakteristieke terugkoppelingsmechanismen tussen de hydrodynamische krachten en de bodemligging.

Wanneer de transversale stroming dominerend is, is het dwarsprofiel na de eerste decennia constant. Het behouden dwarsprofiel kan worden verklaard door een stabiliserende onderlinge afhankelijkheid tussen de lokale bodemhoogte en de getij-geïnduceerde bodemerosie op een groot deel van het intergetijdengebied. Als daar de bodem hoger komt te liggen, neemt de gemiddelde (d.w.z. gemiddeld over een getijdencyclus) waterdiepte af, terwijl de hoeveelheid water die eroverheen stroomt onveranderd blijft (bij gelijke landwaartse bodemligging). Dit vergroot de stroomsnelheden en leidt lokaal tot meer bodemerosie. Deze onderlinge afhankelijkheid tussen de variabelen stuurt naar een lokaal evenwicht.

Echter, op het hoogste stuk van het intergetijdengebied (vlakbij hoogwaterniveau) wordt de relatie tussen de lokale bodemhoogte en de lokale bodemerosie juist gedomineerd door een *positieve* terugkoppeling, doordat de tijdsvariatie in de waterstand daar sterk afneemt met een toenemende bodemhoogte. Doordat een verhoging van de bodem hierdoor leidt tot kleinere stroomsnelheden en bodemschuifspanningen, stabiliseert de bodem zich hier niet. Horizontaal gezien leidt dit tot een afname van de bodemerosie in de landwaartse richting, waardoor er netto sedimenttransport plaatsvindt in de landwaardse richting. Het steeds aangroeiende hogere intergetijdengebied beïnvloedt vervolgens de sedimentbalansen op het lagere wad via een afhankelijkheid tussen de bodemerosie en de landwaartse bodemligging. Onder invloed van deze afhankelijkheid bouwt de kust zeewaarts uit met een behouden dwarsprofiel. Als de bodemerosie op het hogere intergetijdengebied echter wordt gedomineerd door windgolven is een eroderend systeem mogelijk, waarbij de kust zich terugtrekt. De toestand waarin de kustlijn zich op deze manier met behouden dwarsprofiel uitbouwt of terugtrekt wordt in dit proefschrift een 'lagrangiaans evenwicht' genoemd.

Met behulp van de kennis dat er een lagriangiaans evenwicht ontstaat, kunnen kwantitatieve relaties worden afgeleid tussen de uitbouwsnelheid van het intergetijdengebied en (1) de sedimentconcentratie in de aangrenzende wateren, (2) golf- geïnduceerde erosie, en (3) zeespiegelstijging. Deze tonen aan dat de uitbouwsnelheid sterker dan lineair toeneemt met de concentratie in de aangrenzende diepe wateren (geulen). Anderzijds, beïnvloeden zeespiegelstijging en bodemerosie door windgolven de uitbouwsnelheid op een lineaire manier. Ik laat zien dat er een kritisch sedimentconcentratie niveau bestaat waaronder een transitie plaatsvindt van een uitbouwend systeem naar een terugtrekkend systeem. Gegeven een gemeten combinatie van uitbouwsnelheid, golf-geïnduceerde erosie en sedimentconcentratie, kunnen deze relaties worden gebruikt om ruwe projecties te maken voor verschillende scenario's van veranderende sedimentconcentraties en zeespiegelstijging. Voor de monding van de Yangtze rivier kan op deze manier worden bepaald dat grofweg 30% van de sedimentconcentratie in 1990 nodig is om een terugtrekkend intergetijdensysteem te voorkomen (uitgaande van een onveranderd golfklimaat en een lokale zeespiegelstijging van $7mm/yr$).

Het andere type systeem dat ik bekeken heb, is een intergetijdengebied waarop de dominante stromingsrichting parallel is aan de kust. Deze gebieden komen bijvoorbeeld voor aan de oevers van riviermondingen, op plaatsen die ietwat beschermd liggen ten opzichte van de sterkere stromingen in de nabijgelegen geulen, zodat deze stroming af-

neemt in de richting naar de kust toe. Als golven afwezig zijn, is er geen tendens naar een evenwicht of een behouden dwarsprofiel. In dat geval wordt het hogere intergetijdengebied gekenmerkt door permanente aangroei, terwijl op het lagere intergetijdengebied mogelijk permanente erosie optreedt. Echter laten mijn resultaten zien dat zelfs kleine golven (5-10 cm hoog) een belangrijke stabiliserende rol kunnen spelen. De impact van deze kleine golven is maximaal in ondiepe wateren (d.w.z. direct na het opkomen van de zee) en neemt af met toenemende waterdiepte. Deze afhankelijkheid resulteert in een stabiliserend terugkoppelingsmechanisme op het subtidale domein (d.w.z. het stuk onder laag waterniveau), waar de minimale waterdiepte sterk afneemt met een toenemende bodemhoogte. Nadat het subtidale domein gestabiliseerd is, wordt een ander terugkoppelingsmechanisme belangrijk. Namelijk landwaarts van het stabiele domein, leidt een bodemverhoging(verlaging) tot een toename (afname) van de dwarshelling -in de zeewaartse richting- en daardoor tot een toename (afname) van golf shoaling (dit is het effect dat de golfhoogtes toenemen als golven in ondieper water komen). Hierdoor neemt de golf-geïnduceerde erosie toe als het bodemniveau stijgt. Deze onderlinge afhankelijkheid van de variabelen zorgt voor een evolutie naar een stationair evenwicht. De evenwichtstoestand wordt gekenmerkt door een toenemende golf-geïnduceerde bodemschuifspanning in de richting naar de kust, tegengesteld aan de gradiënt in de getijgeïnduceerde bodemschuifspanning. Als de impact van de getijdestroming verwaarloosbaar is (ten opzichte van die van de golven), is de golf-geïnduceerde schuifspanning ongeveer homogeen verdeeld. Deze homogene verdeling kan worden gerelateerd aan een lineair bodemprofiel (d.w.z. een homogene helling in de richting loodrecht op de kust). Op een lineair bodemprofiel is de maximale golf-geïnduceerde bodemschuifspanning (uitgeoefend door kleine windgolven in ondiepe wateren) homogeen verdeeld. Dit resultaat verschilt van de concave evenwichtsprofielen (d.w.z. een steiler wordende bodemhelling in de richting naar de kust) voor grotere golven zoals analytisch bepaald door *Friedrichs & Aubrey* (1996).

REFERENCES

Friedrichs, C.T. & Aubrey, D.G. (1996), Uniform Bottom Shear Stress and Equilibrium Hyposometry of Intertidal Flats, in *Mixing in Estuaries and Coastal Seas, Coastal and Estuarine Studies*, Vol. 50, edited by C. Pattiaratchi, pp. 405-429, AGU, Washington, D.C., doi:10.1029/CE050p0405

PREFACE

Do you sometimes have the feeling that you are simplifying a problem too much? That your solution is too theoretical for real application? Are you sometimes treating variables as constants (to make a problem 'solvable'), whereas in reality the variable is everything but really constant? In that case, I would recommend the book 'Thinking in Systems - A Primer', written by Donella Meadows (*Meadows & Wright*, 2009). She was a pioneering American environmental scientist at MIT and a master in systems thinking and systems analysis. Her work is recognized in many different academic fields, as also outside the academic world, which shows the wide (practical) application of systems thinking and system analysis.

The field of morphodynamics is an example of where an understanding of system theory is indispensable for solving the most challenging problems; those in which the interaction between the morphology and the hydrodynamics plays a dominant role; those at the time-scales in which neither can be treated as independent from the other.

Despite its power, applying system theory does not have to be difficult. It actually yields a very natural and intuitive way of thinking. You just need to 'acknowledge the complexity of nature' here and there, and to concentrate on 'how to solve a complex problem' instead of focusing on how to simplify one with (erroneous) linear regressions. For me, complex systems yield the most fascinating and challenging puzzles to solve.

Writing this thesis has been a pleasure. I want to thank Bram van Prooijen, Zheng Bing Wang and Huib de Vriend for giving me this particular opportunity, and for supporting me in taking an approach that differs from the more traditional (reductionistic) methods in the field of hydraulic engineering. I found confirmation and inspiration from other scientists in the field who follow the approach of complex system science, and from the ongoing shift towards the 'building with nature' philosophy. The interaction between ecologists and hydraulic engineers, and the integral way of thinking it involves, is promising and inspiring.

Debora Cynthia Maan
Delft, August 2018

REFERENCES

Meadows, D.H.& Wright, D. (2009), Thinking in Systems: A Primer. London: Earthscan, ISBN 9781844077267.

1

INTRODUCTION

Systems of information-feedback control are fundamental to all life and human endeavor, from the slow pace of biological evolution to the launching of the latest space satellite.... Everything we do as individuals, as an industry, or as society is done in the context of information-feedback system.

Jay W. Forrester

1.1. BACKGROUND AND MOTIVATION

Many of our biggest cities worldwide are situated in delta's. These low-lying coastal areas are extremely vulnerable to climate change and accelerated sea level rise (SLR) (*Syvitski et al.*, 2009). In meantime, human interferences can weaken our coastal defense, especially if dams inside the upstream river reduce the sediment supply towards the estuary (*Syvitski et al.*, 2007, 2009). Decreasing sediment availability, in combination with SLR and human fixation of the coastline, strongly impacts the coastal environment. Extremely sensitive are the intertidal flats, lying in-between the mean low water and mean high water spring tide. The intertidal flats (including salt marshes and mudflats) form the start for land reclamation; serve as buffers for coastal defense; are sinks of pollutants and nutrients; and are important habitats for flora and fauna (*van de Kam et al.*, 2010). Loss of these coastal wetlands means a loss of biodiversity and an increased coastal vulnerability to extreme events and SLR. It is therefore of utmost importance to predict the morphological development of the intertidal flats with regard to climate change and anthropogenic activities. The better we understand the processes that underlie the evolution of the intertidal system, the more effectively we can manipulate the system, to stimulate its rise and maintain its elevation relative to mean sea level (MSL).

The difficulties in understanding the long-term morphodynamics are related to the many interacting factors that play a role: the (bio)morphology affects the shear stresses induced by wind waves and tidal currents, as well as the patterns of sediment transport. In turn, it is shaped by the same factors. These interactions make the morphodynamic

system behave like a 'complex system' (*D.H. Meadows*, 2009), characterized by the occurrence of stable states (*van Goor et al.*, 2003; *Fagherazzi et al.*, 2006, 2007; *Bearman et al.*, 2010; *Friedrichs*, 2011) and sudden transitions between these states (*Wang et al.*, 2015). This kind of systems are difficult to unravel and to simplify. We have to be careful not to treat dependent variables -that are embedded in a system- as independent drivers (*D.H. Meadows*, 2009).

However, system theory provides a framework for working with and understanding complex systems. It implies that the interactions between the variables should be identified. The type of interactions give (qualitative) understanding of the system's behavior, its states and transitions between those states. Sometimes it is even possible to quantitatively express system variables in terms of independent system drivers. Especially the knowledge that a system tends to an equilibrium state can greatly simplify problems.

1.2. SYSTEMS AND FEEDBACK LOOPS

Quantities and processes are often steered or regulated by feedback loops. In this introduction we discuss the two basic types of feedback loops, the stabilizing feedback loop and the reinforcing feedback loop, by considering two examples of systems. We consider a very simple model for two different students who make exams and get influenced by their results:

- Imagine a student who wants to pass his (or her) exams with as little effort as possible. Initially, he (she) does not know how much effort it takes to pass an exam. But after each exam, feedback is given in the form of a mark. Each inadequate result gives the signal 'work harder'. Each high mark gives the signal 'work less'. After many exams, the student is well 'calibrated' and knows exactly what is required to score just enough points to pass. In this example, the mark for the exam is the quantity that gets controlled via the behavior of the student, that depends on the mark itself (i.e. a feedback loop). The marks get stabilized around the 'passing point'.

- Now imagine another student who needs good results as confirmation of his/her own ability and to stay motivated. Full of enthusiasm he/she starts with the studies and soon the first results come. Is the hard work rewarded by high marks? Then the self-confidence and enthusiasm increases; next time he/she works even harder. Are the first scores disappointing? Then he/she loses motivation to study for the next exam. Hence, also for this student, the marks and the willingness to study are entangled, but now by a reinforcing feedback loop (with a tipping point around the student's own expectations).

Of course no student can be modeled by a routine with one single feedback loop. In reality, a system often consists of many different feedback loops. Different loops working simultaneously; competing to pull the system toward different 'goals'. At different 'stages' another feedback loop can dominate. A student who loses motivation to excel after the first (disappointing) marks can adjust his/her goals to the aim of 'just passing the exams', i.e. a shift from a reinforcing stage to a balancing stage. Or a student who initially was 'trapped' by loop 1, can lose motivation after one very low mark. Hence,

"every balancing feedback loop, has its breakdown point, where other loops pull it away from its goal more strongly than it can pull back" (*D.H. Meadows*, 2009).

To do some more justice to the complexity of a student's behavior, let us consider yet another 'type' of student; one that is studying purely out of interest in the matter. Hence, the behavior of this student will not be affected by the marks he/she achieves. But the enthusiasm of the student can be influenced by the enthusiasm of the teacher. What if the enthusiasm of the teacher, in turn, is influenced by the behavior/ enthusiasm of the whole group of students or their (midterm) marks? See, things easily get complex. Depending on the typical interactions and hierarchies, a system can be too big and complicated to resolve.

However, the functioning of our students is even more complex than the matter they study, so let us now move to the field of morphodynamics. One very simple and direct feedback loop that often influences the overall behavior of morphodynamic systems is the feedback loop between the bed level and the bed shear stress, as indicated in Figure 1.1. Depending on the typical hydrodynamic forcing, stabilizing or reinforcing feedback loops occur. By these loops, bed level changes are respectively diminished or amplified by its own action (via its effect on the erosion rates that in turn directly affect the sediment balances), see Fig1.1.
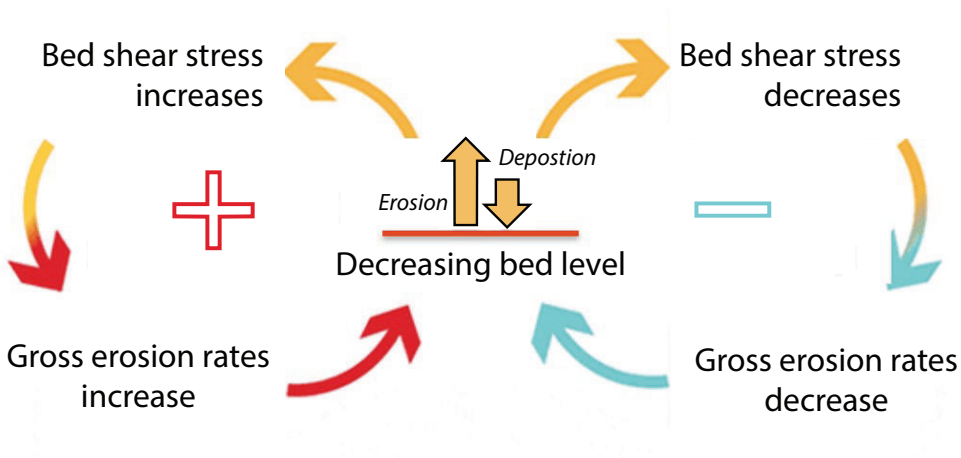
Figure 1.1: Diagram of two different types of feedback loops in a morphodynamic system. The arrows indicate the consecutive consequences of a decrease in the bed level for two different cases. Left (reinforcing) loop: a decrease in the bed level results in larger bed shear stresses and larger gross erosion rates, i.e. bed level changes get amplified. Right (stabilizing) loop: a decrease in the bed level results in smaller bed shear stresses and smaller gross erosion rates, i.e. bed level changes get smaller in time.

Also in the morphodynamic system, multiple feedback loops can act simultaneously, competing or reinforcing each other. This makes the system hard to unravel. System theory is the theory that states arise that are understandable and possible to determine and describe exactly, despite the many interactions between the variables and the apparent complexity of the system. We here define the 'steady states' as states in which certain

properties of a system remain constant in time, controlled by negative feedback loops. Observations and numerical studies show that the evolution of intertidal flats (and morphodynamic systems in general) often converge towards these states (*Roberts et al.*, 2000; *Pritchard et al.*, 2002; *Fagherazzi et al.*, 2006, 2007; *Bearman et al.*, 2010; *Friedrichs*, 2011; *Liu et al.*, 2011; *Hu et al.*, 2015). Following a top-down approach, where we learn from the observed system behavior and states, is a useful strategy to get towards an understanding of dynamical systems. Hence, we can ask the question: 'what are the feedback loops/ the physical mechanisms that can explain the observed behavior (i.e. the states, trends, patterns, events, etc.)?' In special, the observation of conserved properties leads to the important question: 'why are they conserved?' The answers to these questions can reveal much of the system's dynamics. This is the typical systems approach that will be taken in this thesis to discover the processes that drive the morphodynamic system.

1.3. OBJECTIVES AND RESEARCH QUESTIONS

In this thesis we investigate the behavior of 'intertidal flats' as systems. The first goal of this PhD thesis is to increase our understanding of the processes and feedback loops that underlie the long-term morphodynamic evolution of intertidal flats. Instead of a one-sided focus on how the bathymetry steers the hydrodynamic flow and sediment transport, or how the bed shear stresses and sediment transport shape the bathymetry, we explicitly want to know how these variables are reinforced or reversed by its own action. We aim to answer the following research questions: How do the physical processes interplay and together determine the behavior of intertidal systems? Do steady states exist? How resilient or sensitive are these states to environmental changes such as sea level rise and reduced sediment supply? If possible, we want to use this understanding to express state variables quantitatively in terms of the independent driving factors.

1.4. METHODOLOGY

System analysis based on experiments with idealised process-based models were carried out to obtain better understanding of the development of intertidal systems and the underlying processes and mechanisms. By using idealised model set-ups, the behavior can be studied in a systematic way. Unraveling the behavior of a numerical model also has the great advantage that the mutual dependencies are already quantified well in the model. The physics is already in there, but we still need a better understanding of which processes and feedback loops dominate the system's behavior. We consider two types of intertidal systems: (1) wide (open coast) intertidal flats that are dominated by cross-shore tidal currents and wind waves, and (2) fringing intertidal flats in the close vicinity of a tidal channel, on which long-shore currents and wind waves dominate over cross-shore tidal currents. We describe and analyze the time-evolution of the state variables (e.g. the bathymetry, the bed shear stresses, the wave heigth). Considering how these factors change over time and are (positively or negatively) correlated, reveals important information about the interdependencies and morphodynamic feedback mechanisms (reinforcing or stabilizing) that control the observed long-term evolution of the intertidal flats.

1.5. OUTLINE

This thesis is based on a set of three journal papers. One of the papers is split up in Chapters 2 and 3, while the other two papers have been almost literally taken over as Chapter 4 and 5. Because these are stand-alone papers, the introductions of the chapters show some overlap.

In the next chapter (Chapter 2), we describe the behavior and underlying processes of (wide and gently sloped) intertidal flats under influence of cross-shore tidal currents and onshore prograding wind waves. We investigate the steady states of these systems. In Chapter 3, the model is expressed in a moving reference frame, a way to derive the stable profile shapes and progradation speeds for given wave climates and sediment supplies. In Chapter 4, the basis of the 'Lagrangian equilibrium state' is used to derive quantitative relationships between the progradation speed of intertidal flats and (1) the sediment supply, (2) the wave-induced erosion and (3) sea level rise. In Chapter 5, we consider fringing intertidal flats. As in contrast with the wide and open tidal flats, these systems are characterized by small distances between the intertidal area and the adjacent channels and by strong long-shore tidal current velocities on much of the tidal flat. A two dimensional process-based morphodynamic model (Delft3D) is constructed to perform a case-study in the Western Scheldt Estuary. Based on long-term simulations, the system behavior is considered and the underlying feedback loops are identified (Chapter 5). Finally, Chapter 6 summarizes the overall conclusions of the thesis and provides an outlook to future applications and open research questions.

REFERENCES

Bearman, J.A., Friedrichs, C.T., Jaffe, B.E. & Foxgrover, A.C.(2010), Spatial Trends in Tidal Flat Shape and Associated Environmental Parameters in South San Francisco Bay, *Journal of Coastal Research*, *262*, 342-349, doi:10.2112/08-1094.1

Fagherazzi, S., Carniello, L., D'Alpaos, L. & Defina, A. (2006), Critical bifurcation of shallow microtidal landforms in tidal flats and salt marshes, *Proceedings of the National Academy of Sciences of the United States of America*, *103*(22), 8337-8341, doi:10.1073/pnas.0508379103

Fagherazzi, S., Palermo, C., Rulli, M.C., Carniello, L. & Defina, A. (2007), Wind waves in shallow microtidal basins and the dynamic equilibrium of tidal flats, *Journal of Geophysical Research: Earth Surface*, *112*, F0204, doi:10.1029/2006JF000572

Friedrichs, C.T. (2011), Tidal Flat morphodynamics: A synthesis, in *Treatise on Estuarine and Coastal Science*, E. Wolanski and D. McLusky (eds.), Academic Press, Waltham, pp 137-137, ISBN 9780080878850, http://dx.doi.org/10.1016/B978-0-12-374711-2.00307-7

Hu, Z., Wang, Z.B., Zitman, T.J., Stive, M.J.F., & Bouma, T.J. (2015), Predicting long-term and short-term tidal flat morphodynamics using a dynamic equilibrium theory, *Journal of Geophysical Research: Earth Surface*, *120*, 1803-1823, doi:10.1002/2015JF003486

Liu, X.J., S. Gao, Y.P. Wang (2011), Modeling profile shape evolution for accreting tidal flats composed of mud and sand: A case study of the central Jiangsu coast, China, *Continental Shelf Research*, *31*, 1750-1760, doi:10.1016/j.csr.2011.08.002.

Meadows, Donella H (2009), Thinking in Systems: A Primer. London: Earthscan, ISBN 9781844077267 D.H. Meadows (2009), Thinking in Systems - A Primer, Edited by Diana Wright, London, Earthscan,

Passeri, D. L., Hagen, S. C., Medeiros, S. C., Bilskie, M. V., Alizad, K. & Wang, D. (2015), Earth's Future Special Section: The dynamic effects of sea level rise on low-gradient coastal landscapes: A review, *Earth's Future,3*, 159-181, doi:10.1002/2015EF000298

Pritchard, D. A.J. Hogg and W. Roberts (2002), Morphological modelling of intertidal mudflats: the role of cross-shore tidal currents, *Continental Shelf Research*, *22*, 1887-1895, doi:10.1016/S0278-4343(02)00044-4.

Roberts, W., P. Le Hir and R.J.S. Whitehouse (2000), Investigation using simple mathematical models of the effect of tidal currents and waves on the profile shape of intertidal mudflats, *Continental Shelf Research*, *20*, 1079-1097, doi:10.1016/S0278-4343(00)00013-3.

Syvitski, J. P. M., and Saito, Y. (2007). Morphodynamics of deltas under the influence of humans. *Global and Planetary Change*, *57*(3-4), 261-282. https://doi.org/10.1016/j.gloplacha.2006.12.001

Syvitski, J. P, Kettner, A. J., Overeem, I., Hutton, E. W., Hannon, M. T., Brakenridge, G. R., et al. (2009). Sinking deltas due to human activities. *Nature Geoscience*, 2(10), 681-686. https://doi.org/10.1038/ngeo629

van de Kam, J., Battley, P.F., McCaffery, B.J., Rogers, D.I., Hong, J.S., Moores, N. et al. (2010), Invisible connections: why migrating shorebirds need the Yellow Sea, *South Australian Ornithologist,37*(1)

van Goor, M.A., Zitman, T.J., Wang, Z.B. & Stive, M.J.F. (2003), Impact of sea-level rise on the morphological equilibrium state of tidal inlets, *Marine Geology*, *202*(3-4), 211-227, doi:10.1016/S0025-3227(03)00262-7

van Maanen, B., Coco, G., Bryan, K.R. & Friedrichs, C.T. (2013), Modeling the morphodynamic response of tidal embayments to sea-level rise, *Ocean Dynamics*, *63*, 1249-1262, doi:10.1007/s10236-013-0649-6

Wang, Z.B., Van Maren, D.S., Ding, P.X., Yang, S.L., van Prooijen, B.C., De Vet, P.L.M. et al. (2015), Human impacts on morphodynamic thresholds in estuarine systems, *Continental Shelf Research*, *111*, 174-183, doi:10.1016/j.csr.2015.08.009

Zhou, Z., Coco, G., Townend, I., Olabarrieta, M., van der Wegen, M., Gong, Z. et al. (2017), Is 'Morphodynamic Equilibrium' an oxymoron?, *Earth-Science Reviews*, *165*, 257-267, doi:10.1016/j.earscirev.2016.12.002

2

DO INTERTIDAL FLATS EVER REACH EQUILIBRIUM?

Various studies have identified a strong relation between the hydrodynamic forces and 'the equilibrium profile' for intertidal flats. A thorough understanding of the interplay between the hydrodynamic forces and the morphology, however, concerns more than the equilibrium state alone. We study the basic processes and feedback mechanisms underlying the long-term behavior of the intertidal system. In this chapter, we focus on intertidal flats that are controlled by cross-shore tidal currents and wind waves and apply a 1-D cross-shore morphodynamic model. The results indicate that, by an adjustment of the profile slope and shape, an initial imbalance between deposition and erosion is minimized within a few decades. What follows is a state of long-term seaward progradation or landward retreat of the intertidal flat, in which the cross-shore profile shape is largely maintained and the imbalance between deposition and erosion is not further reduced. These long-term trends can be explained by positive feedback loops between the morphology and the hydrodynamic forces on the flat: initial accretion (erosion) decreases (increases) the shear stresses over the flat, which induces further accretion (erosion). This implies that a static equilibrium state cannot exist, the flat either builds out or retreats.

2.1. INTRODUCTION

Intertidal flats, soft sediment beds located between the mean low water and mean high water spring tide, exist in a variety of environments ranging from tidal basins to estuaries and open coasts (*Flemming*, 2002). Above mean sea level, intertidal flats generally merge with vegetated salt marshes. Together, salt marshes and intertidal flats form important habitats, where organic material accumulates and numerous types of living organisms gather, feed, rest, breed and nurse their offspring. The intertidal environment is indispensable to the ecosystem far outside its boundaries and therefore often protected by

international legislation, such as the Ramsar Convention for the protection of migratory birds, or the European Natura2000 legislation.

On the other hand, intertidal flats and marshes are highly sensitive to changes in their environmental conditions. Engineering works, aimed to protect the coast or facilitate navigation, as well as anthropogenic climate change and sea-level rise, often drastically affect the intertidal area. The Eastern Scheldt Estuary in the Netherlands is an example of a system where an anthropogenic interference (building of a storm surge barrier) resulted in ongoing erosion of the intertidal flats (*Eelkema et al.*, 2013). In the Yangtze Estuary (China), the seaward expansion of the intertidal flats slowed down due to the construction of plentiful dams in the Yangtze River (*Yang et al.*, 2011). The Venice Lagoon, on the other hand, is an example of systems where the future of the intertidal flats and salt marshes critically depends on the rate of sea-level rise in the next century (*Marani et al.*, 2007).

Erosion of intertidal flats is generally undesirable, as a smaller area or a lower elevation of the flats implies less food or a shorter dry period for wading birds to forage. It also implies a smaller buffer between (migrating) channels and dikes; intertidal flats protect the dikes by providing geotechnical stability and dissipating wave energy (*Dyer*, 1998; *Kirby*, 2000). In order to support management decisions, a proper understanding of the dynamics of the intertidal system and their response to engineering works and sea-level rise is needed.

The functionality of intertidal flats for ecology and coastal defense depends on the shape of their cross-shore profiles (*Kirby*, 2000). For ecology and safety issues, high and convex-upward (decreasing slope towards the top of the tidal flat, henceforth simply called 'convex') profiles are generally preferred over low and concave-upward (increasing slope towards the top of the flat, henceforth called 'concave') ones for their relatively wide upper intertidal area (*Kirby*, 2000). Relationships between the cross-shore 'equilibrium profiles' of intertidal flats and the environmental factors (sediment availability, wave climate and tidal range) have been derived in various studies (*Friedrichs and Aubrey*, 1996; *Roberts et al.*, 2000; *Friedrichs*, 2011), both numerically and analytically. Such a 'morphodynamic equilibrium state' is commonly defined by a constant bed level over some characteristic time span. It has been shown that the intertidal cross-shore profile, once in equilibrium with the environment, tends to be convex under the influence of tidal currents, whereas the action of wind waves yields more concave equilibrium profile shapes. For situations in which waves and tidal currents are both present, several authors have suggested that the cross-shore equilibrium profile can be classified according to the 'dominance' of waves over tides, i.e. to the relative magnitude of the wave- and tide-induced bed shear stresses (*Kirby*, 2000; *Roberts et al.*, 2000; *Friedrichs*, 2011).

However, numerous studies show that a stationary morphodynamic equilibrium state is rather exceptional and that coastlines are in general in an accretive or erosive state (*Kirby*, 2000; *Pritchard et al.*, 2002; *van der Wegen*, 2010; *Mariotti and Fagherazzi*, 2010; *Tambroni and Seminara*, 2012). Numerical studies by *Pritchard et al.* (2002) and *Waeles et al.* (2004) show that under influence of cross-shore tidal currents, intertidal flats prograde or retreat in the long run, whereas the cross-shore profile shape is stable after a few decades of evolution. *Mariotti and Fagherazzi* (2010) and *Tambroni and Seminara* (2012), both accounting for the effects of wind waves and vegetation, show similar

trends. Other studies show correlations between the accretive (erosive) state and the convexity (concavity) of the cross-shore profile (*Lee and Mehta*, 1997; *Dyer*, 1998; *Kirby*, 2000, 2002; *Liu et al.*, 2011; *Friedrichs*, 2011), as well as the influence of net sedimentation on the profile slope and the width of the intertidal area (*Pritchard et al.*, 2003; *Liu et al.*, 2011; *Friedrichs*, 2011). Convex and accreting flats have furthermore been linked to tidal dominance and concave and retreating flats to wave dominance (*Mehta et al.*, 1996; *Kirby*, 2000; *Friedrichs*, 2011), although *Pritchard et al.* (2002) showed that tidal asymmetry can significantly change the effect of tides and that ebb-dominance can cause the tidal flat to retreat with a convex profile shape.

Subsequent studies sought for the criteria for which intertidal flats prograde or retreat and for which an equilibrium state develops. *Waeles et al.* (2004) incorporated the effect of wind waves in their 1-D cross-shore model and found that the possibility of an equilibrium state depends on the typical wave regime. *Mariotti and Fagherazzi* (2010) showed that the state (progradation or retreat) furthermore depends on the sediment supply and that the presence of vegetation influences the rate of progradation or retreat. In the same study, the evolution of the marsh boundary and adjacent flat was determined for different scenarios of sea-level rise. Their results show that sea-level rise (in time) is an important factor, which can determine whether an intertidal flat will prograde or retreat.

Additional relevant studies on the intertidal morphodynamic equilibrium were carried out within 0-D frameworks (*Fagherazzi et al.*, 2006, 2007; *Marani et al.*, 2007; *de Swart and Zimmerman*, 2009; *Marani et al.*, 2010), i.e. based on the assumption of a homogeneous bed level (platform). This approach is based on observations of characteristic intertidal landscapes in which large tidal platforms lie within specific ranges of elevation (separated by much steeper transition zones). Results of these studies suggest that wave-dominated intertidal platforms migrate to stable equilibrium elevations (*Fagherazzi et al.*, 2006; *Marani et al.*, 2007; *de Swart and Zimmerman*, 2009; *Marani et al.*, 2010) and that the presence of vegetation and biomorphodynamic feedbacks can further intensify the discrepancy between different stable elevations (*Fagherazzi et al.*, 2006, 2007; *Marani et al.*, 2007, 2010).

The present study is motivated by the wish to predict the consequences of engineering works for the status of the intertidal flats in the Yangtze Estuary. The mudflats around the mouth of the Yangtze River are characterized by the exposure to wind waves and the large supply of fine sediment from the Yangtze River (*Yang et al.*, 2008). Studies show that both, wind wave- and tide-induced forces play a significant role in the morphodynamics of these flats (*Yang et al.*, 2001, 2008). In the period between 1982 and 1990, the intertidal flats prograded with a smooth and convex shape (see Fig.2.1), presumably as a consequence of the abundant sediment supply from the river. In the last few decades, the construction of dams in the river basin has resulted in a strong reduction of the sediment supply. Subsequently, the progradation of the tidal flats has stopped and the profiles have become more and more concave (*Yang et al.*, 2011). Yet, the future of the intertidal flats in the Yangtze Estuary remains uncertain: will the flats further prograde after a change in shape, will a stationary balance be established or is the change in shape an early indication for (long-term) erosion?

In this chapter we aim to determine (qualitatively) the influence of the sediment sup-
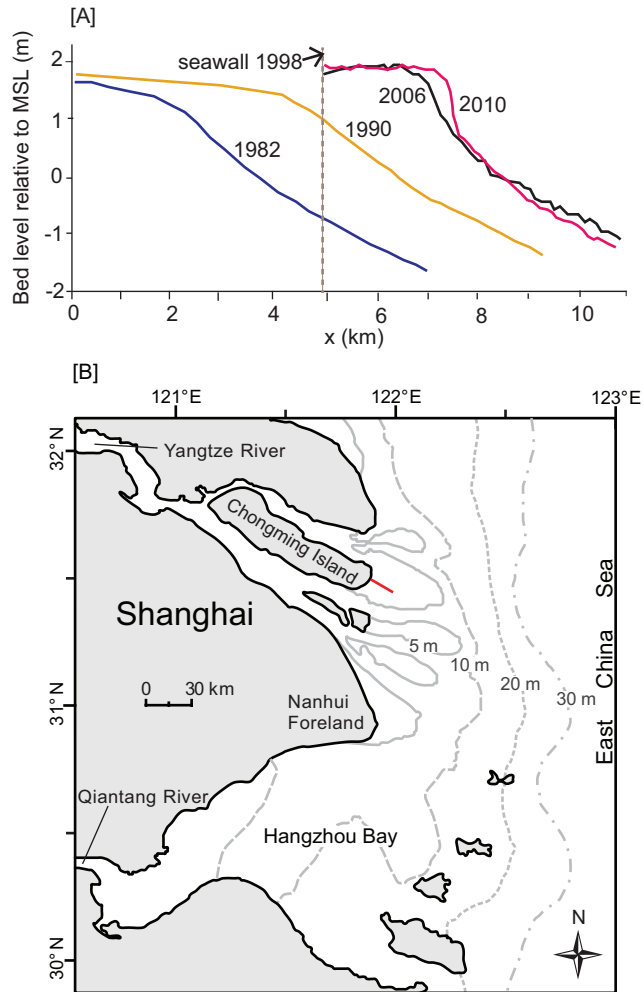
Figure 2.1: (A) Observed cross-shore profiles near mean sea level at Eastern Chongming Island, modified from Yang et al. (2011). Indicated distances are relative to the 1980 seawall (km). The figure shows similar convex-up cross-sections in 1982 and 1990 in combination with a horizontal progradation of the coastline. The profiles in 2006 and 2010 show concave lines.(B) Map of the Yangtze River Delta, the red line indicates the transect of Panel A.

ply and the wave climate on the state (prograding, retreating or in equilibrium) of intertidal flats that are dominated by cross-shore processes (cross-shore tidal currents and wind waves), and to describe the morphodynamic feedback mechanisms that underlie their long-term trends. We explicitly focus on the response of the intertidal system to constant environmental conditions. Understanding the behavior of such a simplified system is a first step in predicting the effect of changing boundary conditions and the consequences of engineering works and sea-level rise for the status of intertidal flats.

The behavior of the intertidal system is investigated by analyzing the evolution of the bathymetry and the patterns of suspended sediment concentration and bed shear stresses, as well as the horizontal sediment fluxes, over developing tidal flats. To this end, we apply a 1-D cross-shore morphodynamic model. In Section 2.2 we will first have a look at the applied model. The model settings (parameters and boundary conditions) are summarized in Section 2.3. The results are presented and discussed in Sections 2.4 and 2.5 respectively. Conclusions are drawn in Section 2.6.

2.2. MODEL DESCRIPTION

2.2.1. FLOW MODULE

Process-based numerical models provide the framework to study the basic processes underlying the intertidal flat evolution. For this study, a 1-D cross-shore model has been developed that computes cross-shore tidal flow and the growth (shoaling) and decay (dissipation and breaking) of incoming wind waves over a tidal flat, the associated tide- and wave-induced bed shear stresses, the sediment transport and the induced morphological changes. By using a cross-shore model, we neglect the effect of the long-shore current and long-shore sediment transport on the cross-shore profile. The study is therefore applicable for wide, gently sloping tidal flats, normally found at locations with a large supply of fine sediment (*Flemming*, 2002). The model is however more comprehensive than the 1-D cross-shore models used by *Roberts et al.* (2000) and *Pritchard et al.* (2002), because it includes a more detailed description for the effects of wind waves on the bed shear stress. Furthermore, we do not neglect the dispersion term in the sediment transport equation (Eq.2.4). Actually, our model is quite similar to the one used by *Waeles et al.* (2004), although we do not include the effects of nonlinear current and wave interactions and the presence of biota on the bed shear stress.

The model is forced by a constant external sediment concentration at the boundary, which is assumed to be independent of the intertidal flat morphodynamics and the gain or loss of sediment over the tidal flat. This boundary can be formed by a tidal channel, for instance, or the mouth of a river, in which the sediment concentration is largely determined by other (larger-scale) processes.

The water depth and cross-shore tidal currents are evaluated in time by the conservation equations for mass and momentum:

$$\frac{\partial h}{\partial t} + \frac{\partial uh}{\partial x} = 0, \qquad (2.1)$$

$$\frac{\partial u}{\partial t} + u\frac{\partial u}{\partial x} = -g\frac{\partial \zeta}{\partial x} - \frac{\tau_{bc}}{\rho_w h} \qquad (2.2)$$

where h is the water depth, u is the cross-shore flow velocity, ζ is the water level, g is the acceleration due to gravity, ρ_w is the density of water and τ_{bc} represents the bed shear stress (i.e. bed-induced friction on the flow). τ_{bc} is given by the quadratic drag law:

$$\tau_{bc} = \rho_w C_d u^2. \tag{2.3}$$

in which C_d is a constant drag coefficient (specified in Table 2.1 in Section 2.3), see *Soulsby* (1997). The effect of wind on the depth-averaged flow is not calculated. Wind waves are however included by making an assumption for the height of the incoming wind waves at the model boundary (see Sec. 2.2.2).

The sediment concentration is described by the advection-dispersion equation:

$$\frac{\partial ch}{\partial t} + \frac{\partial uch}{\partial x} - \frac{\partial}{\partial x}\left(Kh\frac{\partial c}{\partial x}\right) = E - D, \tag{2.4}$$

where c is the suspended sediment concentration, K is the dispersion coefficient and E and D are the erosion and deposition fluxes. The erosion and deposition fluxes are computed by (*Ariathurai*, 1974; *Winterwerp and Van Kesteren*, 2004):

$$E = \max\left[m_e\left(\frac{\tau'_b}{\tau_{cr}} - 1\right), 0\right] \tag{2.5}$$

and

$$D = c \cdot w_s, \tag{2.6}$$

where m_e is the erosion rate coefficient, τ'_b the total skin friction acting on the grains (i.e. that part of the total bed shear stress that directly acts on the sediment particles (*Fredsoe and Deigaard*, 1992), see Eq.2.7), τ_{cr} the critical bed shear stress for erosion and w_s the settling velocity. This description, which does not include a critical bed shear stress for deposition, implies that erosion and deposition occur simultaneously when the shear stress exceeds its critical value for erosion (*Winterwerp and Van Kesteren*, 2004).

The total skin friction consists of a tide- and a wave-induced part, which are assumed to be additive (neglecting nonlinearities due to wave-current interactions, see *Soulsby* (2005)):

$$\tau'_b = \tau'_{bc} + \tau'_{bw}. \tag{2.7}$$

The tide-induced skin friction is derived from the tidal flow velocity (*van Rijn*, 1993):

$$\tau'_{bc} = \frac{1}{8}\rho_w f_c u^2, \tag{2.8}$$

with friction factor

$$f_c = 0.24\left(\log\left(\frac{12 \cdot h}{2.5 \cdot d_{50}}\right)\right)^{-2}, \tag{2.9}$$

where d_{50} is the median sediment diameter. The wave-induced skin friction τ'_{bw} is calculated by Eq.2.19 (Section 2.2.2).

Bedload transport is not taken into account; we focus on intertidal flats that are composed of fine sediments. For the computation of the flow and sediment transport we apply a minimum depth of $10cm$ for the flooding-drying procedure (i.e. at smaller depths the flow velocity and the sediment transport rates are taken equal to zero). After calculating the erosion and deposition fluxes, bed level changes are computed from:

$$\frac{d\eta}{dt} = \frac{1}{\rho_{dry}}(D - E),\qquad(2.10)$$

in which ρ_{dry} is the dry bed density (specified in Table 2.1, Section 2.3). ρ_{dry} is assumed to be constant in time, i.e. the difference in compaction between freshly deposited mud and the older bed is neglected.

For some simulations, a so called 'morphological factor' M is used to speed up the calculation process (*Lesser et al.*, 2004; *Roelvink*, 2006). To this end, the bed level changes are multiplied by M at each hydrodynamic time step. Bed level changes over full spring-neap cycles are then considered; they represent bed level changes over a period of M spring-neap cycles. This method can only be applied when the bed level changes within the considered time period (M times the spring-neap period) are so small that they do not significantly affect the hydrodynamics. The effect of this factor was therefore always verified at different stages of the simulation by running a similar model with smaller factors in parallel during certain time intervals. The values for the applied factors are indicated in Table 2.2 (Section 2.3).

The shallow-water equations were implemented on a staggered grid following *Stelling and Duinmeijer* (2003), with the only difference that the flow velocity in the water level points are approximated by a midpoint scheme (taking the average of the two faces; this gives a more accurate approximation of the flow velocities near the tidal front, compared with an upwind scheme).

2.2.2. Wave module

The wave module calculates the energy gain and loss (by shoaling and dissipation) over the model domain by the continuity equation for the wave energy flux (*Christoffersen*, 1985),

$$\frac{dE_f}{dx} = \frac{d}{dx}\left(\frac{1}{8}\rho_w g H^2 c_g\right) = -D_w,\qquad(2.11)$$

in which E_f is the wave energy, H the wave height, c_g the group velocity and D_w the energy dissipation. c_g is given by linear wave theory;

$$c_g = \frac{c_w}{2}\left(1 + \frac{2\kappa h}{\sinh(2\kappa h)}\right),\qquad(2.12)$$

in which c_w is the phase velocity:

$$c_w = \sqrt{\frac{g}{\kappa}\tanh(\kappa h)}.\qquad(2.13)$$

The wave number κ is related to the water depth and the wave period (see Table 2.1) via the dispersion relation according to linear wave theory (computed via a numerical iteration algorithm based on Newton's method).

The energy dissipation in the wave boundary layer can be related to the amplitude of the wave orbital velocity, U_δ, and the 'energy loss factor' f_e (*Justesen*, 1988; *Fredsoe and Deigaard*, 1992):

$$D_w = \frac{2}{3\pi} \rho_w f_e U_\delta^3. \tag{2.14}$$

U_δ is given by (*van Rijn*, 1993):

$$U_\delta = \frac{\pi H}{T \sinh(\kappa h)}, \tag{2.15}$$

The energy loss factor can be approximated by the wave friction factor (*Justesen*, 1988; *Fredsoe and Deigaard*, 1992), which is calculated by (*Swart*, 1976):

$$f_w = \min \left[\exp \left(-6 + 5.2 \cdot \left(\frac{A_\delta}{2.5 \cdot d_{50}} \right)^{-0.19} \right), 0.3 \right], \tag{2.16}$$

in which A_δ is the amplitude of the wave orbital excursion,

$$A_\delta = \frac{U_\delta}{\omega}, \tag{2.17}$$

with $\omega = 2\pi / T$ the wave angular velocity.

Furthermore, the change in wave height due to wave-breaking in the surf zone is taken into account by limiting the wave height H to a fraction f_r of the water depth h, i.e.

$$H = \min \left[H, f_r h \right] \tag{2.18}$$

This criterion is applied after the derivation of the wave height by Eq.2.11. Our results are produced with $f_r = 0.7$, but the model has been run for different fractions as well, ranging from 0.5 to 0.8. Although the distribution and the peak value of the wave energy on the flat are altered significantly by this parameter, this is not relevant for the concepts that are presented in this chapter.

The wave-induced skin friction is calculated by (*van Rijn*, 1993):

$$\tau'_{bw} = \frac{1}{4} \rho_w f_w U_\delta^2, \tag{2.19}$$

which is related to the wave height and water depth via Eq.2.15. The model does not account for any extra bed shear stress due to wave breaking induced turbulence. The continuity equation for the wave energy flux (given by Eqs.2.11 and 2.14) is discretizised by a simple first order forward difference scheme.

2.3. PARAMETERS AND BOUNDARY CONDITIONS

To run the model, several physical and numerical parameters have to be set (see Table 2.1 for an overview). One of the most uncertain parameters is the horizontal dispersion coefficient K. Following *Ter Brake and Schuttelaars* (2010) and *van Prooijen and Wang* (2013), we assume $K = 100 \, m^2 \, s^{-1}$, in order to empirically represent a number of mixing processes that cannot be resolved in a 1-D framework. Note that mixing does not only

occur due to (small-scale) turbulence, but also, for instance, by larger-scale flow patterns and circulations that result from irregularities in the 2-D bathymetry and geometry (*Fischer*, 1976; *Zimmerman*, 1976; *Geyer*, 1992). As we cannot include any of these underlying processes in a 1-D model, we account for their mixing effect by a dispersion term in Eq.2.4. The sensitivity to this parameter has been tested by a comparison with results for $K = 1\,m^2\,s^{-1}$ (Section 2.4).

Table 2.1: Settings for model parameters

parameter	value	description
w_s	$0.2 \cdot 10^{-3}$	Settling velocity (ms^{-1})
m_e	$5 \cdot 10^{-5}$	Erosion coefficient ($kgm^{-2}s^{-1}$)
τ_{cr}	0.1	Critical shear stress for erosion (Nm^{-2})
K	100	Dispersion coefficient ($m^2 s^{-1}$)
ρ_{dry}	900	Dry bed density (kgm^{-3})
d_{50}	30	Mean sediment diameter (μm)
T	2	Wave period (s)
H_0	0.2	Average wave height at the model boundary (m)
C_d	0.003	Drag coefficient (*Soulsby*, 1997)
$[T_{M2}, H_{M2}]$	[12.4167, 1.356]	M2 tidal constituent [period(hours),amplitude(m)]
$[T_{S2}, H_{S2}]$	[12, 0.6440]	S2 tidal constituent [period(hours),amplitude(m)]
dt	40	Time step (s)
dx	200	Grid size (m)

Since the evolution of the Yangtze tidal flats has our particular interest, many of the other parameters were chosen to correspond with the conditions in the Yangtze Estuary (*Hu et al.*, 2009; *Chu et al.*, 2010; *Shi et al.*, 2012). The sensitivity of the results to a limited amount of parameter variations has been tested (Section 2.4). Although the values of the model parameters influence the morphodynamic evolution for a given set of boundary conditions, they were found to have much less effect on the different types of solutions that can be found by varying the boundary conditions; our qualitative results are therefore valid for a rather wide range of parameter values.

Also boundary conditions have to be imposed. At the seaward boundary, the water level is described by a symmetric spring-neap tidal cycle:

$$\zeta(t) = H_{M2} \cdot \cos\left(\frac{2\pi}{T_{M2}}\, t\right) + H_{S2} \cdot \cos\left(\frac{2\pi}{T_{S2}}\, t\right), \tag{2.20}$$

in which H_{M2} and T_{M2} and H_{S2} and T_{S2} are the amplitude and period of the *M*2 and *S*2 harmonic constituents respectively (Table 2.1). The effect of an asymmetric tidal variation at the boundary on the equilibrium profile shapes and the long-term trends is captured by *Pritchard et al.* (2002). They found that a flood-dominant regime enhances the tendency of the flat to accumulate sediment and prograde, while an ebb-dominant regime leads to export of sediment and a retreating flat. Both types of asymmetries furthermore resulted in steeper cross-shore profiles compared with a symmetric tidal variation. In the current study we describe the dependencies of the state of the flat (stationary,
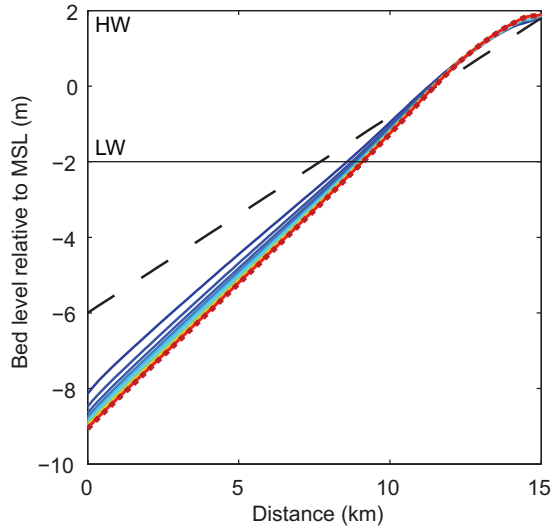
Figure 2.2: [Simulation $E1$, see Table 2.2] Evolution from an initial bathymetry (from the dashed black line, via the solid colored lines, towards the dotted red line), forced with tidal currents only and without suspended sediment at the boundary ($c_0 = 0 kg\,m^{-3}$) , plotted for a total time span of 240 years and time intervals of 40 years.

prograding or retreating) on the sediment availability and the wave climate in case of a symmetric tidal variation. However, the effect of the superharmonic $M4$ tide for the situation in the Yangtze Estuary (i.e. for ratio's between the amplitude of the $M4$ tide and the semi-diurnal tide of ≤ 0.2, as found by *Chu et al.* (2010)), was investigated. The inclusion of the $M4$ tide, tested for different phase lags, did not significantly affect our results.

Table 2.2: Simulation codes with boundary conditions and parameter values.

code	$c_0(kg\,m^{-3})$	waves (m)	$K(m^2 s^{-1})$	$w_s(m s^{-1})$	M
$E1$	0	no	100	$0.2 \cdot 10^{-3}$	50
$E2$	0.15	no	100	$0.2 \cdot 10^{-3}$	10
$E3$	0.05	0.2	100	$0.2 \cdot 10^{-3}$	20
$E4$	0.3	0.2	100	$0.2 \cdot 10^{-3}$	20
$E5$	$5 \cdot 10^{-4}$	0.2	1	$0.2 \cdot 10^{-3}$	20

At the same boundary, a constant value is imposed for the sediment concentration (i.e. tidal variation in the sediment concentration at the boundary is not taken into account; see Table 2.1 for the imposed values). During ebb tide the boundary concentration can influence the computation domain through dispersion. The wave height at the model boundary is set at each time step by a random draw from the Rayleigh distribution around a constant mean value (Table 2.1). At the landward boundary the flow velocity

is set equal to zero, representing a closed boundary (sea wall). The reflection of wind waves at the closed boundary is neglected.

The initial profiles are straight lines. The obtained steady profile shapes are independent of the initial shape and slope, but it is important that the initial profile is chosen not too high and steep (because the top of the intertidal range cannot easily erode once it is established). Systems with limited available space, on the other hand, will be the focus of Chapter 5.

2.4. Results

Tides Only - Stationary

The response of intertidal flats to a constant sediment concentration at their boundary is investigated for two different settings of the hydrodynamic forcing: (1) tidal currents only and (2) tidal currents plus wind waves. Furthermore, the simulations differ in the sediment concentration at the boundary. Each simulation is given a code as indicated in the caption of the figures, and an overview of the corresponding boundary conditions is given in table 2.2. For reasons of convenience, the time intervals and time spans indicated in the captions are rounded values. The exact timestep does always correspond with a whole number of tidal periods.

We first consider the simulations without wind waves. Figure 2.2 shows a simulation for a sediment concentration of 0 $kg\,m^{-3}$ at the boundary. Starting from a linear profile, the adjustment of the profile slope and shape is rapid in the first decades. After approximately 200 years, the flat is stable. At this stage, the (real-time) shear stresses on the profiles do not exceed the critical value for erosion ($\tau_{cr} = 0.1\,N\,m^{-2}$, Fig.2.3), so that there is no sediment transport.

Tides Only - Progradation

Also for a boundary concentration of 0.15 $kg\,m^{-3}$, the adjustment of the profile slope and shape is rapid in the first decades (Fig.2.4). In this case, the intertidal flat evolves into a state of steady progradation. Roughly three phases can be distinguished in this simulation, indicated by $P1 - P3$ in Panel B of Fig.2.4:

1. Within the first few decades, the slope and shape adjusts from an initial profile to a relatively stable shape. Hence the initial erosion of the lower flat, which steepens the profile before accretion starts to dominate everywhere on the flat.

2. A longer period follows in which accretion is mainly translated into a horizontal progradation.

3. The shape changes significantly when the intertidal area (above MSL $-2m$ in the figure) reaches the model boundary. This phase is physically irrelevant, since long-shore processes (which we neglect) will be dominant if the intertidal flat approaches the model boundary (note that the boundary represents the conditions in a tidal channel, see Sec.2.2.1).

The tide-averaged gross erosion and deposition fluxes (Fig.2.5A) have a maximum at the boundary and decrease towards the top of the flat. The concentration field in
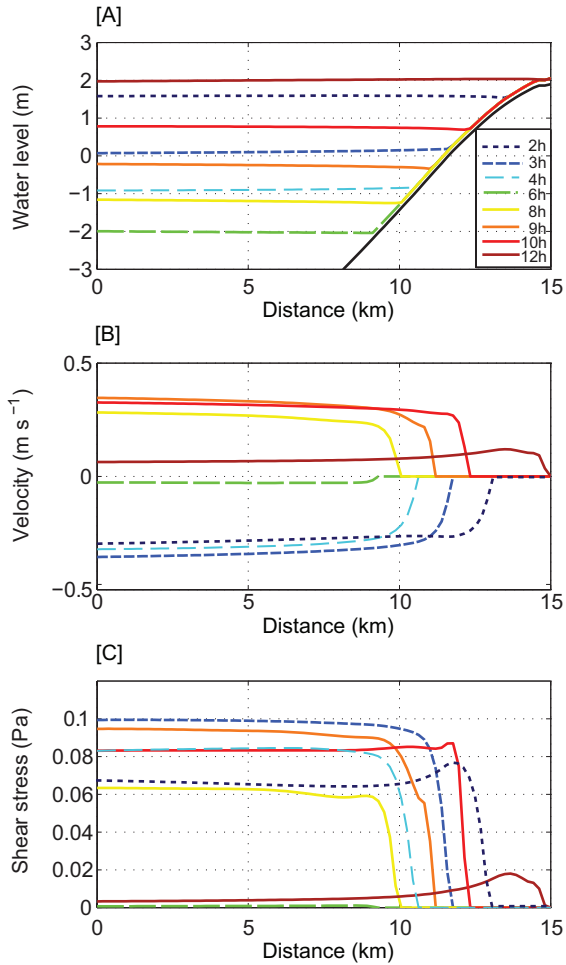
Figure 2.3: [Sim.E1] Water levels (Panel A), flow velocities (Panel B) and shear stressess (Panel C) at different moments during a tidal cycle (at spring tide) on the equilibrium profile after 240 yrs of morphodynamic evolution under influence of tidal currents only and $c_0 = 0 kg\, m^{-3}$, i.e. on the dotted red profile in Fig.2.2.

Figure 2.4: [Sim.*E*2] (A) Evolution from an initial bathymetry (from the dashed black line, via the colored lines, towards the red line), in case of tides only and $c_0 = 0.15\,kg\,m^{-3}$. The total time span is 160 yrs with plotting time steps of 10 yrs. The gray horizontal lines refer to the bed levels of the lines in panel B. (B) Distance towards the open boundary against time for different bed levels in the intertidal zone. Straight lines indicate that the progradation speed is constant in time (constant celerity). Parallel lines indicate a pure horizontal shift (uniform celerity). Convergence or divergence of the lines indicate shape changes. At a relative short time scale, the flat evolves into a prograding system in which the shape is largely maintained and the progradation speed is constant in time (phase 2).
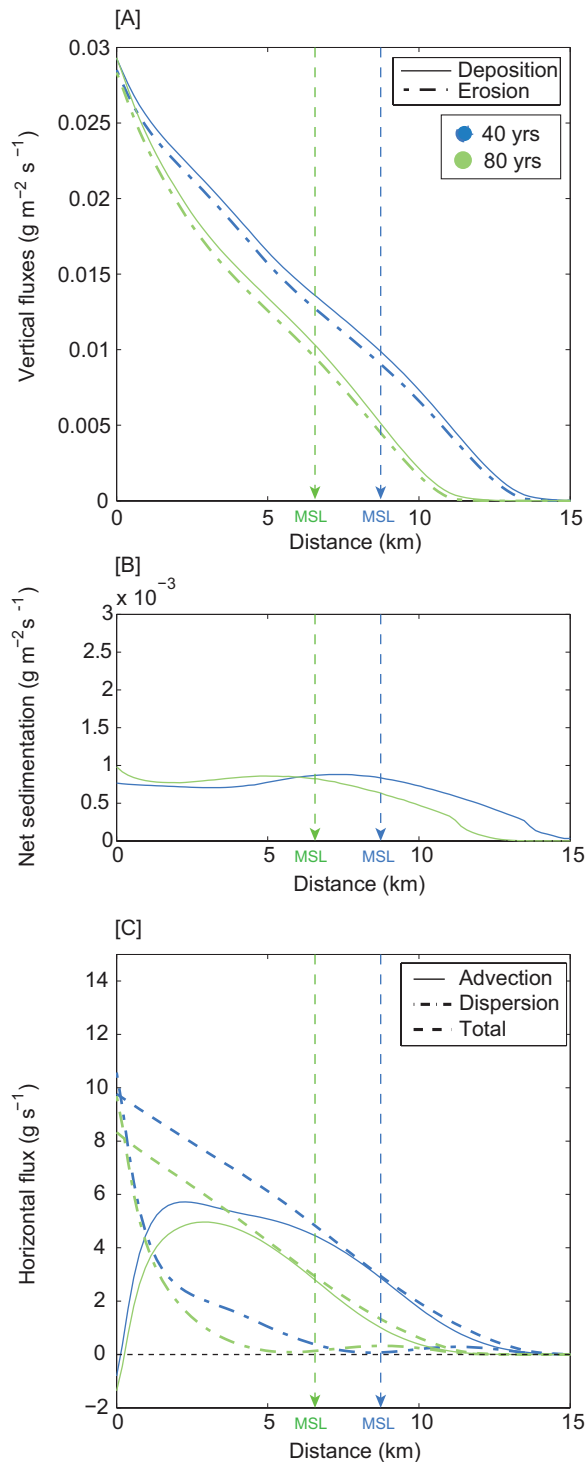
Figure 2.5: [Sim.*E*2] Tide-averaged sediment fluxes over the developing flat of Fig.2.4 after 40 yrs (dark blue) and 80 yrs (light green) of evolution, i.e. correponding with the thick dark blue and light green profiles in Fig.2.4A resp. (A) Deposition and erosion fluxes. (B) Net sedimentation. (C) Horizontal advection and dispersion fluxes. Landward is defined positive.

the intertidal domain does not clearly depend on the distance to the model boundary (Panel A; note that the deposition is directly proportional to the concentration, Eq.5.2) and shifts together with the bed during Phase 2. In the closer vicinity of the boundary, however, the concentration field gets influenced by the decreasing distance.

The sedimentation rates are much smaller than the gross erosion and deposition fluxes (compare Panel A and B). An exact balance is however not reached: the tide-averaged sedimentation rates remain of the same order of magnitude throughout the steady progradation stage. Horizontally, advection is the dominant process over most of the flat (Fig.2.5C). Both the advection and dispersion fluxes induce a landward sediment transport, i.e. in the direction down the tide-averaged concentration gradient (compare Panels A and C).

TIDES & WIND WAVES - RETREAT

Subsequently, we consider the simulations with wind waves. For $0.05\,kg\,m^{-3}$ at the open boundary, a long-term erosive state develops (Fig.2.6). The uppermost part of the tidal range fills up in the very early stage of the evolution (within the first decades), so that a bank is formed at the top. A stationary equilibrium state is reached eventually, but only after a large part of the intertidal area is eroded away (see Fig.2.6). During the erosive stage, the cross-shore shape of the profile (excluding the top), is largely maintained, as can be seen from the parallel lines in Fig.2.6B. The maintenance in cross-shore shape implies that the whole intertidal flat, except for the top, retreats landward (henceforth we will therefore refer to this state as 'retreating', despite the fixed position of the bank).

The tide-averaged gross erosion and deposition fluxes have a wave-induced maximum on the intertidal flat and the peaks shift landward with the migration of the flat (Fig.2.7 A, i.e. the concentration field in the intertidal domain is independent of the distance to the boundary). Note that the maximum of the tide-averaged fluxes is determined by a combination of (1) the magnitude of the bed shear stresses during the period in which a section is underwater (which increases with increasing bed elevation due to maximum wave-induced bed shear stress in very shallow waters, see Panel A and C of Fig.2.8) and (2) the period in which the section is underwater (which decreases with increasing bed elevation).

The net sedimentation rates are small, but do not significantly decrease during the state of gradual retreat (Panel B of Fig.2.7).

Horizontally, the gross landward advection and dispersion terms are of similar magnitude, but of opposite direction (Fig.2.7C). The tide-averaged dispersion flux is seaward over almost the entire intertidal flat, indicating that the real-time concentration is (generally) maximal close to the tidal front (i.e. at every moment in time the concentration gradient drives a seaward dispersion flux). This is in accordance with Fig.2.8, which shows sharp peaks in the instantaneous wave-induced bed shear stresses close to the tidal front (Panels A and C of Fig.2.8) that drive the instantaneous dispersion fluxes (see Panel E in Fig. 2.8). The tide-averaged advection flux, on the other hand, is landward over the intertidal area, but seaward on the lower (subtidal) flat. The net transport is seaward during the period of long-term retreat, indicating a predominance of dispersion processes on the intertidal flat. In the stationary equilibrium state, a net horizontal sediment transport remains over every tidal cycle. Over multiple tidal cycles the net transport balances out, so that the bed level remains steady in the long run.
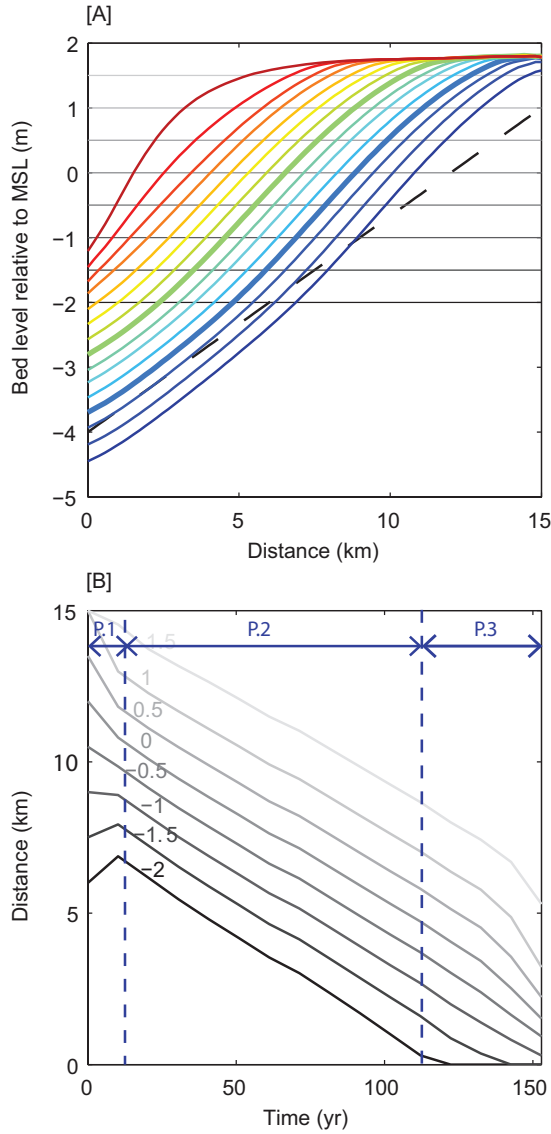
Figure 2.6: [Sim.$E3$] (A) Evolution from an initial bathymetry (from dashed black, via solid colored, towards dotted red) in case of tides and wind waves ($0.2m$) and a suspended sediment concentration at the boundary of $0.05kg$ m^{-3}. The total time span is 600 yrs with steps of 40 yrs. In the last 200 years the bathymetry (red line) did not change any longer. (B) Distance towards the open boundary against time for different bed levels in the intertidal zone. Straight lines indicate a constant celerity. Parallel lines indicate an uniform celerity. Convergence or divergence of the lines indicate shape changes. The intertidal flat below the top part shifts horizontally with a stable cross-shore profile.
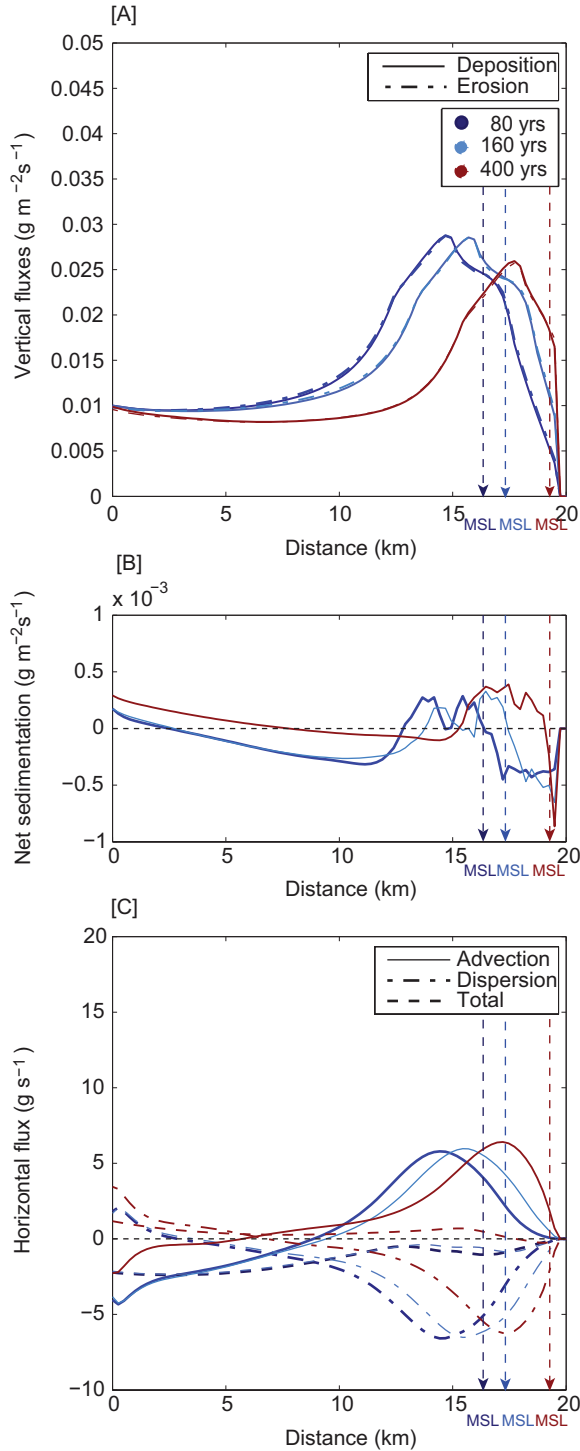
Figure 2.7: [Sim.*E*3] Tide-averaged sediment fluxes over the developing flat of Fig.2.6 after 80 yrs (dark blue) and 160 yrs (light blue) and over the equillibrium state after 400 yrs of evolution (dark red).(A) Deposition and erosion fluxes. (B) Net sedimentation. (C) Horizontal advection and dispersion fluxes. Landward is defined positive.

2
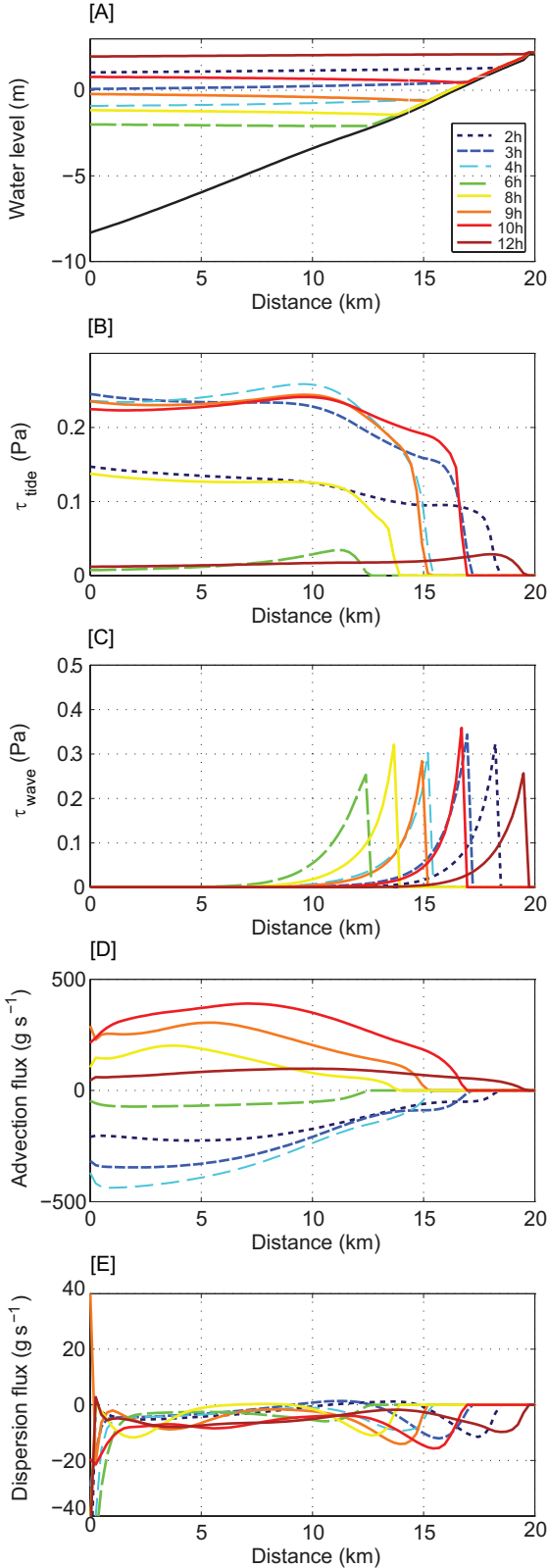
Figure 2.8: [Sim.*E*3] Water levels (Panel A), tide- and wave-induced bed shear stresses (Panels B and C) and horizontal fluxes (Panels D and E) at different moments within a tidal cycle (during spring tide) on a profile that is obtained after 80 yrs of morphodynamic evolution under influence of tidal currents and wind waves and $c_0 = 0.05 kg\ m^{-3}$, i.e. on the thick dark blue profile in Panel A of Fig.2.6. In order to better compare the wave-induced force at different elevations, a constant wave height at the boundary has been chosen ($H_0 = 0.2m$), instead of the random draw from the Rayleigh distribution that has been used for the morphodynamic calculations.

TIDES & WIND WAVES - PROGRADATION

For a sediment concentration at the boundary of $0.3\, kg\, m^{-3}$, a state of steady prograda-
tion develops within a few decades, see Fig.2.9. The action of wind waves results in local
maxima in the tide-averaged gross erosion and deposition fluxes (and hence in the con-
centration) on the intertidal flat. These shift seaward as the flat prograde s (Fig.2.10A).
The maximum concentration is, however, found at the model boundary. In Panel B of
Fig.2.10 we see once more that the sedimentation rates in the prograding state are small
compared with the gross deposition and erosion fluxes, but the differences are persistent
(i.e do not decrease in time). The horizontal sediment transport is mostly dominated by
advection, which induces a landward transport (Fig.2.10C). Dispersion gives a negative
(seaward) contribution over a large part of the intertidal flat. When the intertidal flat
approaches the model boundary closely, the profile steepens and a stationary equilib-
rium state is reached. Due to the proximity to the channel (in which long-shore currents
dominate), the relevance of this state is questionable.

VARIATION OF THE DISPERSION COEFFICIENT

To test the sensitivity of the results to the dispersion coefficient, the experiments were
repeated with $K = 1\, m^2\, s^{-1}$. Only little sensitivity to such a variation was found for high
boundary concentrations (i.e. boundary concentrations that result in prograding pro-
files for $K = 100\, m^2\, s^{-1}$). This will be demonstrated and further discussed in Chapter
3.

For lower boundary concentrations (that result in retreat for $K = 100\, m^2\, s^{-1}$), the state
of the flat (progradation or retreat) was found to depend critically on the dispersion co-
efficient. For a concentration of $0.05\, kg\, m^{-3}$ and a dispersion coefficient of $K = 1\, m^2\, s^{-1}$,
the dispersion flux is negligible. Under influence of a net landward advection flux, a
prograding state is established (opposed to the retreating state in Fig.2.6).

In order to determine the conditions for which a state of long-term retreat is estab-
lished for $K = 1\, m^2\, s^{-1}$, the boundary concentration was lowered systematically. For a
concentration of $C_0 = 5 \cdot 10^{-3}\, kg\, m^{-3}$, a prograding state is established with a progra-
dation speed of $2\, m\, yr^{-1}$. For $C_0 = 5 \cdot 10^{-4}\, kg\, m^{-3}$, a retreating state was found for the
first time, see Fig.2.11. Note that the relative difference between the gross erosion and
deposition flux is very small (they are even indistinguishable in Fig.2.12A). Small net ero-
sion rates and seaward transport, however, remain during the simulation (Fig.2.12C,D);
in the very long run this intertidal flat is found to be erosive. Note furthermore that the
role of the dispersion flux in the horizontal transport over the intertidal area is significant
(Fig.2.12C), despite the low dispersion coefficient. These results show that net seaward
transport within the intertidal domain only occurs via the dominance of the dispersion
flux, even for small dispersion coefficients (in case of a symmetrical tidal variation at
the model boundary). On the sub-tidal flat, where the real-time concentration gradients
are smaller, the transport is totally determined by (net seaward) advection (in case of a
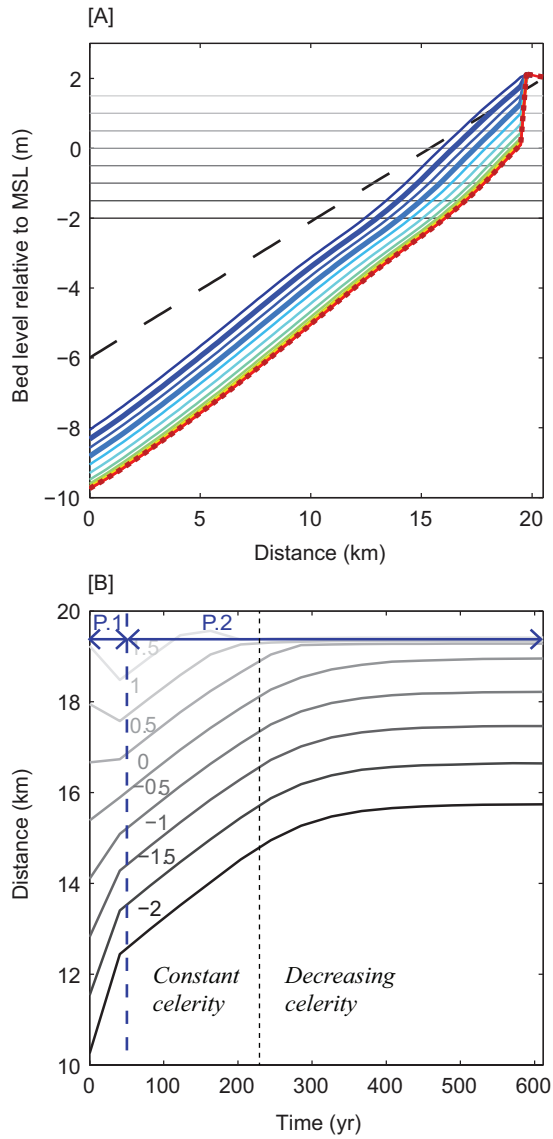symmetric spring-neap tidal cycle).
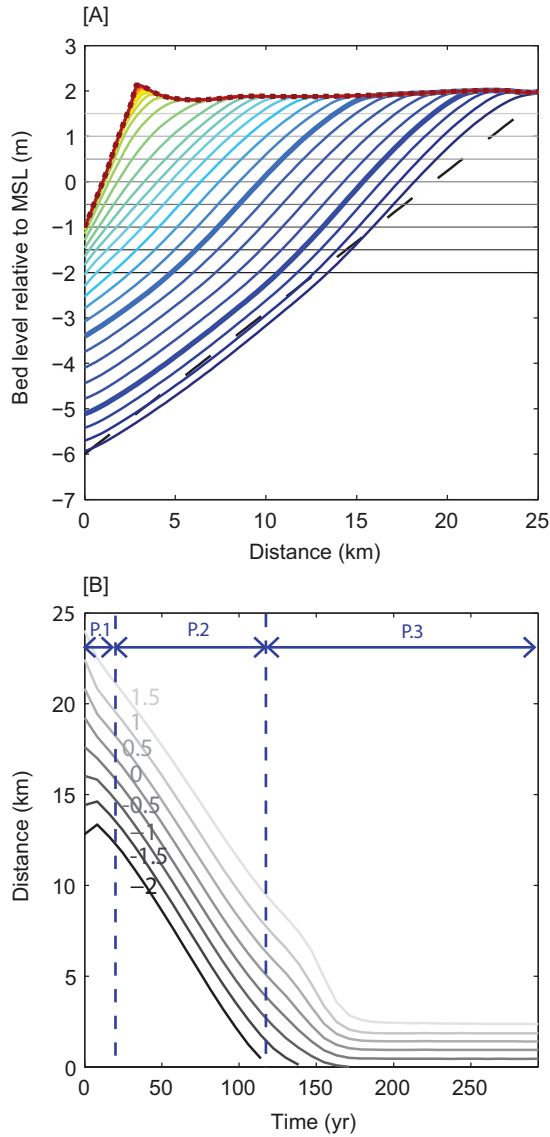
Figure 2.9: [Sim.E4] (A) Evolution from an initial bathymetry (from dashed black, via solid colored, towards dotted red), under influence of tides and wind waves and $c_0 = 0.3 kg\ m^{-3}$. The total time span is 280 yrs, with plotting time steps of 8 yrs. The gray horizontal lines refer to the bed levels of the lines in panel B. (B) Distance towards the open boundary against time for different bed levels in the intertidal zone. Straight lines indicate a constant celerity. Parallel lines indicate an uniform celerity. Convergence or divergence of the lines indicate shape changes. At a relative short time scale, the flat evolves into a prograding system in which the shape and progradation speed is largely maintained (phase 2).
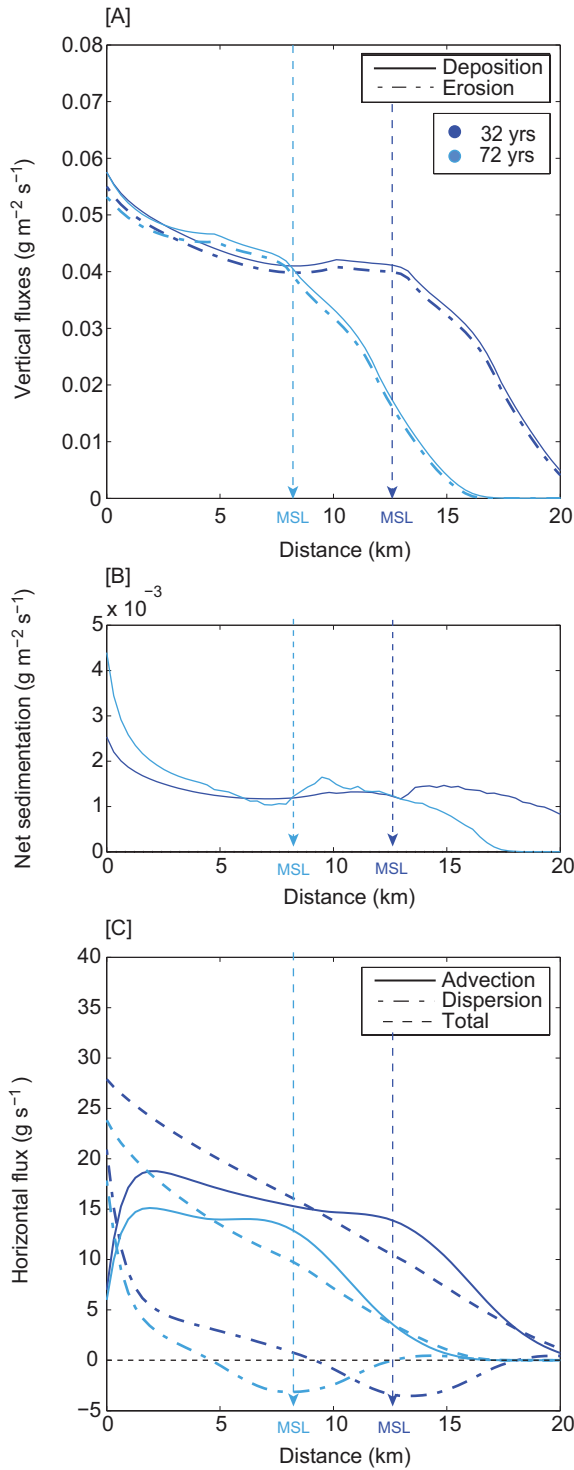
Figure 2.10: [Sim.*E*4] Tide-averaged sediment fluxes over the developing flat of Fig.2.9 after 32 yrs (dark blue) and 72 yrs (light blue) of evolution (i.e. on the thick lines with corresponding color in Fig.2.9).(A) Deposition and erosion fluxes. (B) Net sedimentation. (C) Horizontal advection and dispersion fluxes. Landward is defined positive.
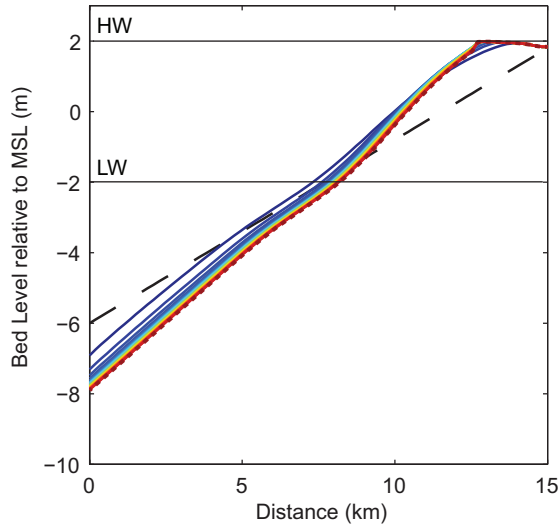
Figure 2.11: [Sim. $E5$] Evolution from an initial bathymetry (from the dashed black line, via the solid colored lines, towards the dotted red line) in case of tides and waves, a suspended sediment concentration at the boundary of $5 \cdot 10^{-4} \, kg \, m^{-3}$ and a dispersion coefficient of $K = 1 \, m^2 \, s^{-1}$. Time steps between two successive lines is 40 yrs and the total time span is 840 yrs.

2.5. DISCUSSION

2.5.1. HORIZONTAL MIGRATION

Our results show that an equilibrium state is generally not (directly) reached. A stationary state can only develop in the following cases:

- Waves are absent and the sediment concentration is zero at the boundary, in which case the bed shear stresses fall under the critical value for erosion. Such a stationary state for $C_0 = 0 \, kg \, m^{-3}$ was also found by *Pritchard et al.* (2002).

- In some cases an equilibrium state is reached eventually after a period of long-term erosion and the formation of a sharp transition towards the top of the intertidal domain (see Fig. 2.6).

More general, a state of long-term progradation or retreat develops. The steady progradation obtained for a symmetric tide at the boundary and in the absence of wind waves is in agreement with the findings of *Pritchard et al.* (2002), *Waeles et al.* (2004) and *Le Hir et al.* (2007). The horizontal migration of intertidal flats in the presence of wind waves has been produced before by *Mariotti and Fagherazzi* (2010) and *Tambroni and Seminara* (2012), while *Waeles et al.* (2004) noted that it depends on the typical wave regime whether a flat migrates horizontally or reaches a stationary equilibrium state. The dependency of the state (progradation or retreat) on the sediment supply (in the presence of wind waves) is in accordance with the studies by *Mariotti and Fagherazzi* (2010) and *Tambroni and Seminara* (2012), that both discuss the importance of the amount of sediment supply in combination with the rate of sea-level rise.

Figure 2.12: [Sim.*E*5] Tide-averaged sediment fluxes over the developing flat of Fig.2.11 after 840 yrs of evolution. (A) Gross deposition and erosion fluxes (these are hardly distinguishable in this plot). (B) Net sedimentation. (C) Horizontal advection and dispersion fluxes. Landward is defined positive.

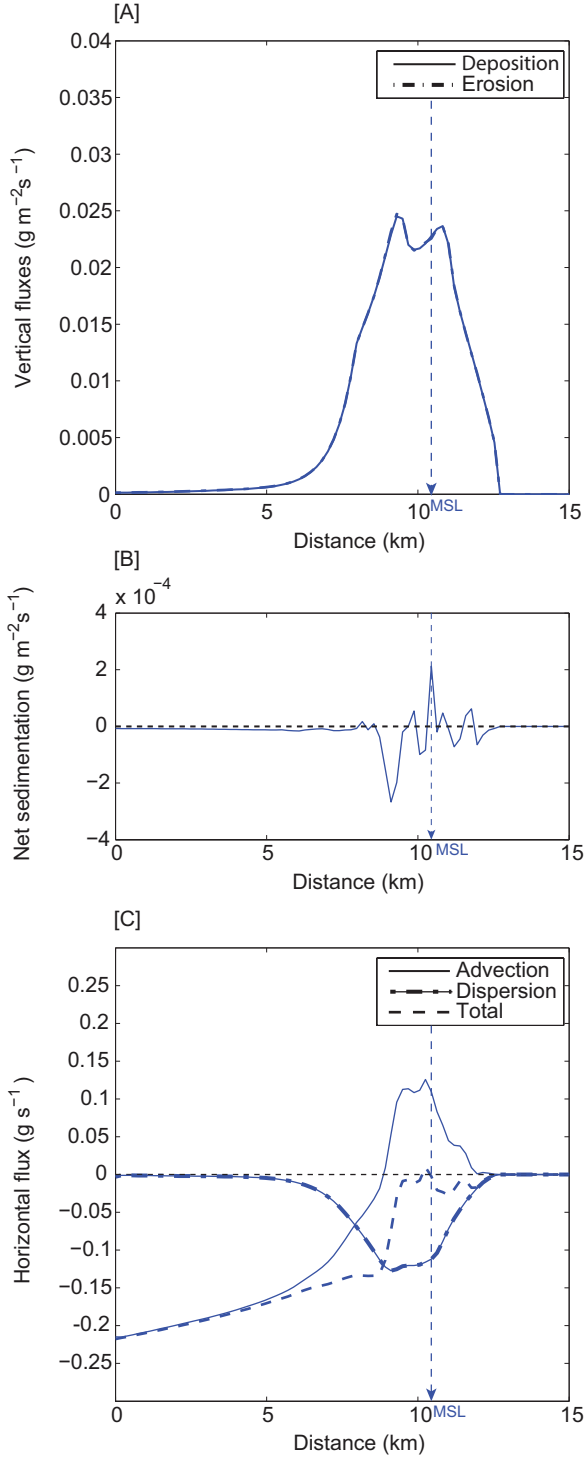To understand the long-term evolution of intertidal flats and the reason why they do not (directly) approach a stationary equilibrium state (on the typical timescale at which the profile shape can adjust), we specify and distinguish the mechanisms which work in favor of such an equilibrium state from those working against it. For the explanation that follows, we first consider an initially accretive intertidal system with a constant sediment concentration at the seaward boundary. This implies that there is a net inflow of sediment and the elevation of the flat is increasing in time. Because the sediment concentration at the boundary is assumed to be constant, an equilibrium state could be approached mainly via an increase of the (tide-averaged) erosion over the intertidal flat, which would reduce the gradient in the seawards-increasing concentration and the net inflow (via both advection and dispersion) of sediment. Hence, the question is whether an increase of the elevation of the flat leads to an increase (favoring equilibrium) or a decrease (resisting equilibrium) of the bed shear stresses on the flat. We will analyze this 'morphodynamic feedback' for (1) tidal currents only, and (2) tidal currents plus wind waves.

Furthermore, in order to understand the stable profile shape of prograding and retreating tidal flats, it is necessary to distinguish different sections of the intertidal area and to consider (1) for each section the 'local morphodynamic feedback' (i.e. the effect of a local bed level change on the local imbalance), as well as (2) the morphodynamic feedbacks between the different sections (i.e. the feedback between a local bed level change and the surrounding tidal flat). In our analyses we assume that local imbalances between the deposition an erosion fluxes are affected (i.e. diminished or intensified) by the local bed level mainly via the erosion flux. This implies that the effect of a bed level change on the deposition flux is assumed to be relatively small. Note that the suspended sediment concentration (to which the deposition flux is linearly related via w_s) is determined by the space-and time-integrated deposition and erosion fluxes. Due to settling lag and scour lag effects, the local deposition flux depends on the erosion and deposition rates on the surrounding tidal flat and is therefore assumed to be less controlled by the local bed level than the local erosion flux.

2.5.2. Underlying Feedbacks - Tides Only

We first consider the situation without wind waves. The cross-shore tidal current velocity on the flat at a certain location and time can be approximated by (*Friedrichs and Aubrey*, 1996):

$$u(x) = \frac{1}{\beta} \frac{d\zeta}{dt},\tag{2.21}$$

where β is the average bed slope from position x towards the position of the tidal front and $\zeta(t)$ the water level (in this derivation assumed to be homogeneous, i.e. uniform over the width of the tidal flat).

For a high concentration at the model boundary, net sedimentation will in first instance be most pronounced on the subtidal and lower intertidal flat, closest to the model boundary (note that the higher flat is too far away to receive sediment directly from the model boundary). On these sections, maximum currents are found during the maximum rate of water level variation and can be approximated by (*Friedrichs and Aubrey*,

1996; *Le Hir et al.*, 2000):

$$u(x) = \frac{\pi R}{\beta T_{tide}}, \tag{2.22}$$

where β is now the average bed slope from position x towards the tidal front at mean sea level, T_{tide} the tidal period and R the tidal range. An increase in the bed level on the subtidal and lower flat would decrease the slope towards the tidal front over the whole period in which the bed is submerged, including the period of maximum tidal current. This would increase the tidal flow velocities, shear stresses and the gross erosion flux over the period in which a section is underwater. This indicates a negative (stabilizing) feedback loop between the local bed level and the hydrodynamic forces: the erosion and deposition fluxes approach a local balance. Due to this negative feedback mechanism, the slopes on the lower tidal flat stabilize within the first decades of the evolution (see Figs.2.4, 2.6 and 2.9), although an exact balance on the lower flat cannot completely be reached before the upper intertidal flat is in balance (because the bed shear stresses are influenced by the upper intertidal flat morphology). At the same time, the increased erosion rates on the lower flat result in an increase in the sediment supply towards the higher sections.

As stated above, a rise in the bed level decreases the slope towards the tidal front over the whole period in which a location is submerged. This effect locally increases the bed shear stresses. However, on the higher sections of the intertidal area, an additional effect dominates the local morphodynamic feedback: Above mean sea level, the time derivative of the water elevation (factor $\frac{d\zeta}{dt}$ in Eq.2.21), during the period in which a section is underwater, decreases with increasing elevation. The most rapid decay of $\frac{d\zeta}{dt}$ occurs on the highest part of the tidal flat, assuming a sinusoidal water level variation in time. On the higher flat, an ascending bed level therefore leads to the exclusion of a period of maximum erosion rates. Hence, a rise in the bed level on this section is expected to cause a decrease in the erosion rates during the period in which a section is underwater. This implies that, once the supply towards the upper flat is abundant (and remains constant), there is no mechanism to increase the local erosion rates. As a result, sediment will accumulate on the upper part of the intertidal profile.

Different sections of the profile do not, however, evolve independently of each other: sedimentation on the upper intertidal flat increases the slopes from the lower flat towards the top of the flat (i.e. increase β in Eqs.2.21 and 2.22) and hence decreases the tidal shear stresses on the lower sections: sedimentation on the upper flat will induce further seaward sedimentation. Because the local feedback loop on the lower flat favors local equilibrium, the slopes over the lower flat are continuously restored while the upper flat accretes. In this way, the flat shifts horizontally while the cross-shore shape, concentration gradients and sediment transport over the flat are conserved: a stationary balance cannot be established. Fig.2.13 outlines this concept.

Conversely, a state of long-term retreat, in which the flat retreats landward while the cross-shore shape is maintained, is to be expected in case of an erosive upper flat in combination with a 'stable' lower flat: erosion on the upper intertidal flat would increase the tidal current velocities, bed shear stresses and erosion rates on the lower sections and therefore induce a state of long-term retreat (i.e. the opposite of the situation in

2
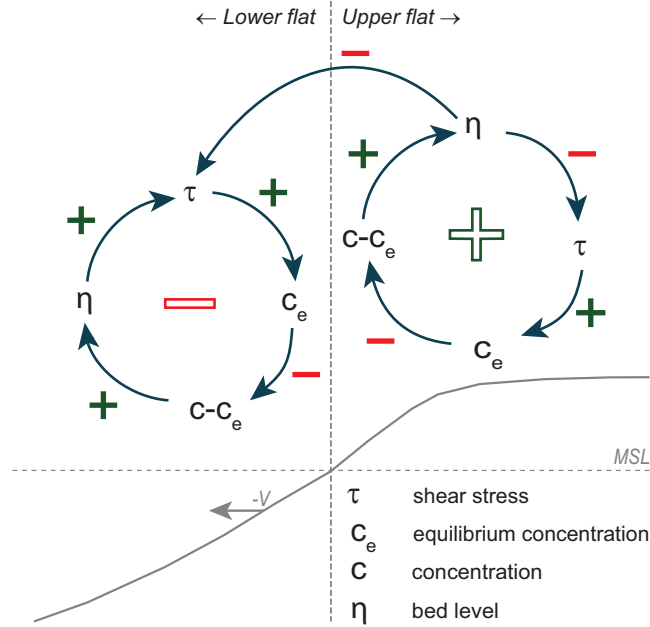
Figure 2.13: Feedback loops on a 'tide controlled' flat. The arrows with positive and negative signs indicate positive and negative influences inbetween the parameters resp. An uneven number of negative influences within a loop results in a balancing feedback loop, whereas an even number of negative influences within a loop results in a reinforcing feedback loop. The bed level on the lower flat is controlled by a balancing feedback loop, i.e. if the depositon flux is initially larger than the erosion flux, i.e. $c - c_e > 0$, net sedimentation occurs and the bed level rises, resulting in locally larger tidal flow velocities and bed shear stresses, which diminishes the initial imbalance. The bed level on the higher flat is controlled by a reinforcing feedback loop; an initial imbalance is amplified, because a rise (decay) in the bed level results in smaller (larger) tidal flow velocities and smaller (larger) shear stresses on the bed. At the same time, a rising upper flat reduces the tidal flow and shear stresses on the lower flat (indicated by the arrow with negative sign inbetween the loops), resulting in a migration of the whole flat.

the foregoing paragraph). We could however not find such a state in case of tides only. The tidal flow velocities and shear stresses generally decrease towards the shore, which favors a net landward sediment transport (see Section 2.5.4).

2.5.3. Underlying Feedbacks - Tides & Wind Waves

Also in the presence of wind waves, the system generally converges to migrating states (long-term coastal progradation or retreat). This tendency indicates a persistent imbalance on the upper flat and a general dominance of the cross-shore tidal current on the lower sections (explaining the horizontal shift). The remaining imbalance on the upper shore can be explained by the limited dependency of the wave-induced bed shear stress on the bed level (this dependency is much smaller than that of the cross-shore tidal current). Because maximum wave-induced bed shear stresses occur close to the tidal front, i.e. in very shallow waters (see Fig.2.8), a section within the tidal domain will experience maximum wave-induced bed shear stresses, independent of the precise bed elevation. Hence, a strong stabilizing feedback loop between the wave-induced bed shear stress and the local bed level is not present. Hence, depending on the specific wave climate and sediment supply, the upper shore is accretive or erosive, resulting in respectively seaward progradation or landward retreat.

Only after an eventual development of a steep transition towards the top of the intertidal range, could an equilibrium state be found (Fig.2.2). On such a configuration, the advection flux converges locally in front of the steep transition. When the transition deepens, the converging flux increases. Hence, a stabilizing feedback loop can be expected between the height of the steep transition and the local deposition in front of this transition. If cliff erosion would play a role, however, continuous retreat can be expected. *Mariotti and Fagherazzi* (2010) used a finer spatial resolution and included a formulation for cliff erosion. Their results suggest that the development of a cliff results in a state of horizontal retreat of the whole profile. This has also been suggested by *Zhao et al.* (2017).

2.5.4. Progradation or Retreat?

Once a stable profile shape is established, the long-term trend can be determined from the direction of the net sediment transport (which is maintained during the stage of steady migration, under the assumption of a constant boundary concentration). Let us now consider the mechanisms that drive these horizontal fluxes.

The tidal flow velocities generally decrease towards the shore (see Section 2.5.2). In the absence of wind waves, this determines the real-time concentration gradients. The real-time dispersion flux, as well as its time-integral, is therefore landward. Decreasing tidal flow velocities and sediment concentrations towards the shore, in combination with settling and scour lag effects, also favor a net landward advection flux (*van Straaten and Kuenen*, 1958). The dominance of the landward advection flux (over the seaward advection flux during ebb) is further enhanced by a larger settling lag in deep water than in shallow water. Note that the sediment that is eroded on the lower flat, typically in larger water depths, stays in the water column for a longer time than sediment that is eroded on the (upper) intertidal flat (in shallower waters). Hence, it travels longer horizontal distances before it settles again. Also see the discussion on the effects of settling and

scour lag provided by *Pritchard et al.* (2003).

In the presence of wind waves, on the other hand, maximum bed shear stresses and erosion rates occur on the intertidal flat. Because at each moment in time the maximum bed shear stresses occur close to the tidal front (where water depths are small, see Fig.2.8), a real-time concentration gradient is generated, which effectively drives a seaward dispersion flux of the eroded sediment (see Fig.2.8 for the real-time and Figs.2.7 and 2.10 for the tide-averaged wave-induced dispersion flux). The wave-induced concentration peaks on the intertidal flat will also enhance the advection flux during ebb and could alter the direction of the net advection flux. However, because the concentration peaks occur in very shallow water, the sediment settles fast again after erosion (i.e. the depth-induced tidal asymmetry is still in favor of a net landward advection flux). Note that our results indicate a generally landward advection flux over the intertidal area, even in the presence of wind waves and concentration peaks on the intertidal flat (Figs.2.7, 2.10 and 2.12). States of steady retreat are then associated with a dominant seaward dispersion flux over the intertidal flat (Figs.2.7 and 2.12). In case of an ebb-dominant tidal asymmetry at the model boundary, however, a net seaward advection flux would be feasible and the dispersion flux could be less relevant.

2.5.5. Technical implications
The influence of the upper intertidal flat morphology on the tide-induced bed shear stresses on the lower intertidal flat implies that the progradation speed of the flat can be influenced by engineering activities on the upper tidal flat. Artificial measures that favor deposition on the upper tidal flat, such as placing wave-breakers or extra vegetation, would also affect the deeper parts and increase the progradation speed of the whole flat. Based on our model results, one could furthermore expect that the construction of a sea dike on the higher flat would decrease the cross-shore tidal flow velocities on the lower sections and induce further seaward sedimentation (i.e. favor coastal expansion). It should however be mentioned that the inclusion of additional processes in the model could alter the dominant feedback mechanisms. In case of a large vegetation cover, biomorphodynamic feedbacks will play an important role (*Mariotti and Fagherazzi*, 2010; *Zhao et al.*, 2017). These, and the effects of wave reflection, should be included for determining the effect of a sea dike (which would influence the salt marsh dynamics).

2.6. Conclusions
This study confirms that intertidal systems that are controlled by cross-shore tidal currents, or a combination of cross-shore tidal currents and wind waves, generally converge to horizontally migrating 'steady states', in which the cross-shore profile is maintained, as shown before by *Pritchard et al.* (2002).

The occurrence of these states is explained by the feedback mechanisms between the hydrodynamic forces and the intertidal flat morphology. A negative feedback loop tends to stabilize the profile slope and shape within the first decades of the evolution. However, this stabilizing feedback loop falls short on the upper flat.

If tidal currents act alone, the upper part of the profile is found to be accretive. This

can be explained by the sharp decrease in the hydrodynamic forces towards this section and a strong effect of tidal asymmetry. The net accretion on this section influences the balances on the lower sections and drives the long-term horizontal migration.

Also in the presence of wind waves, the system generally converges to migrating states (long-term coastal progradation or retreat). This tendency indicates a persistent imbalance on the upper flat and a general dominance of the cross-shore tidal current on the lower sections (explaining the horizontal shift). Because maximum wave-induced bed shear stresses occur close to the tidal front, i.e. in very shallow waters (see Fig.2.8), any section within the intertidal domain will experience maximum wave-induced bed shear stresses, independent of the precise bed elevation. Hence, a strong (stabilizing) feedback loop between the wave-induced bed shear stress and the local bed level is not present. Depending on the specific wave climate and sediment supply, the upper shore is accretive or erosive, resulting in respectively seaward progradation or landward retreat.

The kind of steady states that can be approached is characteristic for the underlying hydrodynamic forces and the morphodynamic feedback mechanisms. Our results only describe the behavior of wide flats that are dominated by cross-shore tidal currents and wind waves. This work can be seen as supplementary to the work of *Fagherazzi et al.* (2006), for instance, which describes the internal feedbacks on intertidal platforms that are controlled by locally generated wind waves only. These systems were found to converge to stationary equilibrium states. In both cases, the local morphodynamic feedback loops reveal the long-term evolution of the intertidal flat.

REFERENCES

Ariathurai, C.R. (1974), A finite element model for sediment transport in estuaries, Ph.D.Thesis. University of California, Berkeley, USA.

Christoffersen, J.B. and I.G. Jonsson (1985), Bed friction and dissipation in a combined current and wave motion, *Ocean Engineering*, *12*(15), 387-423, doi:10.1016/0029-8018(85)90002-2.

Chu, A., Z.B. Wang, H.J. De Vriend, M.J.F. Stive (2010), A process-based approach to sediment transport in the Yangtze Estuary, *Conference on Coastal Engineering*, Shanghai, China, Published by the Coastal Engineering Research Council, Available at: http://journals.tdl.org/icce/index.php/icce/article/view/1387/pdf_352.

De Swart, H.E. and J.T.F. Zimmerman (2009), Morphodynamics of Tidal Inlet Systems, *Annual Review of Fluid Mechanics*, *41*(1), 203-229, doi:10.1146/annurev.fluid.010908.165159.

De Vriend, H.J., M. Capobianco, T. Chesher, H.E. de Swart, B. Latteux and M.J.F. Stive (1993), Approaches to long-term modelling of coastal morphology: a review, *Coastal Engineering*, *21*, 225-269, doi:10.1016/0378-3839(93)90051-9.

Dyer, K.R. (1998), The typology of intertidal mudflats, in Sedimentary Processes in the Intertidal Zone, K.B. Black, D.M. Paterson, and A. Cramp (Eds), Geol. Soc., London, Spec. Publ., *139*, 11-24, doi:10.1144/GSL.SP.1998.139.01.02.

Eelkema, M., Z.B. Wang, A. Hibma and M.J.F. Stive (2013), Morphological effects of the Eastern Scheldt storm surge barrier on the ebb-tidal delta, *Coast. Eng. J.*, *55*(3), doi: 10.1142/S0578563413500101.

Fagherazzi, S., L. Carniello, L. D'Alpaos, and A. Defina (2006), Critical bifurcation of shallow microtidal landforms in tidal flats and salt marshes, *Proc. Natl. Acad. Sci. U.S.A.*, *103*(22), 8337-8341, doi:10.1073/pnas.0508379103.

Fagerazzi, S., C. Palermo, M.C. Rulli, L. Carniello and A. Defina (2007), Wind waves in shallow microtidal basins and the dynamic equilibrium of tidal flats, *J. Geophys. Res.*, *112*, F0204, doi:10.1029/2006JF000572.

Fischer, H.B. (1976), Mixing and dispersion in estuaries, *Annual Review of Fluid Mechanics*, *8*, 107-133, 10.1146/annurev.fl.08.010176.000543.

Flemming, B.W. (2002), Geographic distribution of muddy coasts, In *Muddy Coasts of the World*, T. Healy, Y. Wang and J.-A. Healy (eds.), Elsevier, 99-201.

Fredsoe, J. and R. Deigaard (1992), *Mechanics of coastal sediment transport*, World Scientific, Singapore, Advanced Series on Ocean Engineering, Vol. 3.

Friedrichs, C. T. and D.G. Aubrey (1996) Uniform Bottom Shear Stress and Equilibrium Hyposometry of Intertidal Flats, in *Mixing in Estuaries and Coastal Seas*, *Coastal Estuarine Ser.*, vol. 50, edited by C. Pattiaratchi, pp. 405-429, AGU, Washington, D.C., doi:10.1029/CE050p0405.

Friedrichs, C.T. (2011), Tidal Flat morphodynamics: A synthesis, In *Treatise on Estuarine and Coastal Science* E. Wolanski and D. McLusky (eds.), Academic Press, Waltham, pp 137-137, ISBN 9780080878850, http://dx.doi.org/10.1016/B978-0-12-374711-2.00307-7.

Hu, K., P. Ding, Z.B. Wang and S. Yang (2009), A 2D/3D hydrodynamic and sediment transport model for the Yangtze Estuary, China, *Journal of Marine Systems*, *77*, 114-136, doi:10.1016/j.jmarsys.2008.11.014.

Justesen, P. (1988), *Turbulent wave boundary layers*, Ph.D. Thesis. Techn. Univ. Denmark, Inst. of Hydrodynamics and Hydraulic Engineering, ISVA, Denmark.

Geyer, W.R. and R.P. Signell (1992), A Reassessment of the Role of Tidal Dispersion in Estuaries and Bays, *Estuaries*, *15*(2), 97-108, doi:10.2307/1352684.

Kirby, R. (2000), Practical implications of tidal flat shape, *Continental Shelf Research*, *20*, 1061-1077, doi:10.1016/S0278-4343(00)00012-1.

Kirby, R. (2002), Distinguishing accretion from erosion-dominated muddy coasts, in *Muddy Coasts of the World*, T. Healy, Y. Wang and J.-A. Healy (eds.), Elsevier, 61-81.

Lee, S. and A.J. Mehta (1997), Problems in characterizing the dynamics of mud shore profiles, *Journal of Hydraulic Engineering*, *4*, 351-361, doi:10.1061/(ASCE)0733-9429(1997)123:4(351).

Le Hir, P., Y. Monbet, F. Orvain (2007), Sediment erodability in sediment transport modelling: Can we account for biota effects?, *Continental Shelf Research*, *27*, 1116-1142, doi: 10.1016/j.csr.2005.11.016.

Le Hir, P., W. Roberts, O. Cazaillet, M. Christie, P. Bassoullet, and C. Bacher (2000), Characterization of intertidal flat hydrodynamics *Continental Shelf Research*, *20*(12-13), 1433-1459, doi:10.1016/S0278-4343(00)00031-5.

Le Méhauté, B. (1962), On non-saturated breakers and wave run-up, *Proc. 8th Coastal Engineering Conference*, pp 77-92.

Lesser, G.R., J.A. Roelvink, J.A.T.M. van Kester, G.S. Stelling Development and validation of a three-dimensional morphological model, *Coastal Engineering*, *51*(8-9), 883-915, doi:10.1016/j.coastaleng.2004.07.014.

Liu, X.J., S. Gao, Y.P. Wang (2011), Modeling profile shape evolution for accreting tidal flats composed of mud and sand: A case study of the central Jiangsu coast, China, *Continental Shelf Research*, *31*, 1750-1760, doi:10.1016/j.csr.2011.08.002.

Maan, D.C., van Prooijen, B.C., Wang, Z.B., de Vriend, H.J. (2015). Do intertidal flats ever reach equilibrium? *Journal of Geophysical Research: Earth Surface*, *120*(11). https://doi.org/10.1002/2014JF003311

Marani, M., A. D'Alpaos, S. Lanzoni, L. Carniello and A. Rinaldo, The importance of being coupled: Stable states and catastrophic shifts in tidal biomorphodynamics, *J. Geophys. Res.*, *115*, F04004, doi:10.1029/2009JF001600.

Marani, M., A. D'Alpaos, S. Lanzoni, L. Carniello and A. Rinaldo (2007), Biologically-controlled multiple equilibria of tidal landforms and the fate of the Venice lagoon, *Geophys. Res. Lett.*, *34*, L11402,doi:10.1029/2007GL030178.

Mariotti, G., and S. Fagherazzi (2010), A numerical model for the coupled long-term evolution of salt marshes and tidal flats, *J. Geophys. Res.*, *115*, F01004, doi:10.1029/2009JF001326.

Mehta, A.J., R. Kirby, and S-C. Lee (1996), Some observations on mudshore dynamics and stability. Report UFL/COEL/MP-96/1 (University of Florida, USA).

Pritchard, D. A.J. Hogg and W. Roberts (2002), Morphological modelling of intertidal mudflats: the role of cross-shore tidal currents, *Continental Shelf Research*, *22*, 1887-1895, doi:10.1016/S0278-4343(02)00044-4.

Pritchard, D. and A.J. Hogg (2003) Cross-shore sediment transport and the equilibrium morphology of mudflats under tidal currents *J. Geophys. Res.*, *108*(C10), 3313, doi:10.1029/2002JC001570.

van Prooijen, B.C. and Z.B. Wang (2013), A 1D model for tides waves and fine sediment in short tidal basins -Application to the Wadden Sea, *Ocean Dynamics*, *63*, 1233-1248, doi:10.1007/s10236-013-0648-7.

2

Roberts, W., P. Le Hir and R.J.S. Whitehouse (2000), Investigation using simple mathematical models of the effect of tidal currents and waves on the profile shape of intertidal mudflats, *Continental Shelf Research*, *20*, 1079-1097, doi:10.1016/S0278-4343(00)00013-3.

Roelvink, J.A., Coastal morphodynamic evolution techniques (2006), *Coastal Engineering, 53*(2-3), 277-287, doi:10.1016/j.coastaleng.2005.10.015.

Shi, B.W., S.L. Yang, Y.P. Wang, T.K. Bouma, Q. Zhu (2012), Relating accretion and erosion at an exposed tidal wetland to the bottom shear stress of combined current-wave action, *Geomorphology*, *138*, 380-389, doi:10.1016/j.geomorph.2011.10.004.

Soulsby, R. (1997), Dynamics of marine sands. A Manual for Practical Applications, Thomas Telford, London, UK.

Soulsby, R.L., and S. Clarke (2005), Bed Shear-Stresses Under Combined Waves and Currents on Smooth and Rough Beds, Report TR137, HR Wallingford, `http://books.hrwallingford.co.uk/acatalog/free_downloads/TR137.pdf`

Stelling, G.S. and S.P.A. Duinmeijer (2003), A staggered conservative scheme for every Froude number in rapidly varied shallow water flows, textitInt. J. Numerical Methods in Fluids, *43*(12), 1329-1354, doi:10.1002/fld.537

Swart, D. (1976), Predictive equations regarding coastal transport, *Proc. 15th Conf. Coastal Eng.*, Honolulu, Hawaii, doi:http://dx.doi.org/10.9753/icce.v15.%25p.

Tambroni, N. and G. Seminara (2012), A one-dimensional eco-geomorphic model of marsh response to sea level rise: Wind effects, dynamics of the marsh border and equilibrium, *J. Geophys. Research*, *117*, F03026, doi:10.1029/2012JF002363.

Ter Brake, M.C., H.M. Schuttelaars (2010), Modeling equilibrium bed profiles of short tidal embayments, *Ocean Dynamics*, *60*, 183-204, doi:10.1007/s10236-009-0232-3.

van de Koppel, J., D. van der Wal, J.P. Bakker and P.M.J. Herman (2005), Self-Organization and Vegetation Collapse in Salt Marsh Ecosystems, *Am. Nat.*, *165*(1), E1-E12, doi:10.1086/426602.

Van der Wegen, M. (2010), *Modeling Morphodynamic evolution in alluvial estuaries*, Ph.D.Thesis. Delft University of Technology and UNESCO-IHE Institute for Water Education: The Netherlands.

Van Rijn, L.C. (1993), Principles of sediment transport in rivers, estuaries and coastal seas Amsterdam: Aqua publications.

Van Straaten, L., P.H. Kuenen (1958), Tidal action as a cause of clay accumulation, *Journal of Sedimentary Research*, *28*(4), 406-413, doi:10.1306/74D70826-2B21-11D7-8648000102C1865D.

Waeles, B., P. Le Hir and R. S. Jacinto (2004), Modelisation morphodynamique cross-shore d'un estran vaseux, *Comptes Rendus Geoscience*, *336*, 1025-1033, doi:10.1016/j.crte.2004.03.011.

Winterwerp, J.C. and W.G. Van Kesteren (2004), Introduction to the physics of cohesive sediment dynamics in the marine environment, *Developments in Sedimentology, 56.* Elsevier.

Wolinsky, A.W. (2009), A unifying framework for shoreline migration: 1. Multi-scale shoreline evolution on sedimentary coasts, *J. Geophys. Res., 114,* F01008, doi:10/1092/2007JF000855.

Yang, S.L., P.X. Ding and S.L. Chen (2001), Changes in progradation rate of the tidal flats at the mouth of the Changjiang Yangtze River, China *Geomorphology, 38,* 167180, doi:10.1016/S0169-555X(00)00079-9.

Yang, S.L., J.D. Milliman, P. Li, and K. Xu (2011), 50,000 dams later: Erosion of the Yangtze River and its delta, *Global and Planetary Change, 75*(1-2), 14-20, doi:10.1016/j.gloplacha.2010.09.006.

Yang, S.L., H. Li, T.J. Ysebaert, T.J. Bouma, W.X. Zhang, P. Li, M. Li, and P.X. Ding (2008), Spatial and temporal variations in sediment grain size in tidal wetlands, Yangtze Delta: On the role of physical and biotic controls, *Estuarine, Coastal and Shelf Science, 77,* 657-671, doi:10.1016/j.ecss.2007.10.024.

Zhao, Y., Q. Yu, D. Wang, Y. P. Wang, Y. Wang, and S. Gao (2017), Rapid formation of marsh-edge cliffs, Jiangsu coast, China, *Marine Geology, 385,* 260-273, doi:10.1016/j.margeo.2017.02.001.

Zimmerman, J.T.F. (1976) Mixing and flushing of tidal embayments in the western Dutch Wadden Sea, Part II: Analysis of mixing processes, *Netherlands Journal of Sea Research, 10,* 397-439, doi:10.1016/0077-7579(76)90013-2.

2

3

A LAGRANGIAN FRAMEWORK TO DESCRIBE HORIZONTALLY MIGRATING FLATS

To treat unbalanced systems with a one-dimensional numerical model, we propose a moving (Lagrangian) framework in which a stable cross-sectional profile and a progradation speed can be derived for prograding tidal flats. We study the dependency of the profile and progradation speed on the wave climate, the sediment concentration in their adjacent waters, the dispersion coefficient, the settling velocity and the erosion parameter. It is shown that the cross-sectional shape does not only depend on the hydrodynamic forces, but also on the sediment availability, and is related to the progradation speed of the flat. In turn, the progradation speed increases with increasing sediment availability via a relationship that is stronger than linear. Wind waves and dispersion, on the other hand, lead to lower progradation speeds. Further, it has been shown that a larger settling velocity and a smaller erosion parameter results in a gentler slope, a larger progradation speed and a lower maximum elevation of the flat.

3.1. INTRODUCTION

Having described the feedback loops that underly the state of steady horizontal migration in the previous chapter, we will here further investigate the influence of the sediment concentration at the boundary on the cross-sectional profile and progradation speed of intertidal flats. Also the influence of model parameters will be investigated. For deriving the stable profile shapes and velocities of migrating intertidal flats as a function of hydrodynamic forcing and sediment supply, we found that it is convenient to express the model in a Lagrangian reference frame, so that the boundary conditions determine one single steady state (desribed by a steady profile shape and migration velocity). Note

that this approach is motivated by the observation that the concentration field inside the intertidal domain is invariant to the continuous horizontal shift of the flat. It is (approximately) conserved while the flat steadily progrades seaward, i.e. towards the model boundary (see Chapter 2). The proposed method is incorporated in a purely morphodynamic model and does not require any pre-assumptions on the equilibrium profile shapes (consider *Wolinsky* (2009) for a discussion about morphokinematic models of shoreline migration).

3.2. MODEL DESCRIPTION

We apply the following stategy to make the translation into the Lagrangian reference frame: we assign the boundary conditions (tidal range, wave climate and sediment concentration) to an arbitrary bed level somewhere below the intertidal area. Defining the bed level at the boundary implies that the net sedimentation in the first grid cell is assumed to be completely captured by a horizontal movement of the coastline. The net sedimentation defines a migration velocity, which in turn defines a Lagrangian reference frame with spatial coordinate $x' = x + v \cdot t$ (see Fig.3.1). The equations for the hydrodynamics, sediment transport and bed level changes are reformulated in this reference frame.

Figure 3.1: A stable bathymetry inside the Lagrangian reference frame for a prograding flat, indicated by the colored accentuated area at time t and by the green area at time $t + dt$. $\zeta(x', t)$ is the water level, $\eta(x')$ is the bed level and $h(x', t)$ the water depth. Note that a negative velocity is assigned to seaward progradation.

The conservation equations of (water) mass, momentum and sediment in the Lagrangian reference frame contain an extra term, which couples the time derivatives in the stationary frame to the time derivatives in the moving system. This term has the same form as the flow-advection term. Since the flow velocities of the water (u, in the order of $m\,s^{-1}$) are naturally much larger than the progradation speed of the coastline (v, in the order of $m\,yr^{-1}$), the extra term can be neglected (i.e. the quasi-steady approach).

Equation 2.1 becomes:

$$\frac{\partial h}{\partial t} + \frac{\partial h}{\partial x'}\frac{\partial x'}{\partial t} + \frac{\partial uh}{\partial x'} = \frac{\partial h}{\partial t} + (v+u)\frac{\partial h}{\partial x'} + h\frac{\partial u}{\partial x'}$$

$$\approx \frac{\partial h}{\partial t} + \frac{\partial uh}{\partial x'} = 0. \tag{3.1}$$

Equation 2.2 becomes:

$$\frac{\partial u}{\partial t} + \frac{\partial u}{\partial x'}\frac{\partial x'}{\partial t} + u\frac{\partial u}{\partial x'} = \frac{\partial u}{\partial t} + (v+u)\frac{\partial u}{\partial x'}$$

$$\approx \frac{\partial u}{\partial t} + u\frac{\partial u}{\partial x'} = -g\frac{\partial \zeta}{\partial x} - \frac{\tau_{bc}}{\rho_w h}. \tag{3.2}$$

Equation 2.4 becomes:

$$\frac{\partial ch}{\partial t} + \frac{\partial ch}{\partial x'}\frac{\partial x'}{\partial t} + \frac{\partial uch}{\partial x'} = \frac{\partial ch}{\partial t} + (v+u)\frac{\partial ch}{\partial x'} + ch\frac{\partial u}{\partial x'}$$

$$\approx \frac{\partial ch}{\partial t} + \frac{\partial uch}{\partial x'}$$

$$= \frac{\partial}{\partial x'}\left(Kh\frac{\partial c}{\partial x'}\right) + D - E. \tag{3.3}$$

In the Lagrangian reference frame, we can thus use the conventional conservation equations for mass, momentum and sediment (Eqs.2.1, 2.2 and 2.4). The only equation that significantly changes is the equation for the evolution of the bathymetry. In a moving reference frame, the time derivative of the bathymetry reads:

$$\frac{d\eta}{dt} = \frac{\partial \eta}{\partial t} + \frac{\partial \eta}{\partial x'}\frac{\partial x'}{\partial t}. \tag{3.4}$$

Using $\frac{\partial \eta}{\partial t} = \frac{1}{\rho_{dry}}(D-E)$ and $\frac{\partial x'}{\partial t} = v$, the horizontal migration velocity of the coastline, we find:

$$\frac{d\eta}{dt} = \frac{1}{\rho_{dry}}(D-E) + v\frac{\partial \eta}{\partial x'} \tag{3.5}$$

The profile shape is stable if:

$$\frac{1}{\rho_{dry}}\left(\overline{D} - \overline{E}\right) + v\frac{\partial \overline{\eta}}{\partial x'} = 0, \tag{3.6}$$

in which the bars indicate tidal averages. In this 'Lagrangian balance', net sedimentation is balanced by the velocity term in such a way that the cross-shore shape is maintained while the profile migrates. This implies that the net sedimentation is linearly proportional to the local slope of the profile; the steeper the slope, the more sedimentation (per surface area) is required for the same horizontal progradation (indicated by a thicker green non-accentuated layer in Fig.3.1). Note that in this formulation accretion dominance corresponds with a negative (seaward) velocity of the coastline (in case of

a positive bed-level gradient), whereas erosion dominance corresponds with a positive (landward) velocity term (see Eq.3.6).

The migration velocity follows directly from the assumption of a constant bed level in the first grid cell and is defined by:

$$v = -\frac{\left(\overline{D} - \overline{E}\right)}{\rho_{dry}\left(\frac{\partial \overline{\eta}}{\partial x'}\right)} |_{x'=0} \tag{3.7}$$
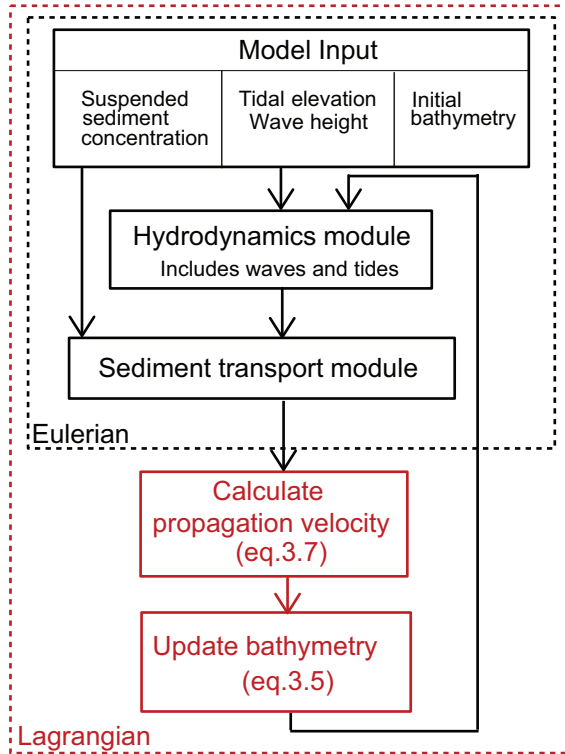

Figure 3.2: Schematic representation of the model in the Lagrangian framework, consisting of a conventional (Eulerian) part and an extra part in which the progradation velocity is calculated and used to update the bathymetry in the Lagrangian reference frame.

Fig.3.2 shows a schematic representation of the model in the Lagrangian framework. The performance of the model in the Lagrangian framework has been tested by an elaborate comparison with the stable prograding profile shapes and migration velocities as obtained in the Eulerian framework. The results were found to be identical (see Fig. 3.3, Panel B).

Because purely retreating profiles were not found in the Eulerian framework (due to the low hydrodynamic forces on the uppermost section of the intertidal area and the exclusion of cliff erosion), we apply the Lagrangian model only to derive seaward prograd-

Table 3.1: Simulation codes with boundary conditions and parameter values.

code	$c_0(kg\,m^{-3})$	waves (m)	$K(m^2 s^{-1})$	$w_s(m\,s^{-1})$	$m_e(kg\,m^{-2}s^{-1})$	M
$Lg1$	0.01	no	100	$0.2 \cdot 10^{-3}$	$5 \cdot 10^{-5}$	5
$Lg2$	0.1	no	100	$0.2 \cdot 10^{-3}$	$5 \cdot 10^{-5}$	5
$Lg3$	0.2	no	100	$0.2 \cdot 10^{-3}$	$5 \cdot 10^{-5}$	5
$Lg4$	0.3	no	100	$0.2 \cdot 10^{-3}$	$5 \cdot 10^{-5}$	5
$Lg5$	0.1	0.2	100	$0.2 \cdot 10^{-3}$	$5 \cdot 10^{-5}$	10
$Lg6$	0.2	0.2	100	$0.2 \cdot 10^{-3}$	$5 \cdot 10^{-5}$	10
$Lg7$	0.3	0.2	100	$0.2 \cdot 10^{-3}$	$5 \cdot 10^{-5}$	10
$Lg8$	0.4	0.2	100	$0.2 \cdot 10^{-3}$	$5 \cdot 10^{-5}$	5
$Lg9$	0.1	0.2	1	$0.2 \cdot 10^{-3}$	$5 \cdot 10^{-5}$	1
$Lg10$	0.2	0.2	1	$0.2 \cdot 10^{-3}$	$5 \cdot 10^{-5}$	1
$Lg11$	0.3	0.2	1	$0.2 \cdot 10^{-3}$	$5 \cdot 10^{-5}$	1
$Lg12$	0.4	0.2	1	$0.2 \cdot 10^{-3}$	$5 \cdot 10^{-5}$	1
$Lg13$	0.1	0.2	100	$0.5 \cdot 10^{-3}$	$5 \cdot 10^{-5}$	1
$Lg14$	0.2	0.2	100	$0.5 \cdot 10^{-3}$	$5 \cdot 10^{-5}$	1
$Lg15$	0.3	0.2	100	$0.5 \cdot 10^{-3}$	$5 \cdot 10^{-5}$	1
$Lg16$	0.4	0.2	100	$0.5 \cdot 10^{-3}$	$5 \cdot 10^{-5}$	1
$Lg17$	0.1	0.2	100	$0.2 \cdot 10^{-3}$	$2.5 \cdot 10^{-5}$	1
$Lg18$	0.2	0.2	100	$0.2 \cdot 10^{-3}$	$2.5 \cdot 10^{-5}$	1
$Lg19$	0.3	0.2	100	$0.2 \cdot 10^{-3}$	$2.5 \cdot 10^{-5}$	1
$Lg20$	0.4	0.2	100	$0.2 \cdot 10^{-3}$	$2.5 \cdot 10^{-5}$	1

3

ing profiles. Note that in principle the same method could be applied to derive retreating profiles as well, but it would require an additional formulation for cliff erosion.

3.3. PARAMETERS AND BOUNDARY CONDITIONS

The model parameters are chosen the same as in Chapter 2 and summarized in Table 2.1. The shape and velocity of the obtained profiles are sensitive to the choice of the model parameters. Yet, our qualitative results about the way in which the sediment supply influences the profile shape and the progradation velocity do not depend on the model parameters. The boundary conditions are assigned to an elevation of $1\,m$ below lowest tide (i.e. MSL $-3\,m$). A constant value is imposed for the sediment concentration at the seaward boundary. The water level variation and wave height at the seaward boundary are imposed in the same way as in Chapter 2. Extra boundary conditions are required for the slopes in Eqs.3.5 and 3.7: The slope at the most landward cell is assumed to be zero and the slope at the most seaward grid cell is assumed to be equal to that of its only neighbor. In order to fix the position of the landward boundary (i.e. an imaginary sea dike) in the Lagrangian reference frame, the length of the last (most landward) grid cell increases with the progradation of the coastline.

As in the previous section, the initial profile is a straight line. When starting from a gentle slope, the first grid cell would be erosive. This results in an initially increasing bed level in the model domain via the last term in Eq.3.5, which steepens the profile slope

(while the bed level in the first grid cell remains unchanged). If a peak in the profile is formed seaward of the most landward cell, the area landward of the maximum bed elevation is omitted from the calculation and its bed level is taken equal to the peak value. Note that this section, which is shielded from the sediment supply and hydrodynamic forces, is not part of the migrating coastline (it will stay behind while the part seaward of the top migrates, or it fills up by aeolian transport) and should be omitted because term 2 in Eq.3.5 keeps acting also if erosion and deposition do not occur any longer.

3.3.1. RESULTS AND DISCUSSION

The effects of the boundary concentration and model parameters on the steady progradation speed and profile shape of the intertidal flats are investigated for (1) tidal currents only and (2) tidal currents plus wind waves. Each simulation is given a code as indicated in the caption of the figures, and an overview of the corresponding boundary conditions is given in table 3.1.

The results show that an increase in the sediment concentration at the model boundary results in gentler slopes and an increase in the progradation speed (Fig.3.3A,B). In Chapter 2 we have seen that the local morphodynamic feedback loop is of a stabilizing type on the lower and intermediate flat, so that local balances between deposition and erosion are approached. Hence, the slopes (affecting tidal erosion) are adjusted via an increase or decrease of the bed levels, until the vertical fluxes are (approximately) in balance (Chapter 2). A higher suspended sediment concentration at the boundary hereby results in a gentler slope towards MSL (Fig.3.3), corresponding with larger tidal currents and tide-induced erosion rates (see Fig.3.3, Panels C and D), see also *Pritchard et al.* (2003). Larger tidal flow velocities correspond with larger landward sediment advection fluxes and more accretion on the upper flat, which is reflected by larger progradation speeds (Fig.3.3A,B)A,B. Fig.4.4 indicates that the relationship between the suspended sediment concentration at the boundary and the progradation speed of the flats is stronger than linear, which will be further discussed in the next chapter.

Adding wind waves to the system (while maintaining the sediment concentration at the boundary), results in steeper profiles on the upper intertidal flat (Figure.3.3B) and in smaller progradation speeds (see Fig.3.3A&B and Fig.4.4). Under influence of wind waves, the bed shear stresses of the upper shore are larger, resulting in smaller net sedimentation rates and a lower progradation speed.

Whereas the tidal erosion increases with an increasing boundary concentration (via the establishment of a local balance, see above), the wave erosion decreases with an increasing boundary concentration (under assumption of a constant wave climate, see Fig.3.3D). For sediment concentrations of $0.1gL^{-1}$, $0.2gL^{-1}$ and $0.3gL^{-1}$ at the boundary, the progradation speed is affected (by $20cm$ wind waves) with 32, 25 and 20 myr^{-1} respectively (see Fig.3.3), i.e. the impact decreases with an increasing boundary concentration (see Fig.3.3). This can be explained by the effect of the morphology on the wave dissipation: on a gentler slope, wave-induced bed friction dissipates more energy, so that the wave height is already reduced before the waves reach the elevation of maximum impact (note, however, that the amount of dissipation and the importance of this effect depends on the wave friction parameter). The dependency of the wave-impact on the suspended sediment concentration at the boundary is, however, much smaller than
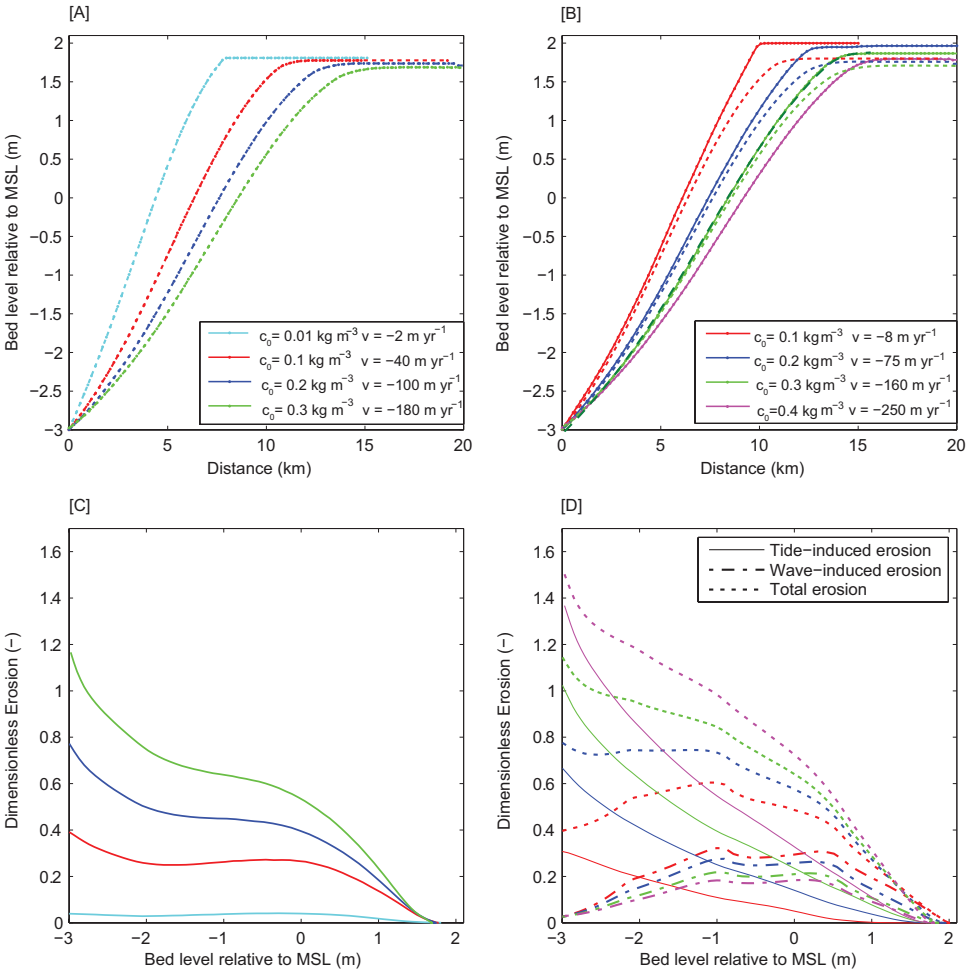
Figure 3.3: (Above) Lagrangian equilibrium profiles and progradation speeds for different concentrations of suspended sediment at the boundary. (A)[Sim.$Lg1 - Lg4$ in Table 3.1] Profiles for tides only. (B) [Sims.$E4$ in Table 2.2 & $Lg5 - Lg8$ in Table 3.1] Profiles for tides and wind waves (solid lines with markers). The dotted lines are copies from panel A. The dark green dashed line is a profile obtained in an Eulerian framework for $c_0 = 0.3 kg\, m^{-3}$, i.e. a copy from Fig.2.9 after 80 yrs of evolution. (Below) Tide-averages of the dimensionless erosion over the Lagrangian equilibrium profiles. (C) Tide-averages of the dimensionless erosion over the profiles in Panel A. (D) Tide-averages of the dimensionless erosion (total, tide-induced and wave-induced) on the profiles in Panel B. (C,D) The values were made dimensionless by $\hat{E} = \frac{1}{m_e} E$ so that they are comparable with the dimensionless concentration $\hat{c} = \frac{w_s}{m_e} c$ (divide the values by 4 to obtain concentrations in $kg\, m^{-3}$ and divide by 20 to obtain erosion rates in $gm^{-2}s^{-2}$). In panel D, the wave- and tide-induced erosion are roughly estimated by the time integrals of $E_W = \max\left[m_e\left(\frac{\tau'_{bw}}{\tau_{cr}} - 1\right), 0\right]$ and $E_T = \max\left[m_e\left(\frac{\tau'_{bc}}{\tau_{cr}} - 1\right), 0\right]$ respectively, and their sum is slightly less than the total erosion rate.
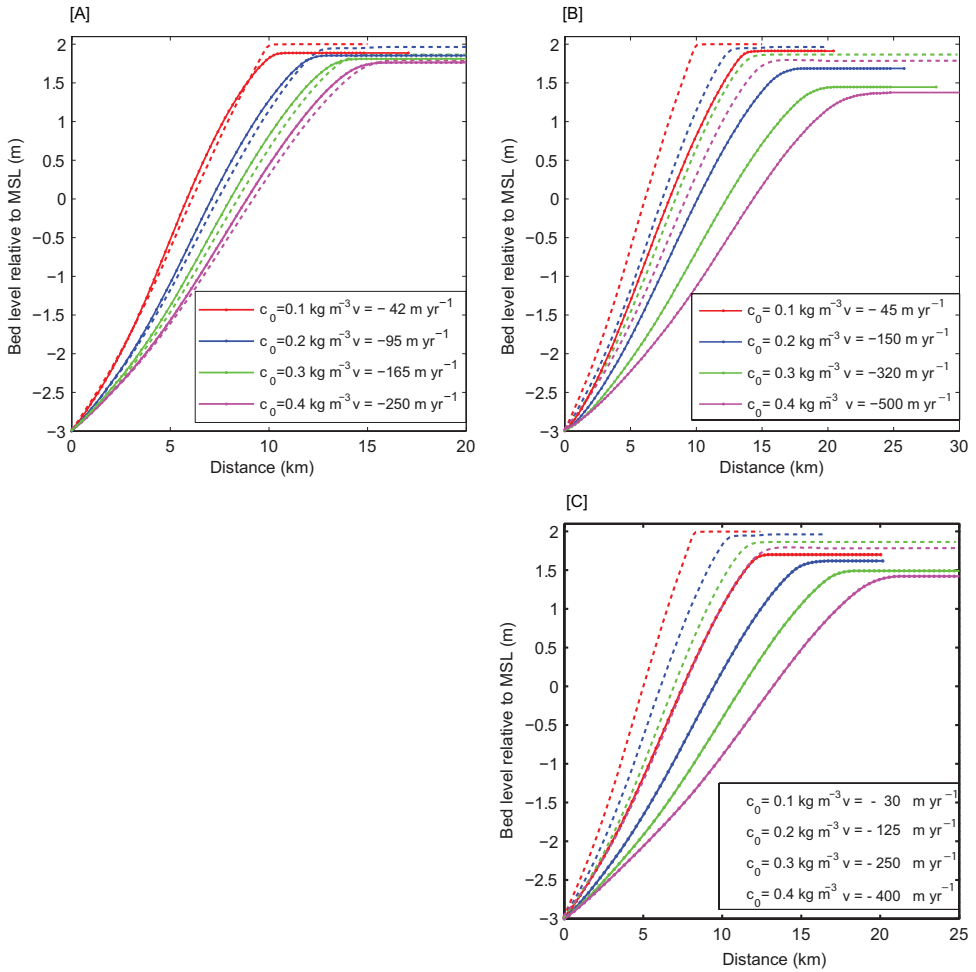
Figure 3.4: (A)[Sim.$Lg9 - Lg12$ in Table 3.1] Lagrangian equilibrium profiles and progradation speeds for $K = 1 m^2 s^{-1}$, under influence of tides and wind waves. The dotted lines are copies from Fig.3.3B, i.e. for $K = 100 m^2 s^{-1}$. (B) [Sim. $Lg13 - Lg16$ in table 3.1] Lagrangian equilibrium profiles and progradation speeds for $w_s = 0.5 \cdot 10^{-3} m s^{-1}$, under influence of tides and wind waves. The dotted lines are copies from Fig.3.3B, i.e. for $w_s = 0.2 \cdot 10^{-3} m s^{-1}$. (C) [Sim. $Lg17 - Lg20$ in table 3.1] Lagrangian equilibrium profiles and progradation speeds for $m_e = 2.5 \cdot 10^{-5} kg m^{-2} s^{-1}$, under influence of tides and wind waves. The dotted lines are copies from Fig.3.3B, i.e. for $m_e = 5 \cdot 10^{-5} kg m^{-2} s^{-1}$.

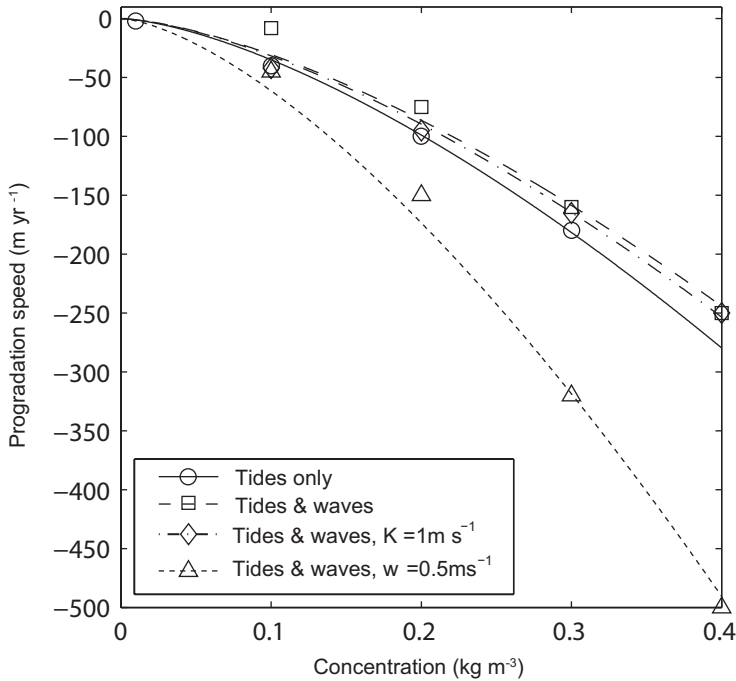the dependency of the tide-induced erosion on the boundary concentration.

Figure 3.5: [Sim.$Lg1 - Lg16$ in Table 3.1] Lagrangian progradation speeds of the profiles in Figs. 3.3 and 3.4 plotted against the sediment concentration at the model boundary and fitted for $v = a * c^{1.5}$. $K = 100 m^2 s^{-1}$ and $w_s = 0.2 \cdot 10^{-3} m s^{-1}$, unless specified differently.

The simulations in Fig.3.3B are repeated for a few different parameter settings (Fig.3.4). The profile slopes and shapes are not very sensitive to a variation of the dispersion coefficient K (comparison Fig.3.4A and 3.3B), but the progradation speeds are sensitive to such a variation (comparison of the squares and the rhombi in Fig.4.4). The seaward dispersion flux, driven by sharp concentration gradients at the tidal fronts (see Chapter 2), is intensified by an increase in the dispersion coefficient, resulting in lower progradation speeds. This effect is most pronounced for low boundary concentrations.

The results are also sensitive to variations of the settling velocity and the erosion coefficient. An increase in the settling velocity results in larger gross deposition fluxes at the boundary, which are balanced by larger gross erosion fluxes. Hence, the slopes get gentler (so that the tidal flow velocities increase) with an increasing settling velocity (Fig.3.4B). In a similar fashion, also the effect of the erosion coefficient can be explained: if the erodibility is lower, higher tidal flow velocities and gentler slopes are needed to balance the deposition flux at the boundary. The increase in the tide-induced erosion rates results in a larger landward sediment advection flux and more accretion on the upper part, which is reflected by larger progradation velocities. Furthermore, the maximum elevation decreases with an increasing settling velocity and a decreasing erosion coefficient (Fig.3.4B&C). This can be explained by an increasing friction on the flow with

decreasing cross-sectional slopes. On a gentler flat, the tidal flow experiences more resistance of the bed and the flow velocities fall to zero at lower elevations.

Despite these dependencies on model parameters, the tendency to evolve into states of steady migration, with a steady profile shape and migration speed, is not influenced by the considered variations of the parameter values.

3.4. CONCLUSIONS

A one-dimensional cross-shore model was expressed in a Lagrangian framework to study the cross-sectional profiles and progradation speeds of prograding tidal flats. The performance of the model was validated against results obtained in an Eulerian framework. It has been shown that the cross-sectional shape does not only depend on the hydrodynamic forces, but also on the sediment availability, and is related to the progradation speed of the flat. For a sufficiently high boundary concentration, we find convex-upward profiles, despite the dominance of wind waves on the upper shore. The progradation speed increases with increasing sediment availability with a relationship that is stronger than linear. Both, wind waves and dispersion processes, on the other hand, lead to lower progradation speeds. Further, it has been shown that a higher settling velocity or a lower erodability results in a gentler slope, a larger progradation speed and a lower maximum elevation of the flat. The tendency to evolve into states of steady migration, with a steady profile shape and migration speed, is not influenced by the considered variations in driving factors and model parameters.

REFERENCES

Maan, D.C., van Prooijen, B.C., Wang, Z.B., de Vriend, H.J. (2015). Do intertidal flats ever reach equilibrium? *Journal of Geophysical Research: Earth Surface*, *120*(11). https://doi.org/10.1002/2014JF003311

Pritchard, D. and A.J. Hogg (2003) Cross-shore sediment transport and the equilibrium morphology of mudflats under tidal currents *J. Geophys. Res.*, *108*(C10), 3313, doi:10.1029/2002JC001570.

Wolinsky, A.W. (2009), A unifying framework for shoreline migration: 1. Multiscale shoreline evolution on sedimentary coasts, *J. Geophys. Res.*, *114*, F01008, doi:10/1092/2007JF000855.

4

PROGRADATION SPEED OF TIDAL FLATS DECREASES NON-LINEARLY WITH DECREASING SEDIMENT AVAILABILITY AND LINEARLY WITH SLR

We use the results of a one-dimensional morphodynamic model and the basis of the 'Lagrangian equilibrium state' [Maan et al., 2015, https://doi.org/10.1002/2014JF003311] to derive a quantitative relationship between the progradation speed of tidal flats, and the suspended sediment concentration in their adjacent waters and show that the speed increases more than linearly with the concentration. We also show that horizontally prograding flats rise vertically with sea level rise (SLR) at the expense of their horizontal speed via a linear relationship. If accretion rates are insufficient to keep up with SLR, however, the intertidal flat submerges and retreats landward at the same time. We apply the obtained relationships to the Yangtze Estuary to estimate the critical sediment concentration level below which a shift from progradation to retreat can be expected.

4.1. INTRODUCTION

Many of our biggest cities worldwide are situated in deltas. These low-lying coastal areas are extremely vulnerable to climate change and accelerated sea level rise (SLR) (*Syvitski et al.*, 2009). In meantime, human activities can weaken our coastal defense, especially if dams on the upstream river reduce the sediment supply to the estuary (*Syvitski et al.*, 2007, 2009). Decreasing sediment availability, in combination with sea level rise and

human fixation of the coastline, strongly impacts the intertidal environment and results in losses of these areas. Loss of coastal wetlands further increases the vulnerability to extreme events and sea level rise, hence undermining the coastal defense. Therefore it is important to understand the dynamics of these intertidal wetlands, their response to sea level rise, and to different types of human activities. The better we understand the processes that underlie the evolution of the intertidal system, the more effectively we can manipulate the system, to stimulate its rise and maintain its elevation relative to mean sea level (MSL).

In this paper we consider the intertidal mudflats at the Yangtze Estuary as examples of intertidal systems at the front of large river mouths. The Yangtze River is one of the biggest rivers in the world in terms of length, discharge and sediment load (Figure 4.1). With half a billion people living in the Yangtze River Basin, it is also one of the most populated and most heavily impacted (*Chen et al.*, 2017). The sediment supplied by the Yangtze River resulted in the development of large coastal wetlands in its estuary, which are important ecosystems. The expanding intertidal flats also provided plentiful new land; two-thirds of Shanghai was reclaimed from tidal wetlands in the past 2000 years. In the last few decades, however, the progradation of tidal flats in the estuary slowed down significantly, and there is serious concern that the system is changing into an eroding regime (*Yafeng et al.*, 2000; *S.L. Yang et al.*, 2006; *Wang et al.*, 2015; *Wei et al.*, 2015; *Luan et al.*, 2016; *Luo et al.*, 2017; *Luan et al.*, 2017).

The changes in the Yangtze Estuary are the effect of human activities inside the coastal system, including land reclamation (*Vriend et al. 2011*, 2011; *Ma et al.*, 2014; *Chen et al.*, 2016), the construction and deepening of navigation channels (*Vriend et al. 2011*, 2011), and the construction of numerous dams on the Yangtze River. The Three Gorges Dam, presently world's largest dam, has particular major consequences for the estuary. The dam blocks most of the sediment in the river from reaching the estuary (*Z. Yang et al.*, 2006; *Yang et al.*, 2007). As a consequence, the supply of suspended sediment by the river declined tremendously. At Datong Hydrological Station, located in the lower reaches of the river, the yearly averaged sediment concentration declined from $0.6 g L^{-1}$ to $0.15 g L^{-1}$ within the last decade (*Yang et al.*, 2015), i.e. a reduction of 75%.

The decrease in sediment supply by the river resulted in a decrease in the suspended sediment concentration (SSC) inside the estuary, although local sediment resuspension in the estuary partly masks the big change in the supply (*Li et al.*, 2012; *Yang et al.*, 2015). Based on long-term observations of suspended sediment discharge and morphological data, *Yang et al.* (2003a) estimated the critical sediment discharge for the conversion to be $260 - 270 Mt/yr$ versus ~ $120 Mt/yr$ that is currently measured (*Li et al.*, 2012). *Luo et al.* (2017) hypothesized that the Yangtze Estuary has already converted to an erosive regime, while *Luan et al.* (2016) projected overall erosion by 2030 for different scenarios of sediment discharge and sea level rise. Overall erosion or retreat of the intertidal flats in the estuary, however, is not yet apparent (*Li et al.*, 2014; *Wei et al.*, 2015).

In previous studies, numerical models have been applied to simulate prograding open coast mudflats that are dominated by transverse tidal currents and wind waves (*Pritchard et al.*, 2002, 2003; *Waeles et al.*, 2004; *Mariotti and Fagherazzi*, 2010; *Tambroni and Seminara*, 2012; *Maan et al.*, 2015). These studies indicate relationships between the suspended sediment concentration in the deeper waters (where longitudinal cur-

Figure 4.1: Suspended sediment in the Yangtze Estuary. Image by NASA.

4

rents dominate) and the transverse profile slope and progradation velocity of the flats *Pritchard et al.* (2003); *Liu et al.* (2011); *Friedrichs* (2011), see Figure 4.2 for an orientation on the considered domain. However, a quantitative relationship between the suspended sediment concentration and the progradation speed has not yet been developed. In this contribution we use the basis of the 'Lagrangian equilibrium state' (*Maan et al.*, 2015), to derive quantitative relationships between the progradation speed, the suspended sediment concentration in the adjacent waters, wave-induced erosion, and sea level rise. By these relationships, a critical sediment concentration level can be derived below which the intertidal system shifts from progradation to retreat. We estimate the critical sediment concentration for the Yangtze Estuary, taking into account the projected rate of sea level rise by the year 2100. Our relationships are applicable to prograding flats in general and can be applied in other river mouth areas as well.

4.2. RELATIONSHIP BETWEEN SEDIMENT AVAILABILITY AND COASTAL PROGRADATION SPEED

4.2.1. TIDES ONLY

From the principle of conservation of sediments it follows that the transverse (perpendicular to the isobaths) progradation speed of a prograding intertidal flat is given by the net landward sediment transport (i.e. advection plus dispersion, integrated over a tide) divided by the vertical distance between the bed (at the location at which the transport rate is considered) and the top of the tidal flat, see Figure 4.2.
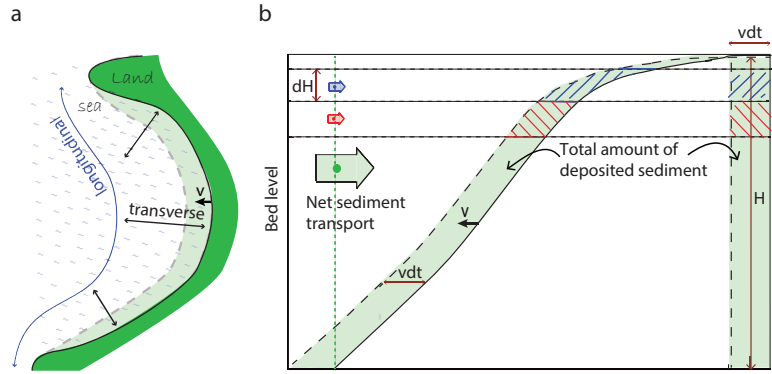

Figure 4.2: (a) Conceptual sketch of the domain declaring the longitudinal (parallel to the isobaths) and transverse (perpendicular to the isobaths) directions. (b) The principle of conservation of sediments on a prograding intertidal flat. The net landward sediment flux (green arrow) is equal to the amount of net deposited sediment, hence: $v\,T\,H\rho = \int_0^T h(t)u(t)c(t)dt$. Because the celerity is uniform, this constraint also holds per (unit) layer dH. Taking $H = a - z$ and $h(t) = \eta(t) - z$ and differentiate with respect to z gives Eq.4.1.

Because the flat progrades with a uniform celerity (i.e. a conserved cross-sectional shape), the net sediment flux needs to be distributed uniformly over the vertical cross-section. This consideration yields the following equation that is valid at any location on the flat, if we neglect the dispersion flux:

$$v\,T\rho = \int_0^T u(t)c(t)dt \tag{4.1}$$

where v is the progradation velocity (in m/s), ρ is the dry bed density and T is the tidal period. $u(t)$ and $c(t)$ are the flow velocity and the suspended sediment concentration respectively.

On much of the tidal flat, the net sediment advection flux contains a landward flood term and a seaward ebb term. However, at the top of the tidal flat, the tidal current velocities fall considerably (*van Straaten and Kuenen*, 1958; *Maan et al.*, 2015), see also Figure 4.3. At the 'top' (see Fig. 4.3) the seaward ebb term becomes negligible relative to the landward flood term (hence, the net flux is locally approximately equal to the flood term). Figure 4.3 shows that the maximum flow velocity during flood tide falls smoothly (almost linearly) over the rest of the flat. Following these findings, we here presume that

the net flux and progradation velocity are proportional to the maximum transverse advection flux at the boundary (the boundary is formed by a channel in which the longitudinal current controls the suspended sediment concentration levels, see Fig.4.2), hence:

$$v = b\frac{T_{top}}{T}\frac{c_b U}{\rho},$$ (4.2)

with c_b and U respectively the sediment concentration and the peak velocity at the boundary. b is the ratio between the maximum landward advection flux at the 'top' and that at the open boundary (Figure 4.2). T_{top} is the period during which (maximum) advection rates occur at the top of the flat (i.e. a small fraction of T). b and T_{top} are presumed to be independent of the suspended sediment concentration and the bed level at the boundary.

The bed shear stress and erosion flux can be related to the peak velocity by the quadratic drag law. From this relationship it follows that:

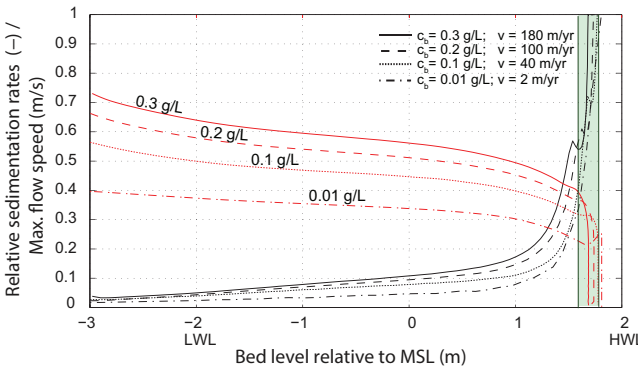$$U \propto \sqrt{\int E dt}.$$ (4.3)

Figure 4.3: Simulated maximum tidal flow velocities during flood tide (red lines) and relative net sedimentation rates (black lines, i.e. the net vertical flux divided by the gross deposition flux) on a steadily prograding intertidal flat (i.e. after a spin-up) for different (constant) sediment concentrations at the open boundary (at *MSL* -3m). In the steadily prograding state, balances are most precise at the open boundary and are increasingly disturbed towards the top of the flat. We here define the 'top of the flat' as the elevation just before the flow velocity becomes zero (for the different simulations this occurs within the green marked domain). The numerical model is based on the conservation equations for mass and momentum (capturing the hydrodynamics) and the advection-dispersion equation (capturing the dynamics of the concentration field) and further explained in *Maan et al.* (2015).

Subsequently, the erosion flux can be coupled to the sediment concentration via the approximation of a local balance at the boundary. Note that the balances between the vertical fluxes are most precise at the open boundary and are increasingly disturbed towards the top of the flat, see Figure 4.3. Thus:

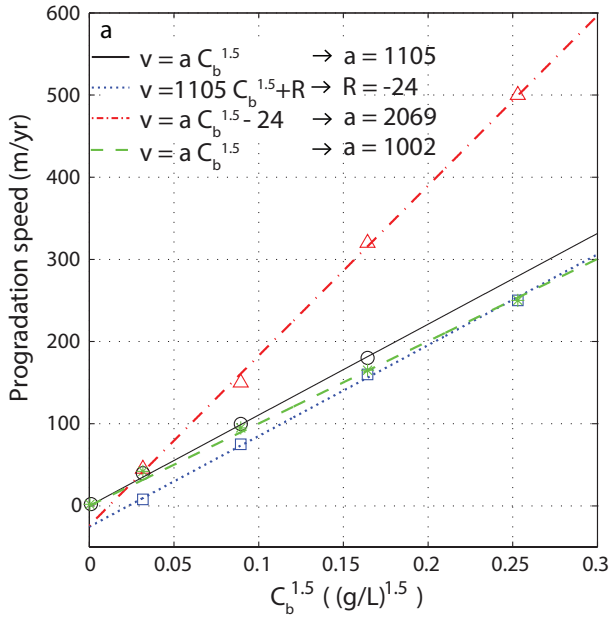$$\int E dt \approx \int D dt = c_b w_s T,$$ (4.4)

Figure 4.4: Simulated steady progradation speeds of intertidal flats versus the SSC in the adjacent waters (see *Maan et al.* (2015) for a description of the model). Data set 1 (black circles) is for tidal currents only, while the other data sets include $20cm$ wind waves. Run 2 (blue squares) and run 3 (red triangles) differ in the fall velocity. $w_s = 0.2 \cdot 10^{-3} \, ms^{-1}$ for set 2 and $w_s = 0.5 \cdot 10^{-3} \, ms^{-1}$ for set 3. Run 2 and Run 4 (green stars) differ in the dispersion coefficient K. $K = 100 m^2 s^{-2}$ for set 2 and $K = 1 m^2 s^{-2}$ for set 4. Every data set is fitted for one free parameter in the indicated function. Coefficient a in the second fit is obtained from the first fit, while coefficient R in the third is obtained from the second fit, i.e. it is assumed that the presence of waves does not affect a, and that w_s does not affect the wave-related R term. For set 4 ($K = 1 m^2 s^{-2}$) the data could be fitted without R.

and hence:

$$v \propto c_b \sqrt{\int E \, dt} \propto c_b \sqrt{c_b w_s} \propto c_b^{1.5}. \tag{4.5}$$

The propagation speed thus scales with the boundary concentration to the power
1.5. This relationship is used to fit the results of the one-dimensional model described
in *Maan et al.* (2015), see the solid black line in Figure 4.4 (the colored data sets repre-
sent simulations including wind waves and are further explained in Section 4.2.2). Note,
however, that another relationship between the flow velocity and the erosion flux would
result in a different power of c_b. Most generally we state a relationship that is stronger
than linear:

$$v \propto c_b^{1+\frac{1}{n}}, \tag{4.6}$$

with n the power between U and E. However, for the derivations in the rest of the
paper we adopt the relationship in Eq.4.5.

The progradation speed can also be expressed in terms of the cross-sectional slope
on the lower intertidal flat. From Eqns. 4.2, 4.3 and 4.4, and taking (*Friedrichs & Aubrey*,
1996; *Le Hir*, 2000):

$$U \propto \frac{2\pi a}{\beta T}, \tag{4.7}$$

with a the tidal amplitude and β the average slope from the boundary towards the
tidal front at mean sea level, it follows that:

$$v \propto U^3 \propto \frac{1}{\beta^3}. \tag{4.8}$$

Combining Eqns. 4.5 & 4.8 gives furthermore:

$$c_b \propto \frac{1}{\beta^2}. \tag{4.9}$$

However, the proportionallities in Equations 4.8 and 4.9 are less accurate than that in
Eq. 4.5, see Figure 4.5. Figure 4.5 shows that an extra term is needed to fit the data. This
can be explained by the critical bed shear stress for erosion, which complicates the re-
lationship between the erosion and the flow velocity (compared with the approximation
in Eq.4.3). More accurate versions of Eqns. 4.8 and 4.9 would be:

$$v \propto \frac{1}{\beta^3} - \frac{1}{\beta_0^3}, \tag{4.10}$$

and

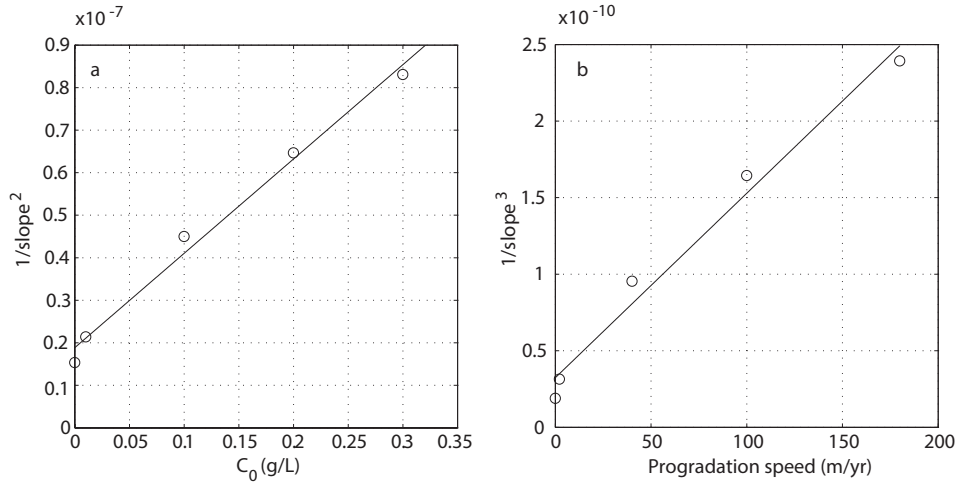$$c_b \propto \frac{1}{\beta^2} - \frac{1}{\beta_0^2}, \tag{4.11}$$

Figure 4.5: (a) Relationship between the cross-sectional slope on the lower tidal flat and the SSC in the adjacent waters (with the tidal currents as only driving factor, see *Maan et al.* (2015) for a description of the model). (b) Relationship between the slope and the progradation speed.

with β_0 the equilibrium slope in case of zero suspended sediment at the boundary. The fit in Fig.4.5A gives $\beta_0 = 7.3 \ 10^{-4}$. The same value has been used to construct the fit in Panel B.

Note that the progradation velocity is found to be (approximately) invariant to the shifting position of the flat. Thus the flat shifts with constant celerity until the intertidal domain reaches the boundary, see also *Maan et al.* (2015). This confirms the direct relationships in Eqn. 4.2, 4.6 & 4.9, independently from the bed level at the boundary and the distance between the boundary and the top of the flat. Thus, the ratio between the advection flux at the top and that at the boundary (parameter b in Equation 4.2) is invariant to the horizontal shift. This implies that larger distances between the boundary and the top (i.e. deeper boundary elevations) correspond with smaller transverse gradients of the flow velocities and the concentration fields towards the intertidal domain. Hence, the deeper the boundary of the transverse system, the more homogeneous the fields in the subtidal domain (i.e. the better an equilibrium state is approached within this domain).

4.2.2. Effect of wind waves on coastal progradation
The net transport is affected by wind waves. In this case, an additional term is needed to fit the data in Figure 4.4. The difference in progradation speed between simulations with and without waves (other settings unchanged) does not significantly depend on the boundary concentration (i.e. the vertical distance between the black circles and the blue squares in Figure 4.4 is approximately constant). Due to this (relative) independency of the wave-impact on the boundary concentration, the effect of wind waves can be taken as invariant to the SSC at the boundary, so that:

$$v - R(H, K, \tau_{cr}) \propto c_b^{1.5}, \tag{4.12}$$

and, in terms of the cross-sectional slope;

$$v - R(H, K, \tau_{cr}) \propto \frac{1}{\beta^3}. \tag{4.13}$$

where $R(H, K, \tau_{cr})$ represents the 'wave induced retreat'. In case of zero sediment supply, the tidal flat would thus retreat with speed R. R typically depends on the incoming wave height H, the dispersion coefficient K and on bed properties as the critical bed shear stress for erosion τ_{cr}. In case of $20cm$ wind waves, a dispersion coefficient of $K = 100 m^2 s^{-2}$ and a critical bed shear stress of $\tau_{cr} = 0.1 Pa$, we found values for R of about of $-24 m/yr$ (Figure 4.4). For $K = 1 m^2 s^{-2}$, R was found to be much smaller (Figure 4.4).

4.3. RELATIONSHIP BETWEEN SEA LEVEL RISE AND COASTAL PROGRADATION SPEED

4.3.1. LINEARITY

As long as the net sedimentation rates ($\frac{D-E}{\rho}$) are larger than the rate of sea level rise (SLR), the bed level change relative to mean sea level can simply be translated into horizontal progradation via the conservation of the cross-sectional slope at the boundary of the tidal flat, see Equation 3.7 in Chapter 3. Hence:

$$v = \frac{1}{\beta}\left(\frac{D-E}{\rho} - SLR\right) = v_0 - \frac{SLR}{\beta}, \tag{4.14}$$

where v_0 is the progradation velocity without sea level rise. Our model results confirm that sea level rise reduces the progradation speed in such a linear fashion as long as the flat prograes seawards, see Figure 4.6. Also *Mariotti and Fagherazzi* (2010) obtained a linear relationship from 1D model simulations.

4.3.2. PASSING THE TIPPING POINT

If accretion rates are insufficient to keep up with sea level rise, the intertidal flat submerges and retreats landward at the same time. This condition is shown in Panels *e* and *f* of Figure 4.7. In panel *e* we see that the flat initially rises with sea level rise, but at a lower rate. Initially the flat builds out seaward (the evolution from dotted black to yellow-orange), but while its relative elevation decreases (see also panel *f*), the transverse flow velocities increase. At some point, erosion starts to dominate at the sea-side of the top, resulting in landward retreat (evolution from orange to red). Landward of the top, however, flow velocities are small and sedimentation occurs. This results in a landward shift of the top. When the top approaches a sea-dike, a 'steady state' develops in which the flat rises with the same rate as the sea level (from red to dark brown; see also the equilibrium state in panel *f*). Similar results were found for rates of sea level rise of up to $5cm/yr$. Note, however, that vegetation is not included in the model. A salt marsh reduces the flow velocities on the upper flat and could maybe prevent accelerated coastal retreat (i.e.
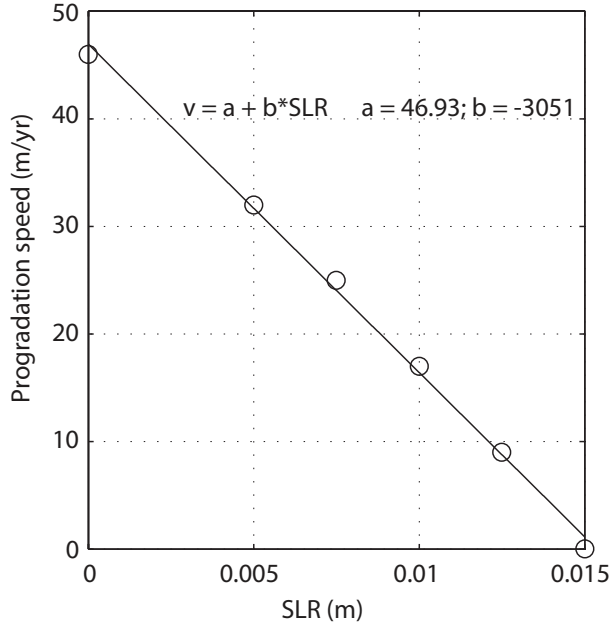
Figure 4.6: Linear relationship between the rate of sea level rise and the progradation speed based on model simulations (*Maan et al.*, 2015) for $c_b = 0.15 g/L$.

prevent the retreat from the orange to the red profile in panel *e* of Figure 4.7). Simulations including vegetation were carried out before by *Mariotti and Fagherazzi* (2010), but they considered wave-dominated flats, with a smaller role for the transverse tidal current. They did not observe accelerated retreat, independent of the presence of a salt marsh.

4.4. APPLICATION TO THE YANGTZE TIDAL FLATS

For practical application of Equation 4.12, we can use measured combinations of the (historical) progradation speeds and the corresponding suspended sediment concentrations, i.e.:

$$\frac{v_{new} - R}{v_{old} - R} = \left(\frac{c_{new}}{c_{old}}\right)^{1.5}, \tag{4.15}$$

Critical values for the SSC can be derived by taking $v_{new} = 0$ or $v_{new} = \frac{SLR}{\beta}$ (including sea level rise), but we first need an estimate for R.

An estimate for R Such an estimate can be obtained from in situ measurements of bed level changes during windy conditions and storms. We thereby need to concentrate on bed level changes on the upper intertidal area, where the tide-induced bed shear stress clearly diminishes (see Figure 4.3). On the lower sections, dominance of transverse tidal
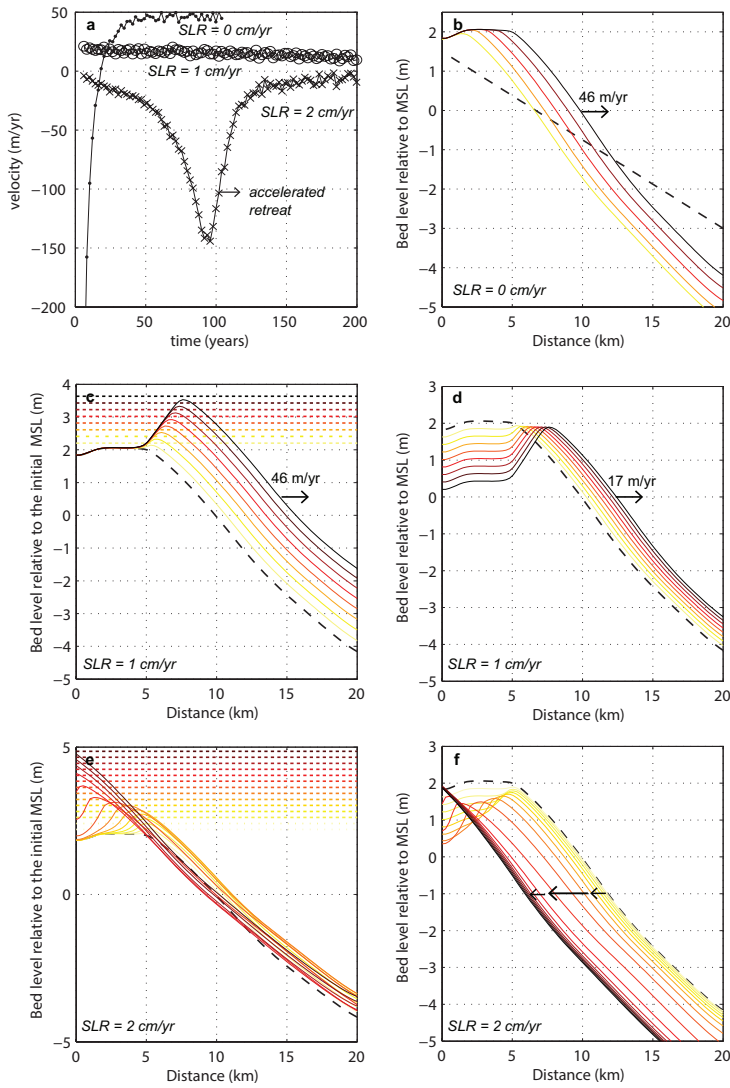
Figure 4.7: (a) Evolution of the migration speed inside a reference frame that rises vertically with mean sea level for the simulations in panels b (no sea level rise, indicated by dots), d ($SLR = 1cm/yr$, indicated by circles) and f ($SLR = 2cm/yr$, indicated by crosses). $c_b = 0.15gL^{-1}$. (c-f) Evolution from the equilibrium profile of panel b with time steps of 20.4 yrs over 165 yrs (panels c&d) and with steps of 10.2 yrs over 165 yrs (panels e&f). (b,c&e) The evolution in a static reference frame, from the dashed initial profile via light yellow to dark red. The dotted lines indicate the top of the tidal range. (d&f) The evolution inside a rising reference frame.

currents induces a strong negative feedback loop (*Maan et al.*, 2015), so that the bed is restored after a storm/wave event. On the upper flat, however, the tide-induced bed shear stress decreases with increasing bed level (implying a positive/reinforcing feedback loop), whereas the wave-induced bed shear stress is rather independent of the local bed level. Thus, there is no (strong) restoring feedback mechanism op the upper flat (*Maan et al.*, 2015). Here, local erosion by wind waves directly influences the long-term sediment budget. On the other hand, salt marsh vegetation dissipates the wave energy and limits the wave impact, so that bed erosion just seaward of the salt marsh is expected to dominate R. Hence, we concentrate on the erosion at the border between the bare flat and the salt marsh. Additional benefits of considering the vegetation line can be (1) its detectability, for instance by remote sensing (*Li et al.*, 2014), and (2) the direct way in which the horizontal retreat can be determined in case of landward retreat of the marsh edge, i.e. without the need to measure vertical bed level changes. Alternatively, however, R can be determined from the vertical bed level changes, divided by the local cross-sectional slope (following Equation 3.6 in in Chapter 3).

Yang et al. (2003b) documented daily bed level changes over a period of two years to study the morphological changes in response to storms versus calm weather of an intertidal flat at the Nanhui coast in the Yangtze Estuary (see Figure 4.8 for the location). The largest event during this 2-yr period was Typhoon Paibaian (12 Beaufort), which resulted in maximum bed level changes of $-21cm$ at the border between the marsh and the bare flat. This corresponds to a landward retreat of about $60m$ (based on Figure 2 of *Yang et al.* (2003b)).

However, of additional importance are the temporally larger accretion rates after storms, benefitting from the temporarily higher suspended sediment concentrations (*Yang et al.*, 2003b; *Zhu et al.*, 2017). These reduce the net effect of the storms. To bring this into account, one can consider the total period during which the bed level was lower than before the storm, in combination with the 'normal' accretion rates (i.e. those in case of calm weather, without prior storm). In case of Typhoon Paibaian, this period was about 10 days during a season with maximum sediment discharge by the Yangtze River (*Yang et al.*, 2003b). Based on the documented information by *Yang et al.* (2003b), we here estimate the normal seasonal accretion rates to be $\sim 7mm/day$ (about twice the yearly average (*Yang et al.*, 2003b)). This implies a missed vertical growth of $70mm$, which can be translated into a horizontal retreat of $\sim 19m$ (using a rough estimate of the local cross-sectional slope of $1:270$, based on Figure 2 of *Yang et al.* (2003b)).

In another study, *Zhu et al.* (2017) reported on the bed level changes on the East Chongming mudflat (see Figure 4.8 for the location) over a full spring-neap cycle with a mean wind speed close to the yearly average. The forces induced by tides and waves were varying during the field campaign, so that periods of erosion and accretion alternated. At the border between the flat and the salt marsh, erosion only occurred during periods of moderate to strong winds ($\geq 5m/s$). The total local erosion during these periods (i.e. neglecting the accretion during the calm periods) was $5mm$, equivalent to a horizontal retreat of $1.13m$ (based on a local slope of 1:227 obtained from the authors). Also in this case, the actual effect might have been smaller due to temporally larger SSCs after the windy periods. However, the field campaign was too short to estimate the average accretion rates during calm weather and from the data it is not possible to determine the
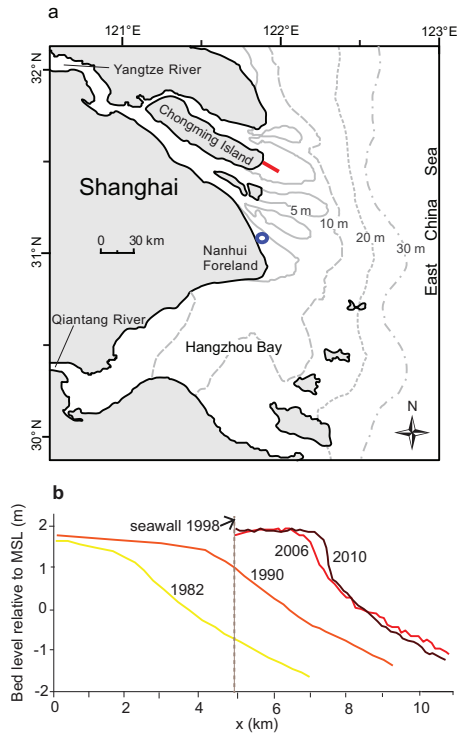
Figure 4.8: (A) Map of the Yangtze River Delta. The red line indicates the transect of Panel A, the blue circle indicates the site where erosion by typhoons was measured by *Yang et al.* (2003b). (B) Observed transverse profiles near mean sea level at Eastern Chongming Island, modified from *Yang et al.* (2001). Indicated distances are relative to the 1980 seawall.

'normal' accretion rates (i.e. without prior storm). Extrapolating the $1.13 m$ per spring-neap cycle gives an upper estimate for the retreat of $27 m/yr$. Note that this value is in the same order of magnitude as the simulated values for $20 cm$ wind waves of $R = -24 m/yr$, which is actually a typical wave height on the Yangtze flats for moderate wind conditions (*Zhu et al.*, 2017). Taking a year of average wave conditions and one major storm for a 'representative impact', we end up with a typical retreat of $R = -46 m/yr$.

An estimate for the critical *SSC* With an estimate of R, we can roughly calculate the critical reduction in the SSC for which the East Chongming flats (Figure 4.8) converge towards retreating systems. To this end, we adopt an historical seaward progradation speed of $300 m/yr$ (*Yang et al.*, 2001) and take $v_{new} = 0$:

$$\frac{v_{new} - R}{v_{old} - R} = \frac{0 + 46}{300 + 46} = \left(\frac{c_{new}}{c_{old}} \right)^{1.5}, \tag{4.16}$$

which yields $\frac{c_{new}}{c_{old}} \approx 0.26$. This fraction is larger than the reduction in SSC in the river, but is yet significantly smaller than the recent reduction factors measured in the estuary, i.e. about 0.8 (*Li et al.*, 2014; *Yang et al.*, 2015). This suggests that the flats at East Chongming can currently still prograde, as is in agreement with observations (*Li et al.*, 2014).

For an estimation of the reduction in the local SSC and progradation speed, we can consider the change in the cross-sectional profile slope. The cross-sectional slope on the lower flat of the transect in Figure 4.8 increased roughly 20% in the recent 20 years. This suggests a reduction in the SSC of approximately 40%, i.e.:

$$\frac{c_{new}}{c_{old}} = \left(\frac{\beta_{old}}{\beta_{new}} \right)^2 = 0.8^2 = 0.64. \tag{4.17}$$

The observed change in cross-sectional slope furthermore suggests a current progradation speed of about $131 m/yr$ (obtained by applying Eq.4.13 with $R = -46 m/yr$), which agrees with the observed expansion of the upper tidal flat (estimated from Figure 4.8 to be about $125 m/yr$). The trend in Figure 4.8 is moreover coherent with the average trend of the intertidal wetland at East Chongming, which already has been shown to be closely correlated with the fluvial sediment supply by previous studies (*Li et al.*, 2014).

The effect of the projected sea level rise Projections of the local sea level rise in the East China Sea for the 21st century vary between $31 cm$ and $1.1 m$ (*Jevrejava et al.*, 2016; *Cheng et al.*, 2017). Taking the average of about $0.7 m$, this implies an average rate of sea level rise of about $7 mm/yr$. Assuming a gentle slope of $1:2000$, this corresponds with a horizontal retreat of $14 m/yr$. Substituting this value for v_{new} in Eq.4.15, gives a shrinkage factor of $\frac{c_{new}}{c_{old}} = 0.31$ relative to the year 1990. For smaller shrinkage factors, a shift from a rising and prograding sytem into a retreating and submerging system (relative to mean sea level) can be expected by the year 2100 for an average scenario of local sea level rise.

4.5. CONCLUSIONS

We showed that the relationship between the progradation speed and the sediment concentration is stronger than linear and provided an explanation for it. Furthermore we found a linear relationship between the progradation speed and the rate of sea level rise. Given a measured combination of progradation speed and suspended sediment concentration, these relationships can be used to make rough projections for different scenarios of changing sediment concentrations and sea level rise. An estimate for the 'wave-induced retreat' is thereby needed. We applied the relationships on the horizontally prograding flats in the Yangtze Estuary to obtain a critical shrinkage factor of about 0.3 relative to the year 1990. This means that at least 30% of the SSC in 1990 is required to keep up with a sea level rise of $7\,mm\,yr^{-1}$ (i.e. the projected mean rate until 2100). When such a tipping point is passed, transverse tidal currents over the submerging flat might increase significantly with rising water levels, resulting in accelerated coastal retreat. Models including salt marshes are needed to get more insight in the non-linear behavior after the tipping point is reached.

REFERENCES

Chen, Y., Dong, J., Xiao, X., Zhang, M., Tian, B., Zhou, Y., Li, B. & Ma, Z. (2016). Land claim and loss of tidal flats in the Yangtze Estuary. *Scientific Reports*, *6*(1), 24018. https://doi.org/10.1038/srep24018

Chen, Y., Zhang, S., Huang, D., Li, B. L., Liu, J., Liu, W. et al. (2017). The development of China's Yangtze River Economic Belt: how to make it in a green way? *Science Bulletin*, 62(9), 648-651. https://dx.doi.org/10.1016/j.scib.2017.04.009

Cheng, H. Q., & Chen, J. Y. (2017). Adapting cities to sea level rise: A perspective from Chinese deltas. *Advances in Climate Change Research*, *8*(2), 130-136. https://doi.org/10.1016/j.accre.2017.05.006

Jevrejeva, S., Jackson, L. P., Riva, R. E. M., Grinsted, A. & Moore, J.C. (2016). Coastal sea level rise with warming above 2 C. *Proceedings of the National Academy of Sciences*, *113*(47), 13342-13347. https://doi.org/10.1073/pnas.1605312113

Friedrichs, C. T. (2011), Tidal Flat morphodynamics: A synthesis, In *Treatise on Estuarine and Coastal Science* E. Wolanski and D. McLusky (eds.), Academic Press, Waltham, pp 137-137, ISBN 9780080878850, http://dx.doi.org/10.1016/B978-0-12-374711-2.00307-7.

Friedrichs, C. T. & Aubrey, D.G. (1996), Uniform Bottom Shear Stress and Equilibrium Hyposometry of Intertidal Flats, in *Mixing in Estuaries and Coastal Seas, Coastal and Estuarine Studies*, Vol. 50, edited by C. Pattiaratchi, pp. 405-429, AGU, Washington, D.C., doi:10.1029/CE050p0405

Le Hir, P., Roberts, W., Cazaillet, O., Christie, M., Bassoullet, P. & Bacher, C. (2000). Characterization of intertidal flat hydrodynamics. *Continental shelf research*, *20*(12-13), 1433-1459. https://doi.org/10.1016/S0278-4343(00)00031-5

4

Li, P., Yang, S.L., Milliman, J.D., Xu, K.H., Qin, W.H., Wu, C. S., Chen, Y. P. & Shi, B. W. (2012). Spatial, Temporal, and Human-Induced Variations in Suspended Sediment Concentration in the Surface Waters of the Yangtze Estuary and Adjacent Coastal Areas. *Estuaries and Coasts*, *35*(5), 1316-1327. https://doi.org/10.1007/s12237-012-9523-x

Li, X. J., Zhou, Y., Zhang, L. & Kuang, R. (2014). Shoreline change of Chongming Dongtan and response to river sediment load: a remote sensing assessment. *Journal of Hydrology*, *511*, 432-442. https://doi.org/10.1016/j.jhydrol.2014.02.013

Liu, X. J., S. Gao, Y. P. Wang (2011), Modeling profile shape evolution for accreting tidal flats composed of mud and sand: A case study of the central Jiangsu coast, China, *Continental Shelf Research*, *31*, 1750-1760. https://doi.org/10.1016/j.csr.2011.08.002

Luan, H. L., Ding, P. X., Wang, Z. B., Ge, J. Z. & Yang, S. L. (2016). Decadal morphological evolution of the Yangtze Estuary in response to river input changes and estuarine engineering projects, *Geomorphology*, *265*, 12-23. https://doi.org/10.1016/j.geomorph.2016.04.022

Luan, H. L., Ding, P. X., Wang, Z. B. & Ge, J. Z. (2017). Process-based morphodynamic modeling of the Yangtze Estuary at a decadal timescale: Controls on estuarine evolution and future trends. *Geomorphology*, *290*, 347-364. https://doi.org/10.1016/j.geomorph.2017.04.016

Luo, X. X., Yang, S. L., Wang, R. S., Zhang, C. Y. & Li, P. (2017). New evidence of Yangtze delta recession after closing of the Three Gorges Dam. *Scientific Reports*, *7*, 1-10. https://doi.org/0.1038/srep41735

Ma, Z., Melville, D. S., Liu, J., Chen, Y., Yang, H., Ren, W, Zhang, Z., Piersma, T. & Li,B. (2014). Rethinking China's new great wall. *Science*, *346*(6212), 912-914. https://doi.org/10.1126/science.1257258

Maan, D. C., van Prooijen, B. C., Wang, Z. B., de Vriend, H. J. (2015). Do intertidal flats ever reach equilibrium? *Journal of Geophysical Research: Earth Surface*, *120*(11). https://doi.org/10.1002/2014JF003311

Maan D.C., B.C.van Prooijen, and Z.B. Wang. (2018), Progradation speed of tide-dominated tidal flats decreases stronger than linearly with decreasing sediment availability and linearly with sea level rise, *Geophysical Research Letters*, *45*. https://doi.org/10.1029/2018GL079933

Mariotti, G. & Fagherazzi, S. (2010). A numerical model for the coupled long-term evolution of salt marshes and tidal flats. *Journal of Geophysical Research: Earth Surface*, *115*(F1). https://doi.org/10.1029/2009JF001326

Pritchard, D., Hogg, A. J. & Roberts, W. (2002), Morphological modelling of intertidal mudflats: the role of cross-shore tidal currents, *Continental Shelf Research*, *22*, 1887-1895, doi:10.1016/S0278-4343(02)00044-4.

4

Pritchard, D. & Hogg, A. J. (2003) Cross-shore sediment transport and the equilibrium morphology of mudflats under tidal currents *J. Geophys. Res.*, *108*(C10), 3313, doi:10.1029/2002JC001570.

Syvitski, J. P. M. & Saito, Y. (2007). Morphodynamics of deltas under the influence of humans. *Global and Planetary Change*, *57*(3-4), 261-282. https://doi.org/10.1016/j.gloplacha.2006.12.001

Syvitski, J. P., Kettner, A. J., Overeem, I., Hutton, E. W., Hannon, M. T., Brakenridge, G. R., et al. (2009). Sinking deltas due to human activities. *Nature Geoscience*, 2(10), 681-686. https://doi.org/10.1038/ngeo629

Van Straaten, L. & P. H. Kuenen (1958). Tidal action as a cause of clay accumulation. *Journal of Sedimentary Research*, *28*(4), 406-413. https://doi.org/10.1306/74D70826-2B21-11D7-8648000102C1865D

Tambroni, N. & Seminara, G. (2012), A one-dimensional eco-geomorphic model of marsh response to sea level rise: Wind effects, dynamics of the marsh border and equilibrium, *J. Geophys. Research*, *117*, F03026, doi:10.1029/2012JF002363.

De Vriend, H. J., Wang, Z.B., Ysebaert, T., Herman, P. M. J. & Ding, P. (2011). Eco-morphological problems in the yangtze estuary and the western scheldt. *Wetlands*, *31*(6), 1033-1042. https://doi.org/10.1007/s13157-011-0239-7

Waeles, B., P. Le Hir & R. S. Jacinto (2004), Modelisation morphodynamique cross-shore d'un estran vaseux, *Comptes Rendus Geoscience*, *336*, 1025-1033, doi:10.1016/j.crte.2004.03.011.

Wang, Z. B., Van Maren, D. S., Ding, P.X., Yang, S. L., Van Prooijen, B. C., De Vet, P. L. M., et al. (2015). Human impacts on morphodynamic thresholds in estuarine systems. *Continental shelf research*, *111*, 174-183. https://doi.org/10.1016/j.csr.2015.08.009

Wei, W., Tang, Z., Dai, Z., Lin, Y., Ge, Z. & Gao, J. (2015). Variations in tidal flats of the Changjiang (Yangtze) Estuary during 1950s2010s: future crisis and policy implication. *Ocean & Coastal Management*, *108*, 89-96. https://doi.org/10.1016/j.ocecoaman.2014.05.018

Yafeng, S., Jiwen, Z., Zhiren, X., Zixiu, J., Zixun, J. & Guishan, Y. (2000). Prediction and prevention of the impacts of sea level rise on the Yangtze River Delta and its adjacent areas. *Science in China Series D: Earth Sciences*, *43*(4), 412-422. https://doi.org/10.1007/BF02959452

Yang, S. L., Ding, P. X. & Chen, S. L. (2001). Changes in progradation rate of the tidal flats at the mouth of the Changjiang (Yangtze) River, China.*Geomorphology*, *38*, 167180. https://doi.org/10.1016/S0169-555X(00)00079-9

Yang, S. L., Belkin, I. M., Belkina, A. I., Zhao, Q. Y., Zhu, J. & Ding, P. X. (2003). Delta response to decline in sediment supply from the Yangtze River: evidence of the recent four decades and expectations for the next half-century. *Estuarine, Coastal and Shelf Science*, *57*(4), 689-699. https://doi.org/10.1016/S0272-7714(02)00409-2

4

Yang, S. L., Friedrichs, C. T., Shi, Z., Ding, P. X., Zhu, J. & Zhao, Q. Y. (2003). Morphological response of tidal marshes, flats and channels of the outer Yangtze River mouth to a major storm. *Estuaries*, *26*(6), 1416-1425. https://doi.org/10.1007/BF02803650

Yang, S. L., Li, M., Dai, S. B., Liu, Z., Zhang, J. & Ding, P. X. (2006). Drastic decrease in sediment supply from the Yangtze River and its challenge to coastal wetland management. *Geophysical Research Letters*, *33*(6). https://doi.org/10.1029/2005GL025507

Yang, Z. S., Wang, H. J., Saito, Y., Milliman, J.D., Xu, K., Qiao, S. & Shi, G. (2006). Dam impacts on the Changjiang (Yangtze) River sediment discharge to the sea: The past 55 years and after the Three Gorges Dam. *Water resources research*, *42*(4). https://doi.org/10.1029/2005WR003970

Yang, S. L., Zhang, J. & Xu, X. J. (2007). Influence of the Three Gorges Dam on downstream delivery of sediment and its environmental implications, Yangtze River. *Geophysical Research Letters*, *34*(10). https://doi.org/10.1029/2007GL029472

Yang, Y. P., Zhang, M. J., Li, Y. T. & Zhang, W. (2015). The variations of suspended sediment concentration in Yangtze River Estuary. *Journal of Hydrodynamics*, *27*(6), 845-856. https://doi.org/10.1016/S1001-6058(15)60547-9

Zhu, Q., van Prooijen, B. C., Wang, Z. B. & Yang, S. L. (2017). Bed-level changes on intertidal wetland in response to waves and tides: A case study from the Yangtze River Delta. *Marine Geology*, *385*, 160-172. https://doi.org/10.1016/j.margeo.2017.01.003

4

5

NEGATIVE FEEDBACK LOOPS CONTROL STABLE FRINGING FLATS

We apply a 2-D horizontal process based model (Delft3D) to study the feedback mechanisms that control the long-term evolution of a fringing intertidal flat in the Western Scheldt Estuary. The hydrodynamic model is validated using a comparison with measurements on the intertidal flat and the sediment transport module is calibrated against long-term morphology data. First, the processes that lead to net sediment exchange between channel and flat are studied. Then, long-term simulations are performed and the dependency of sediment fluxes on the tidal flat bathymetry, and the corresponding morphodynamic feedback mechanisms are explained. In the long run, relatively stable states can be approached, which are shown to be typical for wave-dominated fringing mudflats. The system behavior can be explained by the typical feedback mechanisms between the intertidal bathymetry and the hydrodynamic forces on the flat. In the subtidal domain, the impact of small (5-10cm) wind waves increases with a rising elevation due to decreasing water depths. In the intertidal domain, the wave impact increases with increasing cross-sectional slope due to wave shoaling. These relationships result in negative (stabilizing) morphodynamic feedback loops. The tidal current velocities and tide-induced bed shear stresses, on the other hand, are largely determined by the typical horizontal geometry. A stabilizing feedback loop fails, so that there is no trend towards an equilibrium state in the absence of wind waves.

5.1. INTRODUCTION

During their flyways across the world, many migrating birds make their necessary rest stops on intertidal flats (*van de Kam et al.*, 2010). These are gently sloped mudflats inside tidal seas or estuaries that fall dry during part of the tidal cycle, revealing a rich collection of seafood. Hence, intertidal flats are indispensable for the ecology far outside their boundaries and therefore often protected by international legislation (such as the

Ramsar Convention for the protection of migratory birds and the European Natura2000 legislation).

However, loss of intertidal area, for instance due to climate change (sea level rise) and human activities, is a common phenomenon (*Syvitski et al.*, 2005; *Airoldi & Beck*, 2007; *Fitzgerald et al.*, 2008; *Sampath et al.*, 2011; *Tambroni & Seminara*, 2012; *Eelkema et al.*, 2013; *Kirwan & Megonigal*, 2013; *Ma et al.*, 2014; *Passeri et al.*, 2015; *Hoitink et al.*, 2017; *de Vet*, 2017). The difficulties in 'managing' the long-term morphodynamics are related to the many interacting factors that play a role in the morphodynamic evolution: the (bio)morphology affects the shear stresses induced by wind waves and tidal currents, as well as the patterns of sediment transport. In turn, it is shaped by the same factors. These interactions make the morphodynamic system behave like a 'complex system' (*Meadows & Wright*, 2009), characterized by the occurrence of stable states (*van Goor et al.*, 2003; *Fagherazzi et al.*, 2006, 2007; *Bearman et al.*, 2010; *Friedrichs*, 2011) and sudden transitions between these states (*Wang et al.*, 2015).

One of the main difficulties with complex systems is that they are typically part of and built-up from other (larger and smaller scale) systems. This makes it hard to demarcate an (approximately) closed (sub)system from an overall complex system in order to split-up the system into smaller and simpler parts. Hence, simplification is not always possible. Depending on the typical interactions and hierarchies inside the natural system, a system can be too big and complicated to simulate and resolve. In the field of morphodynamics, the need of high spatial and temporal resolutions in combination with large model domains and time spans easily leads to unacceptably long calculation times.

Yet, to control and design the intertidal environment, and to protect it against SLR, we need an understanding of the system dynamics (*van Maanen et al.*, 2013; *Passeri et al.*, 2015). We have to discover its core and try to make a simpler, understandable, model of the real world (*Zhou et al.*, 2017), including the dominant feedback mechanisms between the interdepenent hydrodynamics, morphodynamics and ecology.

This starts with making a careful and realistic description of the considered system and its boundaries. Boundaries need to be found that are (approximately) independent of the evolution of the modeled factors. Note that the boundary conditions do not have to represent *constant* driving factors. They can be stochastic and varying in time, as long as they behave independently from the evolution inside the model domain. In this paper, we focus on fringing intertidal flats, which are relatively easy to demarcate. These fringing intertidal areas are relatively small compared to the whole coastal or estuarine system, and even to the single adjacent channels. Due to their smaller scale, it is often possible to find model boundaries that behave (approximately) independently of the considered intertidal evolution. This gives the possibility to model these mudflats as relatively small-scale closed systems, which increases their resolvability.

Once we are able to simulate the intertidal evolution, we can look for 'steady states' in the simulations. We here define the 'steady states' as states in which certain properties of the intertidal morphology remain constant in time, controlled by negative morphodynamic feedback loops. Observations and numerical studies show that the evolution of fringing intertidal flats often converges towards these states (*Roberts et al.*, 2000; *Pritchard et al.*, 2002; *Fagherazzi et al.*, 2006, 2007; *Bearman et al.*, 2010; *Friedrichs*, 2011;

Liu et al., 2011; *Hu et al.*, 2015; *Maan et al.*, 2015). Fig.5.1 provides examples of approximately stable profiles for fringing intertidal flats in the Western Scheldt Estuary. Steady states can be seen as signals given by the underlying system, helpful clues to unravel its functioning. As an equilibrium state is not self-evident, the observation of conserved properties leads to the important question: 'why are they conserved?' The answer to this question can reveal the whole dynamics of the system.
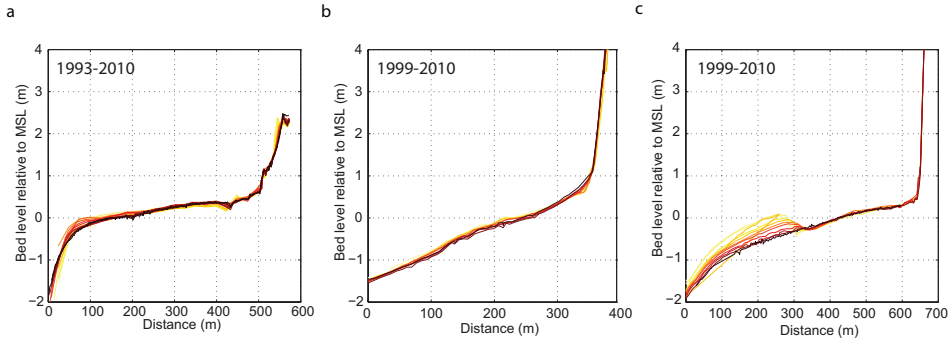

Figure 5.1: (a-c) Cross-shore transects of approximately stable fringing flats at respectively the locations A-C in Fig.5.2 (source: Rijkswaterstaat, part of the Dutch Ministry of Infrastructure and the Environment). Consecutive years are indicated from yellow to dark red over total periods of 17 yrs (a) and 11 yrs (b and c).

The kind of steady states that can be approached is characteristic for the type of intertidal system that is considered. It depends on the particular processes resulting in (net) sediment transport and the typical dependencies of these processes on the intertidal bathymetry. Earlier studies on intertidal flats that could be modeled within 0-D and 1-D frameworks indicated the dominance of feedback mechanisms between the hydrodynamic forcing and the intertidal flat bathymetry (*Friedrichs & Aubrey*, 1996; *Roberts et al.*, 2000; *Le Hir et al.*, 2000; *Fagherazzi et al.*, 2007; *de Swart & Zimmerman*, 2009; *Maan et al.*, 2015).

Systems in which the hydrodynamic forces are controlled by locally-generated wind waves, for instance, were found to converge towards horizontal platforms with a constant (equilibrium) elevation (*Fagherazzi et al.*, 2007; *Marani et al.*, 2007; *de Swart & Zimmerman*, 2009; *Marani et al.*, 2010). These states are controlled by the dominance of a negative feedback loop between the bed elevation and the bed shear stress induced by locally-generated wind waves (*Fagherazzi et al.*, 2007; *de Swart & Zimmerman*, 2009).

Systems in which wind waves act together with cross-shore tidal currents (or in which cross-shore tidal currents act alone), were found to converge into horizontally migrating states with a conserved cross-shore profile (*Pritchard et al.*, 2002; *Waeles et al.*, 2004; *Maan et al.*, 2015). These migrating states can be explained by continuous accretion on the upper intertidal flat (due to generally lower hydrodynamic energy and bed shear stresses), in combination with restoring negative feedback loops between the landward bathymetry and the cross-shore current velocities on the lower tidal flat (*Maan et al.*, 2015).

Systems in which the hydrodynamics and sediment transport are influenced by both

long-shore and cross-shore currents (i.e those that should be described inside 2-D or 3-D frameworks), are in many ways more complicated than systems that can be resolved with a 1-D model. Inside these systems, the intertidal morphology might also have an important effect on the two-dimensional flow and advection patterns over the flat. Hence, the internal feedback mechanisms that control the long-term evolution of this kind of systems are yet to be unraveled.
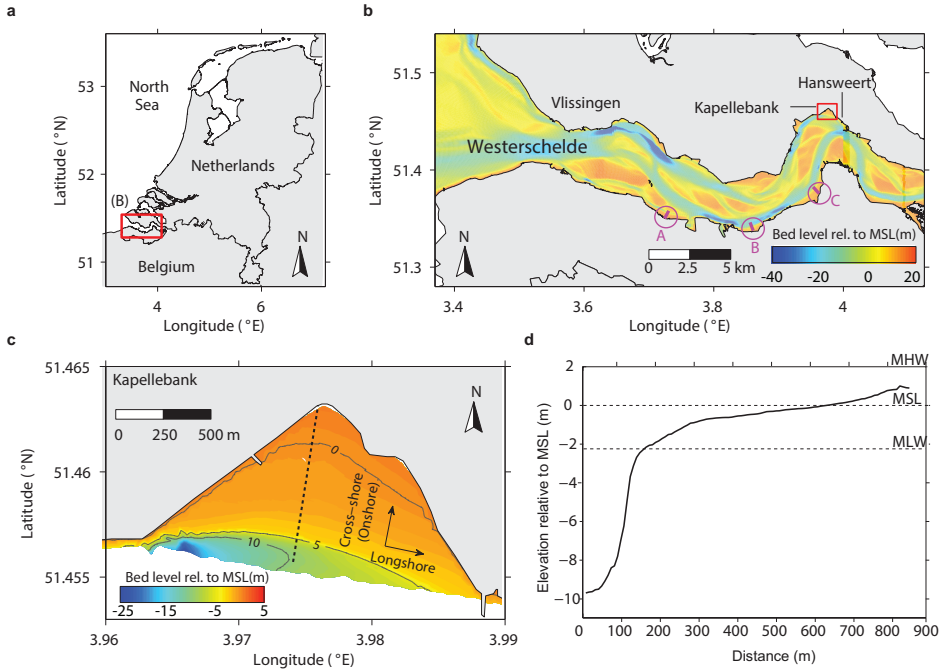

Figure 5.2: (a) Map of the Netherlands with the location of the Kapellebank indicated by the red square. (b) Part of the Western Scheldt Estuary with the location of the Kapellebank indicated by the red square. (c) Schematic representation of the Kapellebank. (d) A transect on the Kapellebank, indicated by the dotted line in panel c.

In this paper, we perform a case study on the *Kapellebank*, a fringing intertidal flat at the outside of a channel-bend in the Western Scheldt Estuary (The Netherlands, Fig.5.2). The hydrodynamic forces are induced by long- and cross-shore tidal currents and wind waves. We investigate the morphodynamic evolution of the flat with a 2-D horizontal process based model (Delft3D). The hydrodynamic model is validated against field observations, which were carried out during a field campaign in April 2014, see also (*Zhu et al.*, 2017). After the validation process, however, the boundary conditions are simplified by considering only the M2 and M4 tidal components. This is a necessary procedure for system analysis, because of the need to compare averages over closed tidal periods.

Hence, the model is applied for studying the response of an initial bathymetry to simplified boundary conditions. We are interested in how this adjustment process looks and whether or not these types of systems evolve into equilibrium states in the long run. For understanding the processes and feedback mechanisms that underlie the long-term

evolution of the intertidal flat, we follow a 'top-down approach'. The morphodynamic evolution is first described. Subsequently, the sedimentation rates and the hydrodynamic forces at different moments in the evolution are determined. Considering how these signals change in time and are correlated with each other, reveals important information about the morphodynamic feedback mechanisms that control the evolution of the intertidal flat. Conclusions will be drawn about (1) whether steady states exist and (2) the feedback mechanisms that underlie the long-term evolution of fringing flats like the Kapellebank.

5.2. STUDY AREA & FIELD DATA

5.2.1. SYSTEM DESCRIPTION: MAIN ACTORS AND DRIVING FORCES

We consider the Kapellebank, a fringing tidal flat along the north bank of the Western Scheldt Estuary in the Netherlands (Fig.5.2). The tidal wave is semi-diurnal, with a mean tidal range of around $4m$. The flat faces a tidal channel on the south, which is delineated by a steep slope in the bathymetry (Panel d of Fig.5.2). Due to the close vicinity of the channel, the long-shore current dominates over the cross-shore current on the intertidal flat. However, due to the typical 2D geometry (i.e. the location of the channel and the enclosure by the two dikes, Fig.5.2), the long-shore current is strongly reduced in the cross-shore direction. This is characteristic for fringing intertidal flats.

The measured cross-shore flow velocities can be compared with the analytically calculated flow velocities resulting from the filling and emptying of the intertidal volume at high tide (i.e. the tidal prism of the Kapellebank). Such a comparison reveals that only a small part (< 20%) of the cross-shore currents represents the filling and emptying of the intertidal volume. Hence, this system is totally different from the ones discussed in *Roberts et al.* (2000); *Pritchard et al.* (2002); *Maan et al.* (2015), where the cross-shore tidal current, caused by filling and emptying of the tidal prism of the intertidal basin, is the dominant eroding force.

The main wind direction is from the south-west, implying that the Kapellebank is often exposed to wind waves. The average wave height in the channel is about $15cm$, and the average of the highest 10% is about $30cm$. During the field campaign at the Kapellebank, wave heights were measured at the interface between the channel and the flat (*Zhu et al.*, 2017). Typical values were found to be $4cm$ during calm conditions and about $13cm$ during strong winds (6 Bft). The sediment on the flat is cohesive, with a median grain size less than $50\mu m$ (*Zhu et al.*, 2017; *Guo et al.*, 2018). The suspended sediment concentration in the channels of the estuary fluctuates strongly in space and time, around an average of about $40mg/L$ (*van der Wal et al.*, 2010).

5.2.2. OBSERVED TRENDS

The channel adjacent to the Kapellebank was subject to morphological changes during the last decades, see Fig.5.3. Both natural processes and human interferences have influenced the channel development (*Jeuken & Wang*, 2010). The change from channel erosion (1965-1990) to channel deposition (1990-2015) is to a great extent attributed to dumping activities that started around 1990 (*Jeuken & Wang*, 2010).

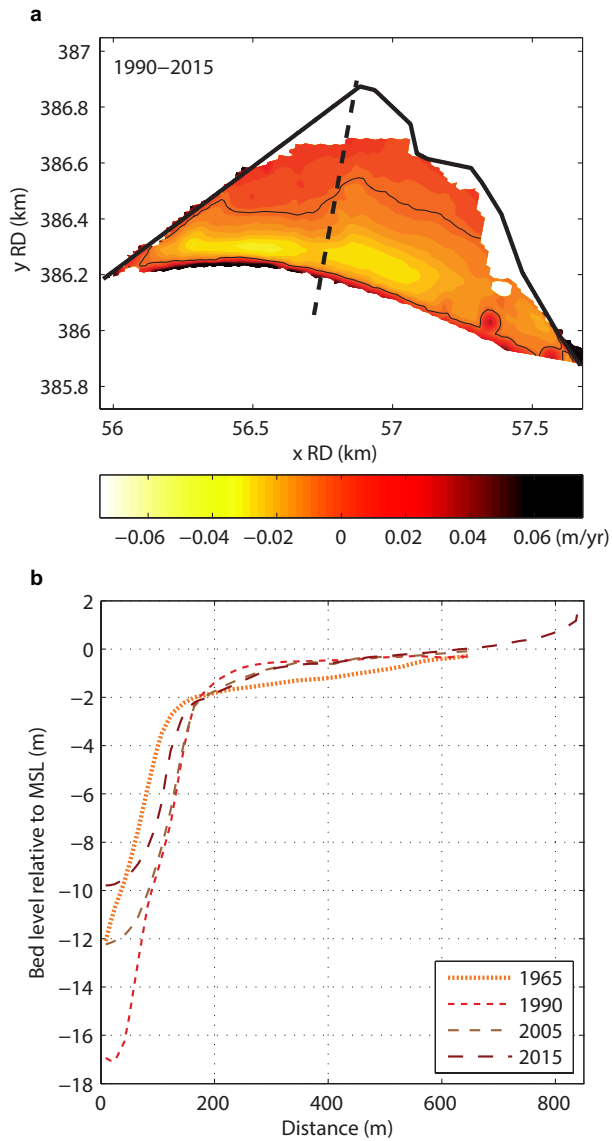It is likely that the morphodynamic trend inside the channel influenced the morpho-

a

b

Figure 5.3: Observed long-term trend on the Kapellebank (based on the 'Vaklodingen' dataset (*Wiegmann et al.*, 2005), see also *de Vet* (2017)). (a) Bed level differences, indicated in yearly averages (in meters) over the period 1990-2015. The black dashed lines indicate the position of the cross-shore transects of panel b. (b) Snapshots of the cross-shore transects in the period 1965-2015. The Kapellebank steepened over the last 25 years. In the last decade, the intertidal bathymetry is relatively stable, despite the large sedimentation rates inside the channel.

dynamic evolution of the flat. Larger (smaller) tidal current velocities inside the channel lead to more (less) erosion at the interface between the channel and the flat. Hence, narrowing of the flat is correlated with an eroding channel and widening of the flat with an accretive channel (see Fig.5.3). Furthermore, variations inside the channel can affect the sediment availability: in case of an erosive channel, more sediment might be available, leading to larger accretion rates on the tidal flat. In case of an accretive channel, on the other hand, fine sediment might settle inside the channel instead (leading to smaller accretion rates on the flat). Variations in the channel might also affect the types of available sediment. Because tidal channels are generally sandier than the intertidal mudflats, an erosive channel might result in a smaller mud-sand ratio on the intertidal flat. The sediment type influences the erodability of the bed and the morphodynamic evolution of the intertidal flat (*Zhu et al.*, 2017).

Despite the influence of the morphodynamically unstable adjacent channel in the past, the intertidal flat (except at its interface with the channel) is found to be rather stable over the last decade (Fig.5.3). Measurements on the site show that the erodibility of the bed is high (*Zhu et al.*, 2017), so that the current relative stability cannot be attributed to an inactive bed. Instead, it should be explained by counteracting gross deposition and gross erosion rates.

The apparent stability of the flat suggests that the current evolution of the intertidal flat is controlled by processes that are rather independent of the morphological developments of the adjacent channel. These include the forces exerted by wind waves and sediment supply from nearby tidal flats, which is hold in suspension by tidal flow in the channel. Note that the changes inside the channel can be dominated by coarser sediment. Stable fringing intertidal flats in combination with highly dynamic (widening or narrowing) adjacent channels has also been noted by *van der Wegen et al.* (2017) for flats in the San Francisco Bay, see also *Bearman et al.* (2010).

5.3. THE MODEL

5.3.1. DELFT3D

We calculate the morphodynamic evolution of the Kapellebank with a process-based morphodynamic Delft3D model (*Lesser et al.*, 2004; *Roelvink*, 2006; *Deltares*, 2014a), coupled to the SWAN (third generation) wave module (*Booij et al.*, 1999; *Ris et al.*, 1999). The flow is calculated by solving the 2-D horizontal shallow water equations (*Deltares*, 2014a) on a high resolution grid with grid sizes varying from about $80m$ inside the channel to less than $10m$ on the Kapellebank (see Fig.5.4). The waves are calculated on a separate grid, with a resolution of about $10m$ on the intertidal flat (Fig.5.4), see *Deltares* (2014b) for a description of the wave module.

Two-dimensional transport of suspended sediment is calculated by solving the two-dimensional advection-dispersion equation:

$$\frac{\partial ch}{\partial t} + \frac{\partial uch}{\partial x} + \frac{\partial vch}{\partial y} = \frac{\partial}{\partial x}\left(Kh\frac{\partial c}{\partial x}\right) + \frac{\partial}{\partial y}\left(Kh\frac{\partial c}{\partial y}\right) + E - D,$$

where c is the suspended sediment concentration, K is the dispersion coefficient,
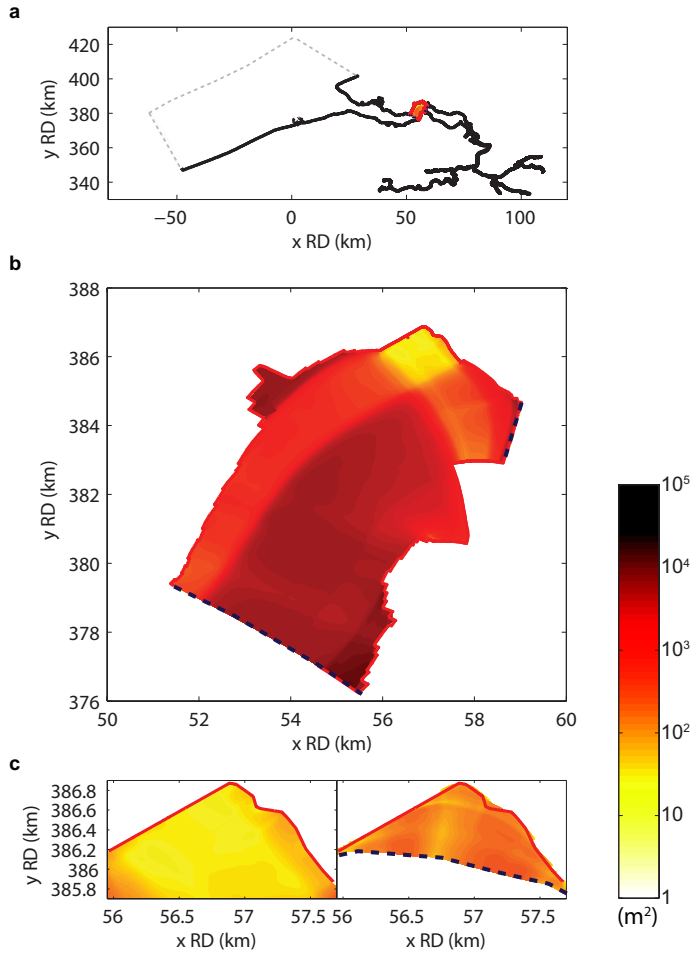
Figure 5.4: The closed (solid lines) and open (dotted lines) model boundaries and the grid resolution (in m^2, indicated in colors) of (a) the larger scale hydrodynamic model 'Nevla' (*Hartsuiker & van Banning*, 2004; *Maximova et. al.*, 2009a,b,c)), (b) the nested flow model, and (c) a close-up view of the nested flow model (left) and the wave model (right).

and E and D are the vertical erosion and deposition fluxes, respectively. These are computed by (*Ariathurai*, 1974; *Winterwerp & Van Kesteren*, 2004):

$$E = \max\left[m_e\left(\frac{\tau_b}{\tau_{cr}} - 1\right), 0\right] \tag{5.1}$$

and

$$D = c \cdot w_s, \tag{5.2}$$

where m_e is the erosion rate coefficient, τ_b the bed shear stress, τ_{cr} the critical bed shear stress for erosion and w_s the settling velocity.

The morphodynamics of the Kapellebank are calculated for elevations above $MSL - 4m$, while the geometry and the surrounding morphology (including the bathymetry of the channel) is fixed. Because we only consider changes on the flat, we use one single sediment class that represents the cohesive sediment on the flats (*Zhu et al.*, 2017). The bed configuration of the Kapellebank in 2015 has been taken as initial condition. The suspended sediment concentration in the adjacent channel is controlled by applying a constant concentration at both flow model boundaries and preventing sedimentation elsewhere than on the Kapellebank.

Note that we need a high resolution grid for calculating the complex tidal currents on the intertidal flat, which makes the calculations time-consuming. To speed up the simulation process, we apply a morphological factor (*Lesser et al.*, 2004; *Roelvink*, 2006). The value of the morphological factor (Table 5.1) is adjusted during the simulation according to the size of the morphodynamic changes. Its effect is validated by using smaller factors at different stages of the evolution.

5.3.2. BOUNDARY CONDITIONS

The model contains two open boundaries (Fig.5.4). Water levels and flow velocities need to be prescribed at the southern and eastern open boundary respectively. Naturally, the boundary conditions are assumed to be independent driving factors. Note that the flow through the boundaries is mainly determined by the larger-scale factors and the geometry of the estuary, so that its dependency on the bathymetry of the Kapellebank is small.

Time series of water levels and flow velocities at the southern and eastern open boundary respectively (see Fig.5.4), were generated by the larger scale model applications *Kustzuid* and *Nevla-Schelde*. These describe the hydrodynamic flow in the North Sea and through the Western Scheldt Estuary respectively (*Hartsuiker & van Banning*, 2004; *Maximova et. al.*, 2009a,b,c), see *Eelkema et al.* (2012) for a description of the Kustzuid model. These models were in turn driven by field observations. For a careful system analysis, we need to compare net sediment fluxes over closed tidal periods at different phases of the morphodynamic evolution. This procedure is much easier if we use a periodic tidal variation. Therefore, we perform a harmonic analysis on the time series and drive the model with the obtained M2 and M4 components only. The tidal amplitudes of the constituents were found the be about $1.9m$ (M2) and $0.1m$ (M4), with a phase difference of about 90° (small spatial variations in these values occur).

At both flow model boundaries, a constant suspended sediment concentration is imposed, which represents the background concentration. Hence, it is assumed that the

fine sediment at the boundaries comes typically from the other (surrounding) tidal flats and is not significantly influenced by erosion on the Kapellebank itself. This approximation can be justified by the relative small-scale of the Kapellebank, compared with the surrounding flats. Tidal variation in the sediment concentration at the boundary is not taken into account. A constant wave height, wave period (see Table 5.1) and wave direction (south-west) is applied at the open boundary of the wave model.

Table 5.1: The model parameter values.

Parameter	Symbol	Value	Unit
Delft3D-Flow			
Manning coefficient	n	0.02	$ms^{-\frac{1}{3}}$
Settling velocity	w_s	$0.3 \cdot 10^{-3}$	ms^{-1}
Specific density for cohesive sediment	ρ_w	2650	kgm^{-3}
Dry bed density	ρ_{dry}	1000	kgm^{-3}
Reference density for hindered settling	C_{ref}	1600	kgm^{-3}
Horizontal eddy viscosity	ν_H	0.1	$m^2 s^{-1}$
Horizontal eddy diffusivity	K	1	$m^2 s^{-1}$
Critical bed shear stress for erosion	$\tau_{cr,e}$	0.35	Nm^{-2}
Erosion coefficient	m_e	$1.7 \cdot 10^{-5}$	$kgm^{-2}s^{-1}$
Time step	Δt	3.75	s
Minimum depth for sediment calculation	h_{dry}	0.3	m
Morphological factor	M	1000-4000	–
Delft3D-Wave:			
Wave height	H	0.075-0.085	m
Wave peak period	T	2	s
Bottom roughness length scale (*Madsen et al.*, 1988)	K_N	0.05	m

5.3.3. VALIDATION AND CALIBRATION

Hydrodynamic model   The hydrodynamic model is validated against field observations. To this end, the model is forced with time series (based on field observations) of water levels and flow velocities at the southern and eastern open model boundary respectively, see Fig.5.4. The model simulations are compared with field observations on the Kapellebank that were carried out by Rijkswaterstaat (part of the Dutch Ministry of Infrastructure and Environment) in May 2014. Figure 5.5 shows a comparison of the measured and simulated flow speeds and directions on the intertidal flat. Driven by the flow from the main channel, the flow direction is from the west towards the east during flood tide. During much of the ebb tide, the flow enters at the east-flank and leaves at the west-flank Fig.5.5), steered by the channel flow. In the end of the ebb tide, eddy circulations occur at the lower west flank of the flat, at the interface with the channel (see L1 in Fig.5.5). The ability of the model to resolve these eddies was improved by refining the grid significantly and using the Horizontal Large Eddy Simulation (HLES) sub-grid module in Delft3D. For the purpose of this study, however, the faster version is applied, not including the eddy circulations. Because the eddies only occur locally, they presumably
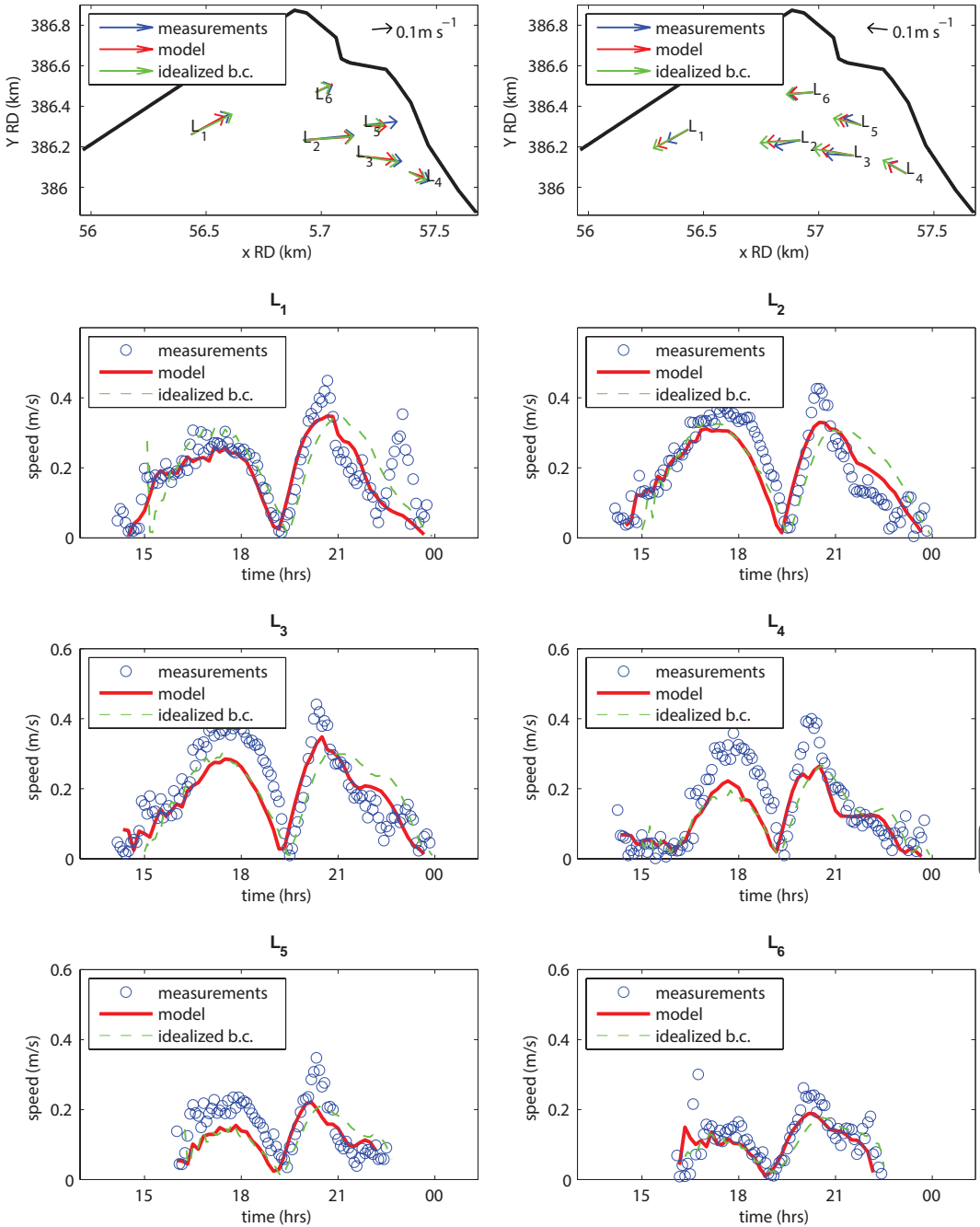
Figure 5.5: (Above) Measured and modeled velocity vectors at the locations L1-L6 during an average tide, time-averaged over flood tide (left panel) and ebb tide (right panel). (Below) Measured and modeled time series of the absolute velocity during an average tide at locations L1-L6 on the intertidal flat. The green dashed line indicates the model simulation for idealized boundary conditions, i.e. including M2 and M4 tidal components only.

do not significantly influence the overall mudflat morphodynamics.

The capability of the model largely depends on the applied spatial resolution (Fig.5.4). Model parameters that influence the flow velocities over the Kapellebank are furthermore the bottom roughness (we use the setting of the Nevla model; a Manning coefficient of $0.02 ms^{-\frac{1}{3}}$) and the horizontal eddy viscosity, which was calibrated against the field observations (determined as $0.1 m^2/s$ for the applied grid).

Sediment transport module   Compared with the hydrodynamic module, the sediment transport module needs a more extensive calibration process. We calibrated the model against the observed long-term trend (Fig.5.3). To this end, simulations were performed that differ in the wave height, the wind force, the erosion threshold, the erosion coefficient, the settling velocity and the (background) sediment concentration inside the adjacent channel. Fig.5.6 gives an overview of the simulated sedimentation/erosion patterns for a limited number of the applied parameter sets.

Measurement data (over the period 1990-2015) shows long-term erosion over the whole width of the lower and intermediate intertidal flat (see the top left panel of Fig.5.6). This pattern corresponds best with simulations that include significant wind waves, in combination with a sufficiently low boundary concentration and settling velocity (for instance with the simulations in the red dotted box of Fig.5.6). The simulations without waves show too much accretion on the east side of the Kapellebank, see Fig.5.6. In combination with significant wind waves, the erosion threshold should be chosen sufficiently high to prevent an overestimation of the net erosion rates.

The effects of increasing the boundary concentration or the settling velocity on the sedimentation/erosion patterns were found to be rather similar to the effect of decreasing the wave height. Also, the effect of decreasing the erosion threshold was found to be comparable with the effect of increasing the wave height, see Fig.5.6. Hence, there exist several different parameter sets that give a fair fit with the observations.

For the main experiments, we chose the parameter values of the black surrounded panel in Fig.5.6. The settling velocity and wave period were taken as $0.3 mm/s$ and $2s$ respectively (corresponding with typical values obtained from the field measurements). To get insight into the sensitivity of the long-term morphodynamic behavior to the forcing parameters, we also performed additional long-term simulations for several different parameter sets (see Sections 5.4.3 & 5.4.4). From these simulations, it followed that a careful calibration process of the parameters in Fig.5.6 is necessary to simulate realistic trends (see section 5.4.3 for a further discussion). The complete set of the model input parameters is listed in Table 5.1.

5.4. Results and discussion

5.4.1. Initial bed shear stress and transport

The simulated (tidally averaged) total bed shear stress decreases towards the shore (Fig.5.7). Due to the presence of the channel and the orientation of the two dikes that enclose it, the long-shore current (and the tide-induced bed shear stress) is strongly reduced on the Kapellebank. The modeled wave-induced bed shear stress also shows a gradual decrease towards the shore. The shorewards decreasing bed shear stress favors net landward sed-
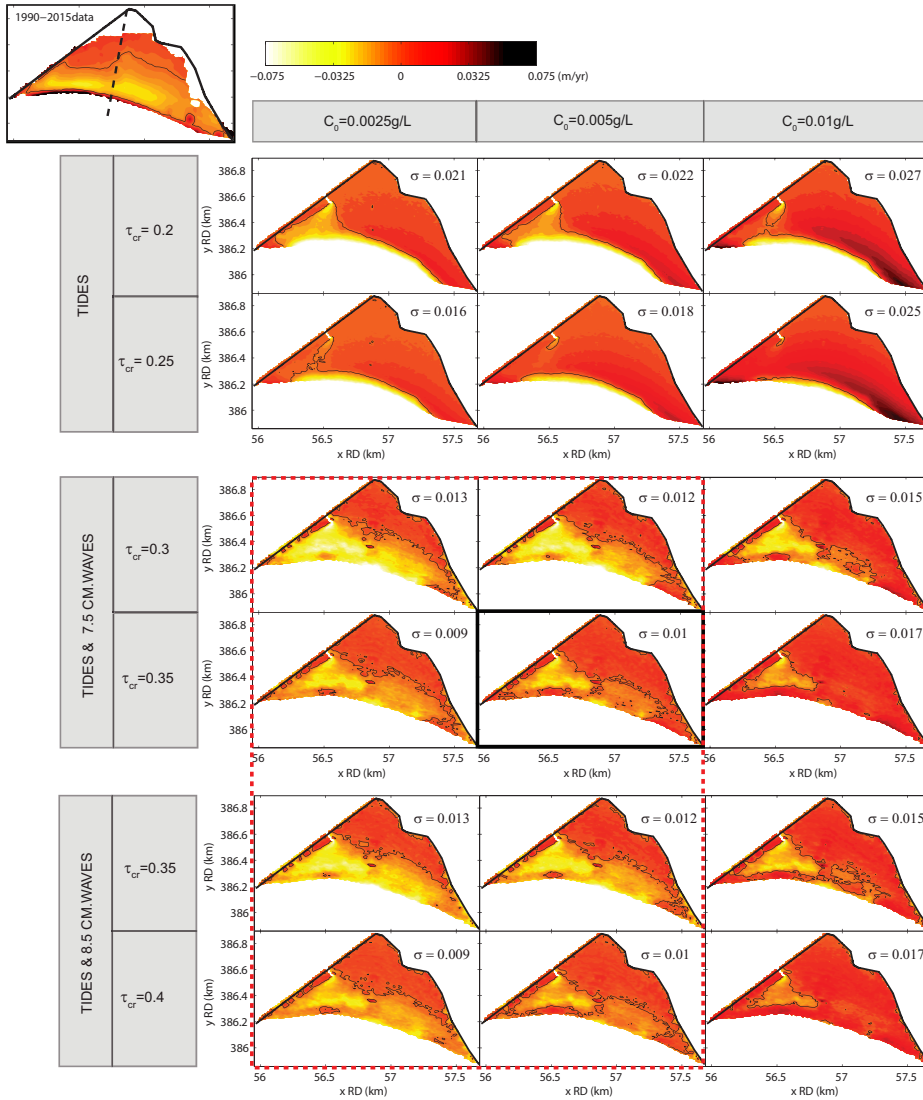
Figure 5.6: Modeled bed level changes over one tidal cycle (normalized to m/yr) on the present bed configuration of the Kapellebank (2015 data), for different boundary concentrations, erosion thresholds, and wave heights. The observed pattern is indicated at the top left. σ indicates the spatial average error of each simulation compared to the field data. The panels in the red dashed square are considered as 'good matches' and the parameters of the solid black surrounded panel are used for the main simulation.

iment advection (*Friedrichs*, 2011; *Gatto et al.*, 2017), see Fig.5.7.
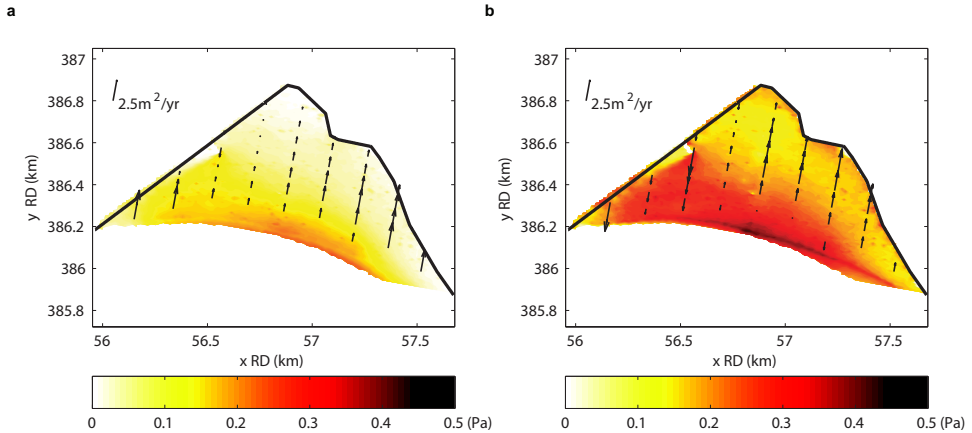

Figure 5.7: Maps of the tidally averaged bed shear stress (averaged over the period during which a location is flooded) and the cross-shore component of the net sediment transport per unit width (indicated by black arrows) on the current bed configuration of the Kapellebank (2015 data) in cases of (a) tidal currents only, and (b) tides plus wind waves. $\tau_{cr} = 0.3$ and $C_0 = 5mg/L$ in both simulations.

5.4.2. FEEDBACKS AND STATES

Long-term morphodynamic evolution is not a simple extrapolation of the initial sedimentation patterns on a (random) initial bathymetry. Instead, the typical internal morphodynamic feedbacks can play an important role in the long run. Through the morphodynamic feedback loops, initial imbalances can be diminished or amplified, resulting in self-maintaining states or trends. In this section, long-term simulations are performed and studied. We try to answer the qualitative questions of (1) whether or not steady states or trends occur and, if they occur, (2) what the underlying feedback mechanisms are. The answers to these questions are often more relevant than the initial response, because they depend less on (the combination of) the initial profile and the specific model parameters and boundary conditions. They are thus less sensitive to uncertainties in these factors. In fact, the use of simplified boundary conditions is only justified when concentrating on qualitative behavior. The states or trends that we are looking for are controlled by feedback loops between the intertidal bathymetry and the hydrodynamic forces and sediment fluxes, i.e. they are intrinsic properties of the system.

An equilibrium state   The long-term evolution of the Kapellebank for the calibrated parameter set is indicated in Fig.5.8. On the subtidal and lower intertidal flat, a balance is quickly established (within 15 years). After stabilization of the lower flat, the equilibrium state builds out landward, so that also the uppermost sections reach equilibrium eventually. The existence of an equilibrium state was further confirmed by a simulation from an alternative initial profile, which evolved into the same equilibrium state in the
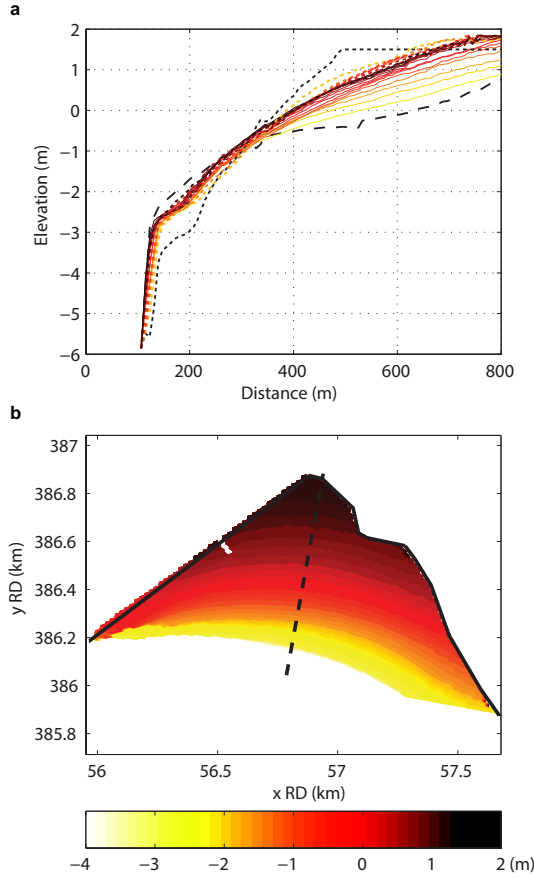
Figure 5.8: (a) Modeled evolution of a cross-shore transect (indicated by the dashed black line in panel b) from two different initial profiles (the dashed and dotted black lines), from yellow to dark red with time steps of 50 yrs and total time spans of respectively 600 yrs and 350 yrs. The initial bathymetries are (dashed) the bed configuration from 2015 and (dotted) that mirrored around the equilibrium bathymetry. The evolutions from the dashed and dotted initial profiles are indicated by solid and dotted lines respectively. The two simulations migrate towards identical equilibrium states (indicated by the red lines). (b) Map of the equilibrium bathymetry. The applied morphological factors varied between 1000 and 4000, maximum values were used towards the end of the simulations.
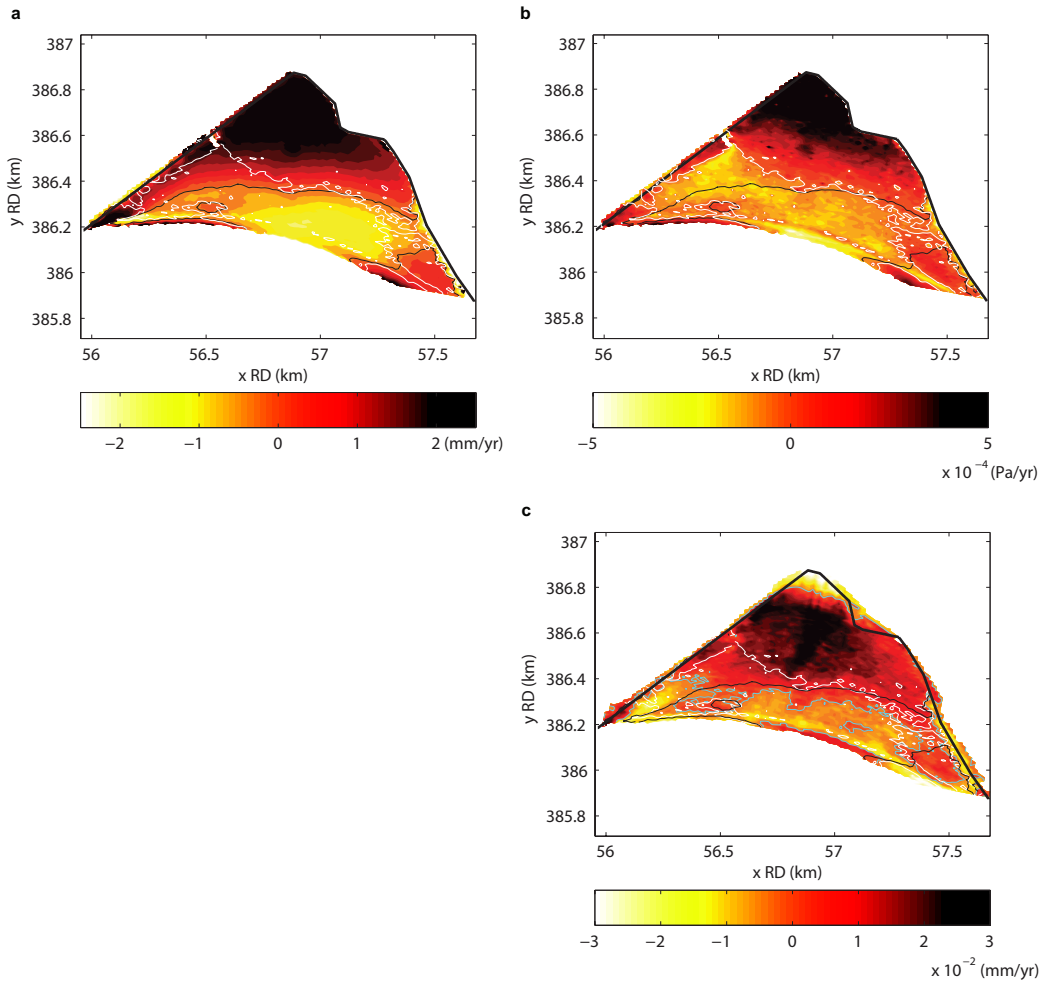
Figure 5.9: (a) Bed level changes over the first 300 years of the modeled evolution (accretion over time is positive), normalized to mm/yr. (b) Corresponding changes in the tidally averaged bed shear stress (in Pa/yr). (c) Corresponding changes in averaged wave height in shallow waters (less than 1 m deep), normalized to mm/yr (with cyan zero-contour lines).(a-c) The thin black and white lines are zero-contour lines of the changes in the bed level and the erosion flux respectively. At most locations, the figure shows positive correlations between the bed level, the erosion rates and the wave height, which suggests a negative (stabilizing) internal feedback mechanism.

same chronological sequence (i.e. from the lower flat towards the shore, see Fig.5.8).

Now that a steady state is recognized, we can search for the underlying controlling feedback mechanisms. We first consider the correlations between changes in the bed level and changes in the bed shear stress over the morphodynamic evolution. On much of the intertidal flat, bed shear stresses increase (decrease) with an increasing (decreasing) bed elevation, which suggests a stabilizing feedback loop between the bed level and the local bed shear stress (see Figure 5.9).

In Fig.5.10 (panel b) it can be seen that the observed changes in the bed shear stress are mainly due to changes in the wave-induced component. Whereas the wave-induced bed shear stress on the upper flat is doubled during the morphodynamic evolution, the tide-induced bed shear stress on the equilibrium profile is almost identical to that on the initial profile (see Fig.5.10). This shows that the tide-induced bed shear stress is approximately independent of the intertidal bathymetry. This makes the long-shore tidal current (and its shoreward decay) an 'independent driving factor', largely determined by the typical horizontal geometry of the site. The wave-induced erosion, on the other hand, is a 'state variable', which adjusts during the bathymetric evolution.

Two wave-related processes are found to play an important stabilizing role. Firstly, the local real-time wave-induced bed shear stress generally increases with a decreasing water depth (see Fig.5.11). With rising and falling tide, maximum wave-induced bed shear stresses were found close to the tidal fronts, i.e. in shallow waters of less than $1m$ deep (Fig.5.11), which corresponds with observations in the field (*Zhu et al.*, 2017), see also (*Roberts et al.*, 2000). The high bed shear stresses in shallow waters effectively result in high local sediment concentration peaks that subsequently result in a dispersive sediment transport in the offshore direction. Because the tidally averaged water depth mainly decreases with an increasing bed elevation, the relationship in Fig.5.11 results in a negative morphodynamic feedback loop on much of the intertidal flat. This stabilizing feedback loop is particularly strong in the subtidal domain, where the minimum water depth strongly increases with an eroding bed.

Around the low water line (LWL), however, a decrease (increase) in the bed level results in a longer (shorter) period of shallow water and associated maximum bed shear stresses (because shallow water here coincides with slack water), see *Waeles et al.* (2004). Note that the bed above the LWL falls temporarily dry, whereas the bed below the LWL is wet during the whole tidal cycle. As a consequence of the longer (shorter) period of shallow water, a lowering (raising) of the bed can locally result in greater (smaller) gross erosion rates. This relationship implies a locally positive feedback loop, so that an unstable section can be expected around the LWL.

However, after the subtidal region reaches an equilibrium elevation that matches its specific supply (which is mainly determined by the sediment concentration inside the channel), another stabilizing feedback loop becomes dominant on the intertidal flat. Namely, landward of the stable section, an increase in the local bed level leads to an increase in the cross-sectional slope (in offshore direction) and thereby to an increase in the relative importance of wave shoaling versus wave dissipation (*Le Hir et al.*, 2000). Fig.5.9 (panel c) indicates a strong correlation between the changes in the tidally averaged erosion rates and in the wave height in shallow waters. This suggests a causal relationship, i.e. the tidally averaged bed shear stress increases as a consequence of an
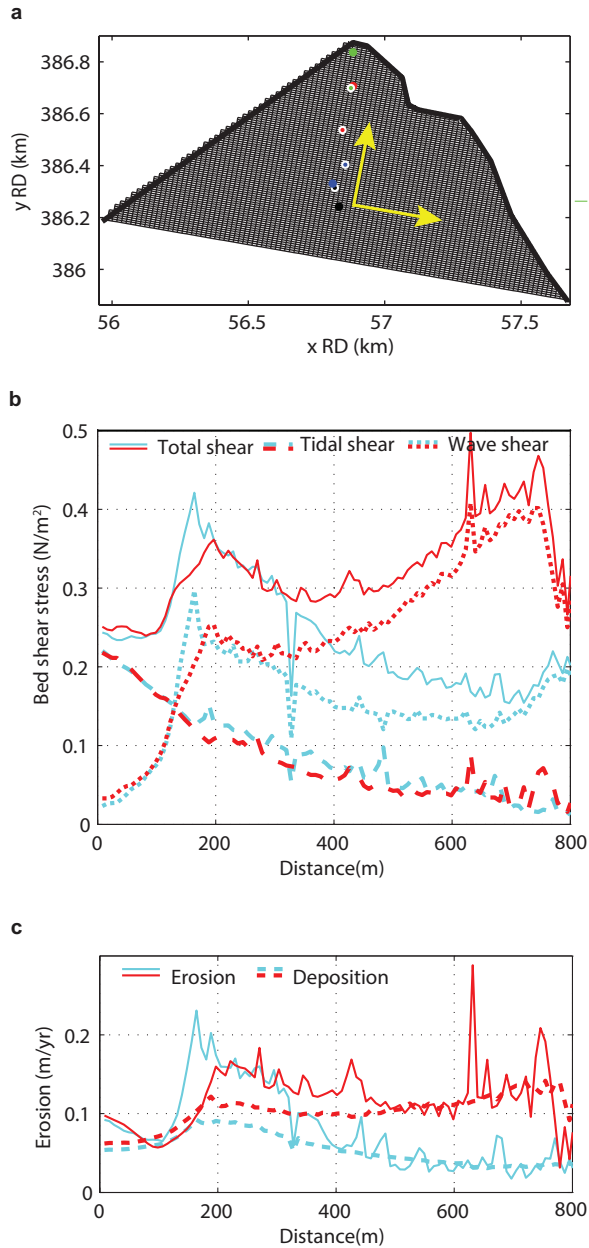
5

a

b

c

Figure 5.10: (a) Grid used for creation of panels *b&c*; the data is translated on this grid for making long-shore averages. The colored dots refer to the locations of the data in Fig.5.11. (b) Cross-shore variation in the bed shear stresses on the initial bathymetry (cyan) and on the equilibrium bathymetry (red), averaged over the long-shore dimension and the tidal (flooded) period. The total and tide-induced bed shear stresses are model output. The wave-induced bed shear stress is roughly estimated by the difference between these components. (c) Cross-shore variation in the gross erosion and deposition rates (in *m/yr*).
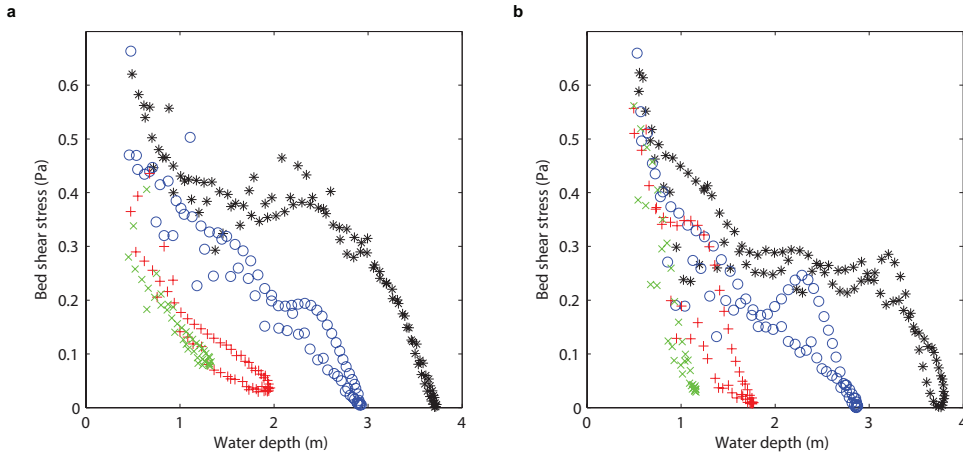
Figure 5.11: Modeled instantaneous total (tide- plus wave-induced) bed shear stress versus water depth during one tidal cycle at different locations, indicated with different colors and markers, on (a) the initial bathymetry, and (b) the equilibrium bathymetry. The locations are indicated in Fig.5.10 by dots in the corresponding color. Those with white edges refer to points on the equilibrium configuration. Maximum bed shear stresses occur in shallow water. In the equilibrium state, the bed shear stresses in shallow water (less than 1m deep) are rather similar at the different locations.

increasing wave height in shallow waters. Hence, wave shoaling is important. Fig.5.12 outlines this concept.

The evolution towards a morphodynamic equilibrium state can now be understood as follows. The water column contains sediment that originates from a range of locations. The deposition fluxes are therefore the spatially integrated (smoothed) counterparts of the locally determined gross erosion fluxes. As a result, each location initially experiences an imbalance between the local gross erosion flux and the more global deposition flux. These imbalances naturally result in net sedimentation/erosion rates. The resulting bed level changes influence the local gross erosion fluxes and, via the stabilizing feedback loop described in the previous paragraphs, the spatial variations in the gross erosion fluxes diminish. This process smoothens the concentration fields further and hence, uniform conditions are approached. Uniform distributions in the tidally averaged hydrodynamic energy, erosion rates and suspended sediment concentrations (Fig.5.10) minimalizes the net sediment exchange by lag effects (*Friedrichs*, 2011; *Gatto et al.*, 2017). Hence, despite the increase in the gross sediment fluxes on the intertidal flat, the net sediment exchange is minimalized. An equilibrium state is reached when the net horizontal sediment transport vanishes. Fig. 5.13 shows a clear reduction in the net horizontal sediment transport. The remaining net transport in the equilibrium state (Panel b) balances out over multiple tidal cycles. Note that the morphodynamic feedback loops between the bathymetry and the hydrodynamic forces are subject to time lags, resulting in (small) oscillatory behavior around a steady bathymetry.

Note that the description above is an approximation. Sediment exchange rates do not only depend on spatial gradients in the suspended sediment concentrations, but
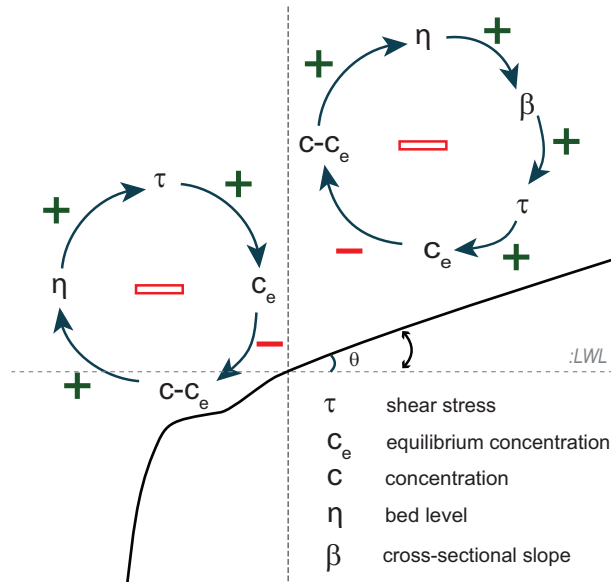
Figure 5.12: Feedback loops on a fringing flat. The arrows with positive and negative signs indicate positive and negative influences in-between the parameters respectively. An uneven number of negative influences within a loop results in a negative feedback loop, whereas an even number of negative influences within a loop results in a positive feedback loop. The bed levels are controlled by two negative feedback loops, i.e. if the depositon flux is initially larger than the erosion flux, i.e. $c - c_e > 0$, net sedimentation occurs and the bed level rises, increasing the wave impact and the bed shear stresses, which diminishes the initial imbalance. On the intertidal flat the feedback loop between the local bed level and bed shear stress occurs via the (seaward) cross-sectional slope, due to wave shoaling.

also on their correlation with the flow velocities (see also *Friedrichs* (2011)). Bed erosion only influences the (im)balances at neighboring sections if the locally eroded sediment is transported before local settling. Although the erosion and concentration fields in the equilibrium state are found to be rather uniform, spatial variations might thus remain. Hence, the erosion rates around MSL can be somewhat smaller than the spatial average (see the red curve in panel c of Fig.5.10), due to the locally more optimal correlation between the erosion peaks and the maximum flow advection velocities. Also, the tidally averaged concentrations on the intertidal flat are higher than those inside the tidal channel (see the red curve in panel c of Fig.5.10), because a larger proportion of the eroded sediment settles locally again, instead of being exchanged. Irrespective of the specific concentration field that results in a vanishing net sediment transport, however, an equilibrium state can only be established via a stabilizing morphodynamic feedback loop as described above.

Due to the large exchange rate with the tidal channel via the long-shore channel flow, the 'background concentration' at the lower flat is relatively independent of the upper sections, so that a balance is first established on the lower (sub-tidal) flat and subsequently expands landward via adjustments in the landward bathymetry (see Fig.5.8).
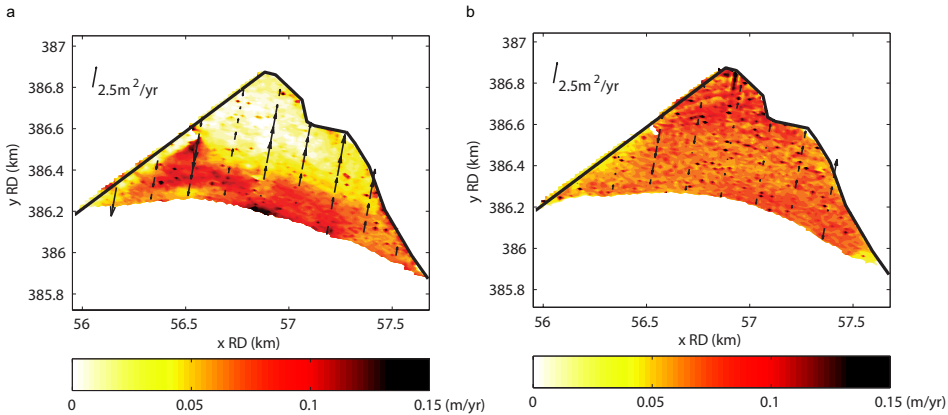
Figure 5.13: Maps of the tidally averaged *gross* erosion (translated in m/yr, indicated in colors) and the cross-shore component of the sediment transport per unit width (indicated by black arrows) on (a) the initial intertidal bathymetry and (b) the equilibrium bathymetry.

The impact of small waves The impact of wind waves on the Kapellebank is principally different from the situation described by *Friedrichs & Aubrey* (1996). *Friedrichs & Aubrey* (1996) derived concave equilibrium profiles by assuming a homogeneous distribution of the maximum bed shear stress. Our model results confirm an (almost) uniform distribution of the maximum bed shear stress and gross erosion rates, but the profiles that we obtain are not concave. This is despite the strong dominance of the wind waves on the upper shore. The difference in the obtained equilibrium profiles can be explained by the different moment of maximum wave impact during the tidal cycle.

Friedrichs & Aubrey (1996) assumed maximum wave-induced forces during high water, when the fetch length is largest and the incoming wind waves are highest. This is probably a good assumption for higher incoming wind waves (*Le Hir et al.*, 2000). For small wind waves ($5 - 10cm$ high), however, maximum bed shear stresses are found in shallow waters, close to the tidal fronts (*Zhu et al.*, 2017), see also *Roberts et al.* (2000). In case of small wind waves, water depths during high tide are generally too large for optimal wave impact. The results of *Le Hir et al.* (2000) indicate that the section on an intertidal flat that experiences highest bed shear stresses a little after covering or before uncovering (instead of during high tide) increases with a decreasing wave height.

Hence, for small wind waves, at each moment in the tidal cycle, another location (always close to the tidal front) experiences maximum bed shear stress. The value of the maximum bed shear stress depends on the seaward bed slope via shoaling and dissipation processes. The assumption of a homogeneous distribution of the maximum bed shear stress (associated with an equilibrium state (*Friedrichs & Aubrey*, 1996), see also Fig.5.11, therefore leads to a homogeneous slope and hence to a linear cross-sectional profile. A linear profile can thus be expected close to the shore, where the tidal currents are negligible. Its slope will depend on parameters as the sediment supply, the incoming

wave height and the wave friction factor.

Note that the cross-shore transect of the modeled equilibrium state in this study (Fig.5.8), as well as the observed equilibrium profiles of other fringing flats in the Western Scheldt Estuary (Fig.5.1), are rather linear close to the shore, i.e. where long-shore currents fall to zero due to the embanked geometry. A linear equilibrium profile was also obtained by *van der Wegen et al.* (2017), who modeled the morphodynamic evolution of a fringing flat in the San Francisco Bay with a 1-D cross-shore model including similar small wind waves (and neglecting the long-shore tidal currents).

5.4.3. ALTERNATIVE PARAMETER SETS

Besides the simulation for the calibrated settings, we also considered long-term simulations for a few alternative parameter sets. From these simulations we found that the presence of wind waves does not necessarily result in an equilibrium state. In cases of a highly abundant sediment supply or a large erosion threshold, states of continuous accretion occur, see Fig.5.14. In cases of low sediment availability or high wind waves, on the other hand, states of continuous erosion occur. In these cases, the feedback mechanisms are in favor of an equilibrium state, but the erosion rates on the tidal flat are never strong enough (or remain too strong) to balance out the landward sediment transport (favored by the landward decay in the tidal energy). Hence the equilibrium state is a rather particular state and sensitive to the model parameters in Fig.5.6. However, equilibrium states were found for wave heights in the range $7.5 - 8.5 cm$ (with the other parameters identical to the 'default' run), see Fig.5.15, whereas wind waves of $9cm$ resulted in an equilibrium state below the intertidal range (Fig.5.16). Based on these results and the comparable effects of the different parameters (Fig.5.6), we estimate that at least the simulations within the parameter space indicated by the red dashed rectangle in Figure 5.6 migrate towards a stable intertidal area.

5.4.4. IN THE ABSENCE OF WIND WAVES

Furthermore, we considered simulations without wind waves. In the absence of wind waves, a stationary equilibrium state is never approached (see Fig. 5.17). The part of the intertidal flat that is initially accretive, remains accretive in the long run. The magnitudes of the net sedimentation rates on the intertidal flat decrease in the long run, but are persistent. The decrease in the net sedimentation rates can be explained by a reduction in the period during which the flat is flooded, and by a decrease in the flow advection rates (which are both consequences of an increasing bed elevation). The change in advection rates affects the effectiveness of the sediment exchange between the channel and the flat (*Pethick*, 1981), but it cannot change the spatial concentration gradients and the direction of the net sediment transport.

For an equilibrium state (different than the total infilling or erosion of the intertidal area) to exist, a mechanism is needed by which the differences between the erosion and deposition rates, and the incoming and outgoing sediment fluxes, are diminished. A trend towards an equilibrium state would for instance be possible if a local increase (decrease) in the bed level would result in an increase (decrease) in the local bed shear stresses and erosion rates.

However, the spatial variation in the erosion rates is largely controlled by the hori-
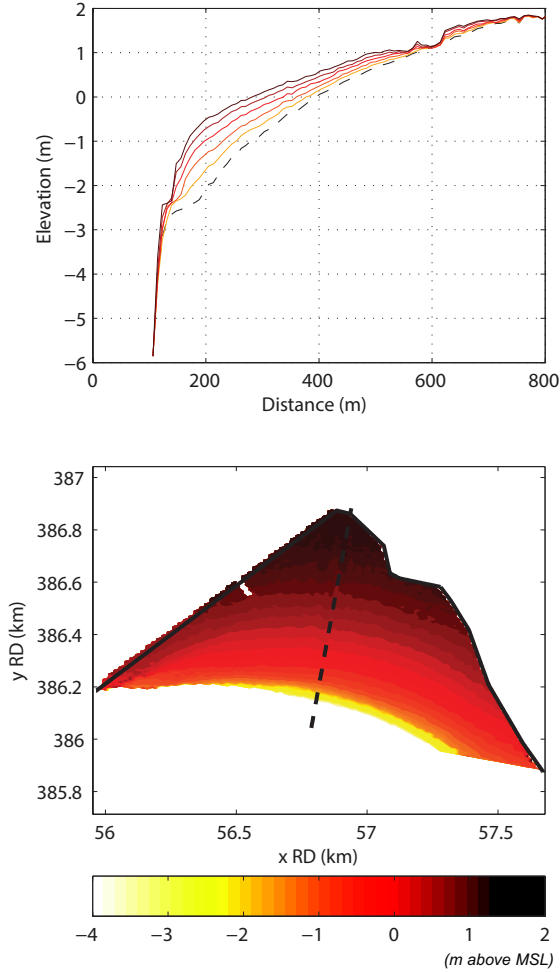
Figure 5.14: (a) Modeled evolution of an indicated bathymetry with 6.5cm wind waves (τ_{cr}=0.2 & C_0=5mg/L), a morphological factor of 4000 has been applied. The cross-section of the initial bathymetry (2015 data) is indicated by the dashed black line and the evolution occurs from yellow towards dark red, with time intervals of 25 yrs and a total time span of 125 yrs. There is no stabilizing trend. (b) Map of the bathymetry after 125 years of morphodynamic evolution.
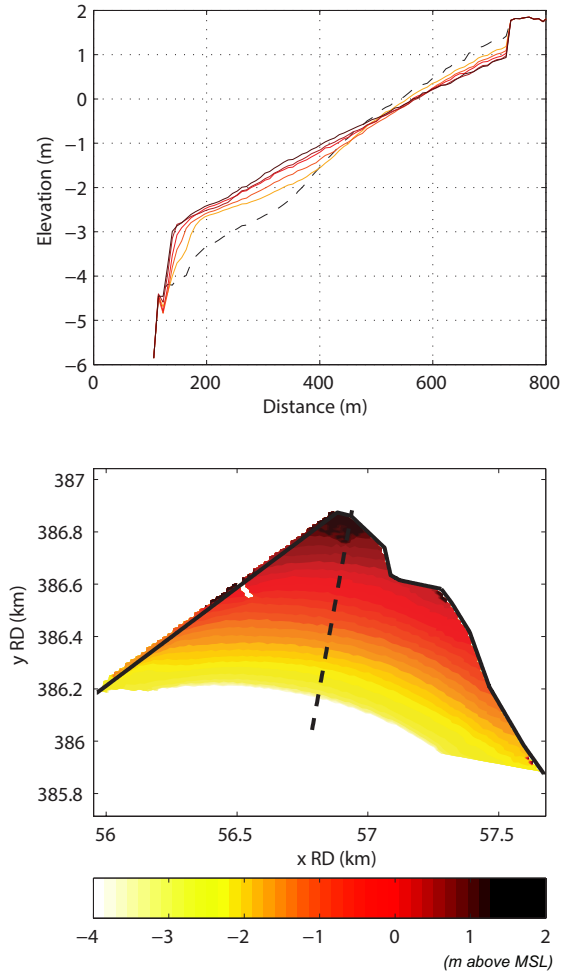
Figure 5.15: (a) Modeled evolution of an indicated bathymetry with $8.5cm$ wind waves (τ_{cr}=0.2 & C_0=5mg/L), a morphological factor of 4000 has been applied. The cross-section of the initial bathymetry (2015 data) is indicated by the dashed black line and the evolution occurs from yellow towards dark red, with time intervals of 25 yrs and a total time span of 125 yrs. A linear equilibrium profile is established. (b) Map of the bathymetry after 125 years of morphodynamic evolution.
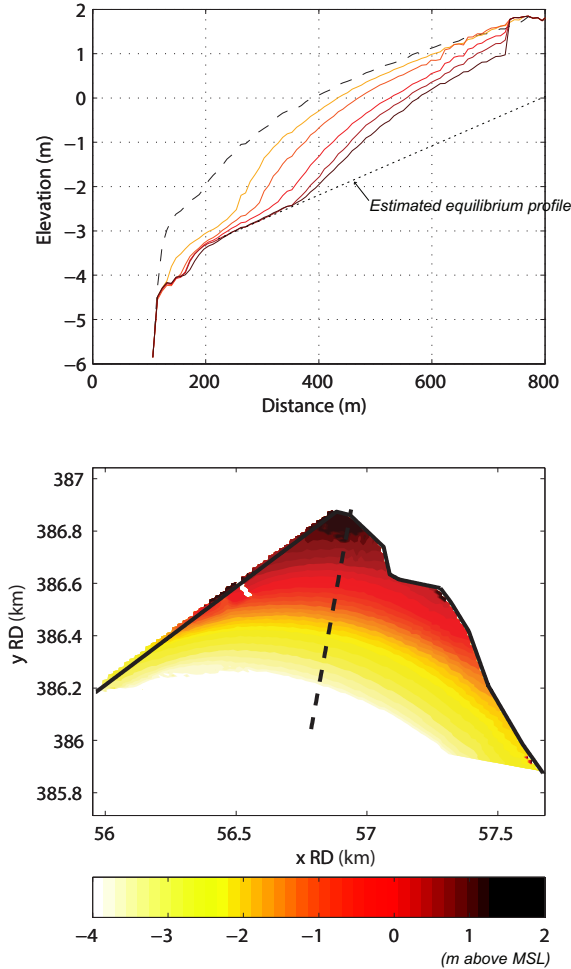
Figure 5.16: (a) Modeled evolution of an indicated bathymetry with $9cm$ wind waves (τ_{cr}=0.2 & C_0=5mg/L), a morphological factor of 4000 has been applied. The evolution occurs from yellow towards dark red, with time intervals of 25 yrs and a total time span of 125 yrs. After 125 yrs, the subtidal domain has been stabilized. Based on the typical evolution of fringing flats, an equilibrium state can also be expected for the rest of the flat. The expected equilibrium profile is indicated by the dotted line in the Figure. (b) Map of the bathymetry after 125 years of morphodynamic evolution.
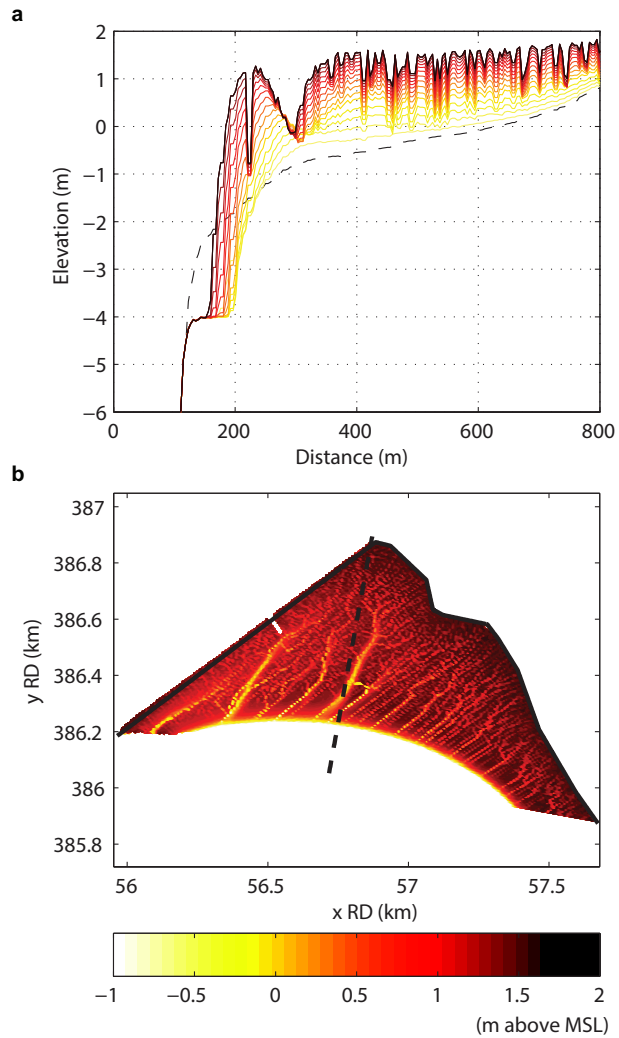
Figure 5.17: (a) The modeled evolution of the indicated transect in panel b, without wind waves (τ_{cr}=0.2 & C_0=5mg/L). The cross-section of the initial bathymetry (2015 data) is indicated by the dashed black line and the evolution occurs from yellow towards dark red, with time intervals of 25 yrs and a total time span of 375 yrs. (b) Map of the bathymetry after 375 years of morphodynamic evolution. A morphological factor of 1000 is applied.

zontal two dimensional geometry (the position of the dikes and the location of the channel), which is an independent driver. Furthermore, correlations between the bed level changes and gross erosion rates suggest a mostly positive (destabilizing) morphodynamic feedback loop between the variables (Fig. 5.18); erosion rates on the tidal flat are decreasing with a rising bed (due to decreasing long-shore tidal flow velocities). Hence, an initial deviation from an imaginary equilibrium state would be intensified by the internal feedback loops in the system. As a consequence, a stable equilibrium state cannot exist in the absence of wind waves.

Channel formation In the first decades, the accretion rates are maximal on the deeper parts of the intertidal area (closest to the channel), so that a flat intertidal platform is formed, see Fig.5.17 (panel b). This gently sloped bathymetry gives rise to the development of a structure of tidal creeks (see Fig.5.17, panel a).

The development of the channel network is a result of a positive feedback mechanism within the intertidal system, earlier described by *van Maanen et al.* (2015), see Fig.5.18. On an uneven bed, the flow finds less resistance on the lower bed elevations where the water depth is larger. Once a weak channel structure is initiated, the flow thus concentrates through the channels, inducing relatively large flow velocities and shear stresses there, which strengthens the channel structure. At a later stage, when the structure is (locally) well-developed, a further increase of the local channel depth does not further increase the amount of water flowing through the channel. From that moment on, a further deepening of the channel leads to a decrease in the local bed shear stress (due to a larger cross-sectional area), i.e. a negative feedback loop, so that the depth of the channels (relative to the surrounding flat) stabilizes (see Fig.5.17).

5.4.5. DO WE NEED A 2-D MODEL TO SIMULATE THE EQUILIBRIUM STATES?
Many previous studies have attempted to predict the equilibrium states of intertidal flats by 1-D cross-shore numerical and analytical models, neglecting the long-shore tidal current (*Friedrichs & Aubrey*, 1996; *Roberts et al.*, 2000; *Pritchard et al.*, 2002; *Mariotti & Fagherazzi*, 2010; *Hu et al.*, 2015; *Maan et al.*, 2015; *van der Wegen et al.*, 2017). The results in this paper can be used to validate this approach for fringing tidal flats. The results show that the long-shore tidal current does not significantly change during the bathymetric evolution. Wave-related feedback loops, on the other hand, underlie the evolution towards an equilbrium state. This suggests that modelling of the long-shore tidal current is not strictly needed. Hence, it is expected that comparable results can be obtained by 1-D cross-shore models including wave dissipation and wave shoaling. Largest deviations can be expected on the lower flat, where long-shore tidal current velocities are largest. 1-D models for fringing flats can therefore be improved by including a description of the decay of the long-shore tidal current (and associated bed shear stress) in the cross-shore direction.

5.4.6. BATTLE BETWEEN WAVES AND CROSS-SHORE TIDAL CURRENTS
Opposite to the bed shear stresses induced by cross-shore tidal currents and wind waves, which co-evolve with the system as state variables, the long-shore tidal current acts (approximately) as an 'independent driving factor'. Hence, the spatial variation in the long-
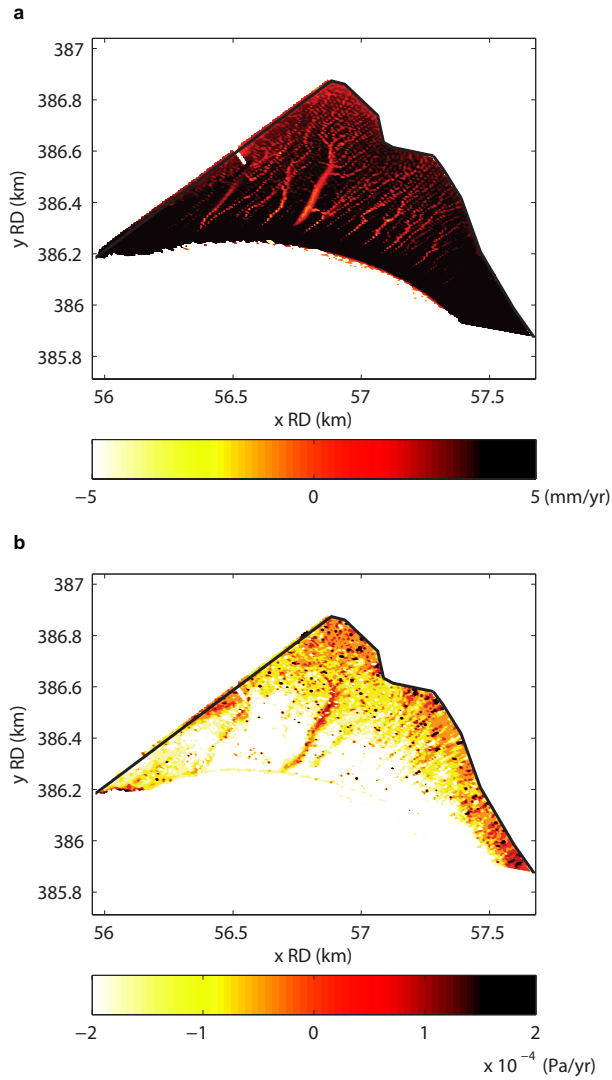
Figure 5.18: (a) Bed level changes (in meters) between 50 and 225 yrs of evolution (accretion over time is positive), normalized to meters per year. (b) Corresponding changes in the tidally averaged bed shear stress (in Pa/yr; positive values correspond with an increase in time). At most locations, the figure shows a negative correlation between the two variables, which in this case suggests a positive (de-stabilizing) internal feedback mechanism.

shore tidal current initially determines where intertidal flats develop (i.e. at those sites where the long-shore current is relatively small/ partly blocked by the typical geometry). It sets an initial energy gradient towards the shore. The energy gradient favors sediment transport (*Friedrichs*, 2011). In an 'equilibrium state' the energy gradient induced by the long-shore tidal current is counteracted by either (1) cross-shore tidal currents or (2) wind waves. In the first case, the flat typically starts at a low elevation in the subtidal domain. The impact of wind waves is reduced by wave-dissipation, but can be significant in the intertidal domain. The dominance of the cross-shore tidal current in the subtidal domain, results in horizontally migrating systems (*Pritchard et al.*, 2002; *Mariotti & Fagherazzi*, 2010; *Maan et al.*, 2015).

In the second case, the mudflat starts not far below the tidal range, at the elevation where wind waves start to affect the bottom. A narrow fringing flat develops and the wave-induced feedback loops control the development towards a stationary equilibrium state. In this system, the impact of cross-shore tidal currents is negligible.

Which of these systems occur, is largely determined by the combination of the available space for the flats (typically the distance between a tidal channel and a dike) and the suspended sediment concentration in the adjacent waters. These settings determine if a balance can be established in the subtidal domain by the action of the cross-shore tidal current. Much (little) space and low (high) concentrations promote the tide (wave) controlled regime.

5.5. Conclusions

The bathymetry of the Kapellebank has become steeper over the last 25 years and seems rather stable during the last decade. Measurements on the site show that the erodibility of the bed is high (*Zhu et al.*, 2017). Thus, the current stability cannot be attributed to an inactive bed. Instead, it should be explained by counteracting gross erosion and gross deposition rates.

Our results show that small wind waves (5-10cm) can have an important stabilizing effect on the long-term morphodynamics of the intertidal flat. For simulations without these wind waves, a stable bathymetry could not be found. The stabilizing effect of the small waves can be explained by a strong relationship between the water depth and the wave-induced bed shear stress. We found that the wave-induced bed shear stress is maximal in shallow waters (i.e. at the tidal fronts) and decreases with increasing water depth. Due to this relationship, the subtidal area stabilizes first. Subsequently, the wave-induced bed shear stress on the landward sections increases with an increasing cross-sectional slope due to wave shoaling. This implies another stabilizing morphodynamic feedback loop. By this feedback loop, the homogeneity of the gross erosion rates increases during the evolution of the flat, until the net horizontal sediment transport vanishes.

Because the tide-induced bed shear stress decreases towards the shore (which is typical for fringing flats), the equilibrium state is characterized by a shoreward increasing wave-induced bed shear stress, so as to counteract the tidal energy gradient. Closer to the shore, where the long-shore current becomes negligible, the wave-induced erosion (and maximum bed shear stress) is approximately homogeneous on the equilibrium bathymetry.

5

Such a homogeneous maximum wave-induced bed shear stress (exerted by small wind waves in shallow waters) is related with a linear cross-shore equilibrium profile. On a straight line, the effects of wave shoaling and wave dissipation at the tidal fronts (where the wave impact peaks) are uniform. This result differs from the concave equilibrium profiles derived analytically by *Friedrichs & Aubrey* (1996). *Friedrichs & Aubrey* (1996) assumed maximum wave-induced bed shear stresses during high water levels, representing situations with larger incoming wind waves.

Our results agree with the study by *van der Wegen et al.* (2017), who simulated the linear equilibrium profile of an intertidal flat in the San Francisco Bay by using a 1-D cross-shore model with similar small wind waves. Our results are also in agreement with the findings of *Hunt et al.* (2015) and *Gatto et al.* (2017). They showed on an estuarine scale that wind waves, acting on the intertidal area, are important for the establishment of an equilibrium state.

We forced our model with an average wave condition, whereas wave conditions are ever changing in reality. For stochastically varying boundary conditions, the concept of a dynamic equilibrium seems appropriate (*Friedrichs*, 2011; *Hu et al.*, 2015). *van der Wegen et al.* (2017) noted that the ability to model a realistic evolution by average forcing only, implies a system's resilience to extreme events. Our results confirm a great stability of the equilibrium configuration and provide an explanation for it. This resilience suggests that extreme events (with a sufficiently low return frequency) do not affect the long-term morphodynamics. Field observations tend to confirm the ability of the system to recover from a storm event (*Zhu et al.*, 2017).

When wind waves were neglected in the simulations, a stable bathymetry was not approached. In that case, most of the flat is found to be accretive in the long run and the internal morphodynamic feedback mechanisms result in the development of tidal creeks. For the development of the tidal creeks a gentle (flat) bathymetry seems important.

5

REFERENCES

Airoldi, L. & Beck, M.W.(2007), Loss, Status and Trends for Coastal Marine Habitats of Europe, *Oceanography and Marine Biology, An Annual Review,45*(January 2007), 345-405, doi:10.1201/9781420050943

Ariathurai, C.R.(1974), A finite element model for sediment transport in estuaries, Ph.D.Thesis. University of California, Berkeley, USA.

Bearman, J.A., Friedrichs, C.T., Jaffe, B.E. & Foxgrover, A.C.(2010), Spatial Trends in Tidal Flat Shape and Associated Environmental Parameters in South San Francisco Bay, *Journal of Coastal Research*, *262*, 342-349, doi:10.2112/08-1094.1

Booij, N., Ris, R.C. & Holthuijsen, L.H. (1999), A third-generation wave model for coastal regions: 1. Model description and validation, *Journal of Geophysical Research: Oceans*, *104*, 76497666.

Deltares (2014a), Delft3D flow user manual. Available at http://oss.deltares.nl/web/delft3d/manuals. Date accessed: 29 june 2018.

Deltares (2014b), Delft3D wave user manual. Available at http://oss.deltares.nl/web/delft3d/manuals. Date accessed: 29 june 2018.

de Swart, H.E. & Zimmerman, J.T.F. (2009), Morphodynamics of Tidal Inlet Systems, *Annual Review of Fluid Mechanics*, *41*(1), 203-229, doi:10.1146/annurev.fluid.010908.165159

de Vet, P.L.M., van Prooijen, B.C. & Wang, Z.B. (2017), The differences in morphological development between the intertidal flats of the Eastern and Western Scheldt, *Geomorphology*, *281*, 31-42, doi:10.1016/j.geomorph.2016.12.031

Eelkema, M., Wang, Z.B., Hibma, A. & Stive, M.J.F. (2013), Morphological effects of the Eastern Scheldt storm surge barrier on the ebb-tidal delta, *Coastal Engineering Journal*, *55*(3), doi: 10.1142/S0578563413500101

Eelkema, M., Wang, Z.B. & Stive, M.J.F., (2012), Impact of Back-Barrier Dams on the Development of the Ebb-Tidal Delta of the Eastern Scheldt,*Journal of Coastal Research,285*, 1591-1605, doi:10.2112/JCOASTRES-D-11-00003.1

Fagherazzi, S., Carniello, L., D'Alpaos, L. & Defina, A. (2006), Critical bifurcation of shallow microtidal landforms in tidal flats and salt marshes, *Proceedings of the National Academy of Sciences of the United States of America*, *103*(22), 8337-8341, doi:10.1073/pnas.0508379103

Fagherazzi, S., Palermo, C., Rulli, M.C., Carniello, L. & Defina, A. (2007), Wind waves in shallow microtidal basins and the dynamic equilibrium of tidal flats, *Journal of Geophysical Research: Earth Surface*, *112*, F0204, doi:10.1029/2006JF000572

Fitzgerald, D.M., Fenster, M.S., Argow, B.A. & Buynevich, I.V. (2008), Coastal Impacts Due to Sea-Level Rise, *Annual Review of Earth and Planetary Sciences*, *36*(1), 601-647, doi:10.1146/annurev.earth.35.031306.140139

5

Friedrichs, C.T. (2011), Tidal Flat morphodynamics: A synthesis, in *Treatise on Estuarine and Coastal Science*, E. Wolanski and D. McLusky (eds.), Academic Press, Waltham, pp 137-137, ISBN 9780080878850, http://dx.doi.org/10.1016/B978-0-12-374711-2.00307-7

Friedrichs, C.T. & Aubrey, D.G. (1996), Uniform Bottom Shear Stress and Equilibrium Hyposometry of Intertidal Flats, in *Mixing in Estuaries and Coastal Seas, Coastal and Estuarine Studies*, Vol. 50, edited by C. Pattiaratchi, pp. 405-429, AGU, Washington, D.C., doi:10.1029/CE050p0405

Gatto, V.M., van Prooijen, B.C. & Wang, Z.B. (2017), Net sediment transport in tidal basins: quantifying the tidal barotropic mechanisms in a unified framework, *Ocean Dynamics*, *67*(11), 1385-1406, doi:10.1007/s10236-017-1099-3

Guo, C., Qing, H., van Prooijen, B.C., Guo, L., Manning, A.J., Bass, S. (2018), Investigation of flocculation dynamics under changing hydrodynamic forcing on an intertidal mudflat, *Marine Geology*, *395*,120-132.doi:10.1016/j.margeo.2017.10.001

Hartsuiker, G. & van Banning, G.K.F.M. (2004), 2Dh Nevla-Scheldemodel (SCALWEST 2000 met verbeterde Belgische roosterschematisatie): bouw en afregeling stromingsmodel. *WL Rapporten.*

Hoitink, A.J.F, Wang, Z.B., Vermeulen, B., Huismans, Y., & Kästner, K., Tidal controls on river delta morphology, *Nature Geoscience, advance online publication*, doi:10.1038/NGEO3000

Hu, Z., Wang, Z.B., Zitman, T.J., Stive, M.J.F., & Bouma, T.J. (2015), Predicting long-term and short-term tidal flat morphodynamics using a dynamic equilibrium theory, *Journal of Geophysical Research: Earth Surface*, *120*, 1803-1823, doi:10.1002/2015JF003486

Hunt, S., Bryan, K.R., Mullarney, J.C. (2015), The influence of wind and waves on existence of stable intertidal morphology in meso-tidal estuaries, *Geomorphology*, *228*, 158-174, doi:10.1016/j.geomorph.2014.09.001

Jeuken, M.C.J.L. & Wang, Z.B. (2010), Impact of dredging and dumping on the stability of ebb-flood channel systems, *Coastal Engineering*, *57*(6), 553-566, doi:10.1016/j.coastaleng.2009.12.004

Kirwan, M.L. & Megonigal, J.P. (2013), Tidal wetland stability in the face of human impacts and sea-level rise, *Nature*, *504*(7478), 53-60, doi:10.1038/nature12856

Le Hir, P., Roberts, W., Cazaillet, O., Christie, M., Bassoullet, P., & Bacher, C., (2000), Characterization of intertidal flat hydrodynamics *Continental Shelf Research*, *20*(12-13), 1433-1459, doi:10.1016/S0278-4343(00)00031-5

Lesser, G.R., Roelvink, J.A., van Kester, J.A.T.M. & Stelling, G.S. (2004), Development and validation of a three-dimensional morphological model, *Coastal Engineering*, *51*(8-9), 883-915, doi:10.1016/j.coastaleng.2004.07.014

Liu, X.J., Gao, S., Wang, Y.P. (2011), Modeling profile shape evolution for accreting tidal flats composed of mud and sand: A case study of the central Jiangsu coast, China, *Continental Shelf Research, 31*, 1750-1760, doi:10.1016/j.csr.2011.08.002

Ma, Z., Melville, D.S., Liu, J., Chen, Y., Yang, H., Ren, W. et al. (2014), Rethinking China's new great wall, *Science, 346*(6212), 912-914, doi:10.1126/science.1257258

Maan, D.C., van Prooijen, B.C., Wang, Z.B., de Vriend, H.J. (2015), Do intertidal flats ever reach equilibrium? (2015), *Journal of Geophysical Research: Earth Surface, 120*(11), https://doi.org/10.1002/2014JF003311

Maan, D. C., van Prooijen, B. C., Zhu, Q., & Wang, Z. B. (2018). Morphodynamic feedback loops control stable fringing flats. *Journal of Geophysical Research: Earth Surface, 123.* https://doi.org/10.1029/2018JF004659

Madsen, O., Poon, Y.-K., & Graber, H. (1988), Spectral wave attenuation by bottom friction: Theory, *Coastal Engineering Proceedings, 21*, 492504, Available at https://icce-ojs-tamu.tdl.org/icce/index.php/icce/article/view/4241. Date accessed: 29 june 2018.

Marani, M., D'Alpaos, A., Lanzoni, S., Carniello, L., & Rinaldo, A.(2007), Biologically-controlled multiple equilibria of tidal landforms and the fate of the Venice lagoon, *Geophysical Research Letters, 34*, L11402,doi:10.1029/2007GL030178

Marani, M., D'Alpaos, A., Lanzoni, S., Carniello, L., & Rinaldo, A. (2010), The importance of being coupled: Stable states and catastrophic shifts in tidal biomorphodynamics, *Journal of Geophysical Research: Earth Surface, 115*(F4), doi:10.1029/2009JF001600

Mariotti, G. & Fagherazzi, S. (2010), A numerical model for the coupled long-term evolution of salt marshes and tidal flats, *Journal of Geophysical Research: Earth Surface, 115*, F01004, doi:10.1029/2009JF001326

Maximova, T., Ides, S., Vanlede, J., De Mulder, T. & Mostaert,F. (2009a), LTV O&M thema Veiligheid Deelproject 1: Verbetering 2D randvoorwaardenmodel. Deelrapport 3: Kalibratie bovenlopen. WL Rapporten, 753_09. Flanders Hydraulics Research, Antwerp, Belgium. Available at http://www.vliz.be/imisdocs/publications/36/155036.pdf. Date accessed: 4 july 2018.

Maximova, T., Ides, S., De Mulder, T., Mostaert, F. (2009b), LTV O&M thema Veiligheid Deelproject 1: Verbetering hydrodynamisch NeVla model ten behoeve van scenarioanalyse. WL Rapporten, 756_05. Flanders Hydraulics Research & Deltares, Antwerp, Belgium. Available at http://www.vliz.be/nl/open-marien-archief?module=ref&refid=142561&printversion=1&dropIMIStitle=1. Date accessed: 4 july 2018.

Maximova, T., Ides, S., De Mulder, T., Mostaert, F. (2009c), Verbetering randvoorwaardenmodel. Deelrapport4: Extra aanpassingen Zeeschelde. WL Rapporten, 753_09. Flanders Hydraulics Research, Antwerp, Belgium. Available at www.vliz.be/imisdocs/publications/237561.pdf. Date accessed: 4 july 2018.

5

Meadows, D.H.& Wright, D. (2009), Thinking in Systems: A Primer. London: Earthscan, ISBN 9781844077267.

Passeri, D. L., Hagen, S. C., Medeiros, S. C., Bilskie, M. V., Alizad, K. & Wang, D. (2015), Earth's Future Special Section: The dynamic effects of sea level rise on low-gradient coastal landscapes: A review, *Earth's Future*,*3*, 159-181, doi:10.1002/2015EF000298

Pethick, J.S. (1981), Long-term accretion rates on tidal salt marshes. *J. Sediment. Petrol.*, *51*, 571-577, doi:10.1306/212F7CDE-2B24-11D7-8648000102C1865D

Pritchard, D., Hogg, A.J., and Roberts, W. (2002), Morphological modelling of intertidal mudflats: the role of cross-shore tidal currents, *Continental Shelf Research*, *22*, 1887-1895, doi:10.1016/S0278-4343(02)00044-4

Ris, R.C., Holthuijsen, L.H., & Booij, N. (1999), A third-generation wave model for coastal regions: 2. Verification, *Journal of geophysical research: Oceans*, *104*, 76677681.

Roberts, W., Le Hir, P. & Whitehouse, R.J.S. (2000), Investigation using simple mathematical models of the effect of tidal currents and waves on the profile shape of intertidal mudflats, *Continental Shelf Research*, *20*, 1079-1097, doi:10.1016/S0278-4343(00)00013-3

Roelvink, J.A., Coastal morphodynamic evolution techniques (2006), *Coastal Engineering*, *53*(2-3), 277-287, doi:10.1016/j.coastaleng.2005.10.015

Sampath, D.M.R., Boski, T., Silva, P.L. & Martins, F.A. (2011), Morphological evolution of the Guadiana estuary and intertidal zone in response to projected sea-level rise and sediment supply scenarios, *Journal of Quaternary Science*, *26*(2), 156-170, doi:10.1002/jqs.1434

Syvitski, J.P., Vrsmarty, C.J., Kettner, A.J. & Green, P. (2005),Impact of humans on the flux of terrestrial sediment to the global coastal ocean, *Science*, *308*(5720), 376-380, doi:10.1126/science.1109454

Tambroni, N. & Seminara, G. (2012), A one-dimensional eco-geomorphic model of marsh response to sea level rise: Wind effects, dynamics of the marsh border and equilibrium, *Journal of Geophysical Research: Earth Surface*,*117*(F3), doi:10.1029/2012JF002363

van de Kam, J., Battley, P.F., McCaffery, B.J., Rogers, D.I., Hong, J.S., Moores, N. et al. (2010), Invisible connections: why migrating shorebirds need the Yellow Sea, *South Australian Ornithologist*,*37*(1)

van der Wal, D., van Kessel, T., Eleveld, M.A., Vanlede, J. (2010), Spatial heterogeneity in estuarine mud dynamics, *Ocean Dynamics*, *60*, 519-533, doi:10.1007/s10236-010-0271-9

van der Wegen, M., Jaffe, B., Foxgrover, A.& Roelvink, D. (2017), Mudflat Morphodynamics and the Impact of Sea Level Rise in South San Francisco Bay, *Estuaries and Coasts*, *40*(1), 37-49, doi:10.1007/s12237-016-0129-6

van Goor, M.A., Zitman, T.J., Wang, Z.B. & Stive, M.J.F. (2003), Impact of sea-level rise on the morphological equilibrium state of tidal inlets, *Marine Geology*, *202*(3-4), 211-227, doi:10.1016/S0025-3227(03)00262-7

van Maanen, B., Coco, G., Bryan, K.R. & Friedrichs, C.T. (2013), Modeling the morphodynamic response of tidal embayments to sea-level rise, *Ocean Dynamics*, *63*, 1249-1262, doi:10.1007/s10236-013-0649-6

van Maanen, B., Coco, G. & Bryan, K.R. (2015), On the ecogeomorphological feedbacks that control tidal channel network evolution in a sandy mangrove setting, *Proceedings of the Royal Society A,471*(2180), doi:10.1098/rspa.2015.0115

Wang, Z.B., Van Maren, D.S., Ding, P.X., Yang, S.L., van Prooijen, B.C., De Vet, P.L.M. et al. (2015), Human impacts on morphodynamic thresholds in estuarine systems, *Continental Shelf Research*, *111*, 174-183, doi:10.1016/j.csr.2015.08.009

Waeles, B., Le Hir, P. & Jacinto, R.S. (2004), Modelisation morphodynamique cross-shore d'un estran vaseux, *Comptes Rendus Geoscience*, *336*, 1025-1033, doi:10.1016/j.crte.2004.03.011

Wiegmann, N., Perluka, R., Oude Elberink, S. & Vogelzang, J. (2005), Vaklodingen: de inwintechnieken en hun combinaties: vergelijking tussen verschillende inwintechnieken en de combinaties ervan Technical Report Adviesdienst Geo-Informatica en ICT (AGI) Delft (in Dutch)

Winterwerp, J.C. & Van Kesteren, W.G. (2004), Introduction to the physics of cohesive sediment dynamics in the marine environment, *Developments in Sedimentology, 56*. Elsevier.

Zhou, Z., Coco, G., Townend, I., Olabarrieta, M., van der Wegen, M., Gong, Z. et al. (2017), Is 'Morphodynamic Equilibrium' an oxymoron?, *Earth-Science Reviews, 165*, 257-267, doi:10.1016/j.earscirev.2016.12.002

Zhu, Q., van Prooijen, B.C., Maan, D.C., Wang, Z.B., Daggers, T., Yang, S.L. (2017), Cross-shore and vertical variability of mudflat erodibility: An integrated approach of in situ measurements and modeling. Manuscript submitted for publication.

5

6

SUMMARY AND CONCLUSIONS

6.1. SUMMARY

Systems thinking and system analysis have been applied to get towards an understanding of the 'intertidal morphodynamical system'. This is the philosophy that states arise that are understandable and possible to determine exactly, despite the many interactions between the variables and the apparent complexity of systems. To find out the dominant feedback mechanisms, we followed a top-down approach. The points below summarize the approach that has been taken and discuss the findings:

1. The procedure starts with a description of the considered system and its boundaries. For intertidal flats, those boundaries are often formed by adjacent tidal channels. The conditions in these channels are mainly determined by larger scale processes and can therefore be considered as (approximately) independent of the evolution of the intertidal flat. In this thesis, we considered two types on intertidal systems: (1) intertidal flats that are dominated by cross-shore tidal currents and wind waves; (2) fringing intertidal flats adjacent to a tidal channel, on which along-shore tidal currents and wind waves dominate over cross-shore tidal currents. The fundamental difference between these systems lies in the dominant flow direction: cross-shore for System 1 and along-shore for System 2. Because the cross-shore tidal current velocities are directly linked to the cross-sectional profile slopes, System 1 is characterized by gentler cross-sectional slopes and wider intertidal areas than the flats in System 2.

2. Secondly, morphodynamic models were constructed to simulate the long-term evolution of the considered systems. System 1 was modeled by a 1-D cross-shore model, in which the longshore flow was neglected. For System 2, we used an extensive 2-D horizontal morphodynamic model to capture the along-shore flow on the intertidal flat.

3. Once we were able to simulate the intertidal evolution (confirmed by field observations), we considered the co-evolution of state variables. For the wide flats that

are dominated by cross-shore tidal currents and wind waves (System 1), we found that an initial imbalance between deposition and erosion is minimized within a few decades. This happens simultaneously with an adjustment of the profile slope and shape. After a while, the imbalance between deposition and erosion is not further reduced and the profile shape stabilizes. What follows is a state of long-term seaward progradation or landward retreat of the intertidal flat, in which the cross-shore profile shape is maintained.

For fringing flats (System 2), we found that the subtidal area at the interface with the channel stabilizes first. Subsequently, the wave-induced bed shear stress on the landward sections increases (decreases) with an increasing (decreasing) cross-sectional slope, until an equilibrium state is reached. We also considered the simultaneous development of the wave-height and found a strong correlation between the evolutions of the bed levels, bed shear stresses and wave heights.

4. Subsequently, we used the model outcomes to answer the question that was stated in the introduction: 'Which feedback loops/physical mechanisms can explain the observed evolution of the state variables?' We found that the feedback mechanisms between the bed configuration and the bed shear stress are often dominant over other types of feedback mechanisms. Under influence of cross-shore tidal currents, a negative feedback loop tends to stabilize the profile slope and shape within the first decades of evolution. Namely, local cross-shore tidal current velocities increase (decrease) with a increasing (decreasing) bed elevation, inducing larger (smaller) bed shear stresses and gross erosion rates. This type of interdependency between the variables steers towards a local equilibrium. On the upper intertidal flat, however, this feedback loop does not exist. If tidal currents act alone, the upper flat is persistently accretive. The impact of wind waves can result in net erosion (depending on the specific wave climate and sediment supply). Net accretion (or erosion) on the upper flat influences the balances on the lower sections, which drives the long-term horizontal progradation or retreat.

For fringing flats, we concluded that small wind waves (5-10cm) have an important stabilizing effect on the long-term morphodynamics. The stabilizing effect of the small waves can be explained by a strong relationship between the water depth and the wave-induced bed shear stress. We found that the wave-induced bed shear stress is maximal in shallow waters (i.e. at the tidal fronts) and decreases with increasing water depth. This relationship results in a stabilizing morphodynamic feedback loop in the subtidal domain, where the minimum water depth strongly increases (decreases) with a decreasing (increasing) bed level. After stabilization of the subtidal region, an additional stabilizing feedback loop gets important on the intertidal flat. Namely, landward of the stable section, an increase (decrease) in the local bed level leads to an increase (decrease) in the cross-sectional slope (in the offshore direction) and thereby to an increase (decrease) in the relative importance of wave shoaling versus wave dissipation. These processes explain the modeled (chronological) development towards a stationary equilibrium state.

5. We used the basis of the steady migrating states (with conserved cross-sectional profiles) to derive relationships between the state variables and the external drivers.

We derived that the progradation speed increases with a power larger than 1 of the concentration in the deep adjacent waters. Sea level rise and erosion by wind waves, on the other hand, affect the progradation speed via a linear relationship. Wave-induced erosion and SLR lead to the existence of a critical sediment concentration level below which intertidal systems shifts from expansion to retreat.

For fringing intertidal flats we concluded that an equilbrium state is characterized by a shoreward increasing wave-induced bed shear stress that counteracts the tidal energy gradient. The tide-induced bed shear stress, was found to be approximately independent of the intertidal bathymetry and can therefore be seen as an independent driving factor. Close to the shore, where the along-shore current becomes negligible, the equilibrium state is characterized by a linear cross-shore equilibrium profile on which the wave-induced erosion is uniform. This result differs from the concave equilibrium profiles for larger incoming wind waves as derived analytically by *Friedrichs & Aubrey* (1996).

6.2. A SYNTHESIS

While we studied the behavior of two different types of intertidal systems, dominated by cross-shore tidal flow (System 1) and along-shore tidal flow (System 2) respectively, an important question that still needs an answer is 'When do we expect a System 1 or a System 2?' The findings of this study give some insight.

We found that the along-shore tidal current acts (approximately) as an 'independent driving factor' for open coast and fringing intertidal systems, as opposite to the cross-shore tidal currents and wind waves, which co-evolve with the system as state variables. This suggests that the spatial variation in the along-shore tidal currents (steered by larger scale features as the typical geometry of an estuary) initially determines where intertidal flats can develop. At the sites where the along-shore current is relatively small/ partly blocked by the typical geometry, sediment can settle. As long as the internally generated cross-shore tidal current velocities and the effect of wind waves on the bottom are small, the spatial decay in the along-shore tidal current velocities set an energy gradient. The energy gradient favors sediment transport (*Friedrichs*, 2011). In an 'equilibrium state' the energy gradient induced by the along-shore tidal current is counteracted by either (1) cross-shore tidal currents or (2) wind waves (or a combination of those).

Which of these forces take the lead, is largely determined by the combination of the available space for the flats (typically the distance between a tidal channel and a dike) and the suspended sediment concentration in the adjacent waters. These settings determine if a balance can be established in the subtidal domain by the action of the cross-shore tidal current. Namely, according to equation 4.9,

$$c_b \propto \frac{1}{\beta^2},$$ (6.1)

Taking $\beta = \frac{h}{W}$ (*Friedrichs & Aubrey*, 1996) with W the distance between the channel and a dike and h the local water depth at the interface between channel and flat (relative to *MSL*), we find:

$$h \propto \frac{W}{\sqrt{c_b}}. \tag{6.2}$$

Hence, much (little) space and low (high) suspended sediment concentrations promote a large (small) h. A large (small) water depth subsequently implies a small (large) wave impact, which promote the tide (wave) controlled regime. Hence, in the tide controlled regime, the flat typically starts at a low elevation (large h) in the subtidal domain. The impact of wind waves is reduced by wave-dissipation, but can be significant in the intertidal domain. The dominance of the cross-shore tidal current in the subtidal domain, however, results in horizontally migrating systems. If h in Equation 6.2 is small (promoted by little space and high suspended sediment concentrations), the mudflat starts at an elevation at which wind waves contribute significantly to the bed shear stress. A narrow fringing flat develops and the wave-induced feedback loops control the development towards a stationary equilibrium state. In this system, the impact of cross-shore tidal currents is negligible.

6.3. APPLICATIONS

Here we summarize the practical applications of our results.

Making projections   We applied our results to the Yangtze Estuary to estimate the critical sediment concentration level below which a shift from progradation to retreat can be expected. Thereby, an estimate of the typical wave-induced erosion was obtained from earlier studies, based on in situ measurements of bed level changes during extreme events. For the Yangtze Estuary we found that at least 30% of the suspended sediment concentration in 1990 is required to keep up with a sea level rise of $7mm/yr$. Our relationships are applicable to prograding flats in general and can be applied in other river mouths as well.

We further discussed the consequences of sea level rise on this system. Beyond the critical value, the intertidal flat initially submerges and retreats landward at the same time. Due to its gentle slope, especially the top of the flat is sensitive to submergence (which increases the tidal flow velocities and erosion rates). Local erosion there, in turn, affects the seaward balances and induces retreat. Only after the 'outer-dike hinterland' has disappeared completely, can the flat stabilize against a sea wall (relative to mean sea level, i.e. the flat will rise at the same rate as the sea).

Also for fringing intertidal flats we shortly discussed the consequences of sea level rise in the thesis. The restoring feedback mechanisms that control the stationary equilibrium states of fringing flats, cause resilience to sea level rise, i.e. the flat has the tendency to rise together with the sea level. The relevant question is then if the sedimentation rates during the recovery process (i.e. the evolution towards equilibrium) are high enough to keep up with SLR. If the net sedimentation rates during this process are higher than the rate of sea level rise, the elevation relative to mean sea level is maintained. The simulations reveal that the accretion rates on the upper flat increase with the degree of distortion from the equilibrium state. Therefore it is possible (depending on the sediment availability) that the flat initially submerges, and starts to rise at the rate of sea level rise at a lower elevation relative to the mean sea level.

The restoring feedback loops that control fringing tidal flats also cause resilience to extreme events (with a sufficiently low return frequency). More specifically, if the typical period between two successive events (with similar strength) is long enough to allow for total recovery, they do not affect the long-term morphodynamic evolution or equilibrium state.

Developing strategies   The obtained understanding can help to find strategies for protecting the intertidal environment against erosion or submergence due to sea level rise. The progradation speed of horizontally migrating mudflats (described as System 1 in Sec.6.1) can be influenced by engineering activities on the upper shore. Placing wavebreakers, extra vegetation, or raising the bed directly, does not only affect the sediment balances locally, but eventually also induce sedimentation on the seaward sections, i.e. it increases the seaward expansion of the whole system. Nurturing salt marsh growth would also decrease the critical concentration level needed to keep up with sea level rise and prevent submergence and accelerated coastal retreat. These effects emphasizes the benefits of these methods and the concepts of 'building with nature'.

Also on fringing tidal flats (System 2 in Sec.6.1) it would be possible to stimulate sedimentation, for instance by nurturing salt marshes (on the upper flat) or placing wave breakers. As opposite to the horizontally migrating systems, however, these measures only have a local effect (they do not affect the balances on the seaward sections).

Our results also suggest that it can be possible to artificially initiate a shift from a 'narrow and stationary system 2' to a 'wide and migrating system 1' (or vice versa) by creating more (less) space for intertidal flats. For instance shifting seadikes landwards, would promote the dominance of the cross-shore tidal currents and the development of a wide and gentle tidal flat (including a extensive subtidal area).

Simplifying and improving model set-ups   Once the dominant processes and feedback loops are identified, simpler models can be constructed that only include a limited selection of components. For instance, this study suggests that fringing flats can be modeled with 1-D cross-shore models including wind waves. Furthermore, a qualitative understanding about the evolution of the components inside a comprehensive model can be used to speed-up simulations. For instance, instead of applying a morphological factor at each hydrodynamic time step, one could speed-up the development of migrating flats by applying horizontal shifts. In this way, the accelerated representation of facts is better in line with the actual course over time, so that larger artificial acceleration factors can be applied in the models.

6.4. OUTLOOK

This research have shown the usefulness of systems thinking in the field of morphodynamics. A range of other morphodynamic systems could be approached in a similar way; by making strict distinctions between system variables and driving factors; by identifying states; by studying time-series and correlations between system variables. A systematical approach to study the complex interactions in morphodynamic systems is needed if one wants to make use of the internal stabilizing or re-inforcing feedback loops of the

natural system itself and to 'build with nature' in the most effective way.

This study indicates that fringing flats can be modeled with one-dimensional (cross-shore) numerical models. This makes modeling faster and can be very helpful in further quantifying this system. Using a faster model, we can further investigate: (1) the relationships between the system drivers (boundary concentration, tidal range, incoming wave height etc.) and system variables as the cross-sectional slope or the elevation at which the fringing intertidal flat starts. (2) the recovery rate after a disturbance or the ability of the system to adjust to SLR. (3) the generality or exceptionality of the stationary equilibrium state. These investigations require many simulations, which were impossible to carry-out with the extensive Delft3D model set-up.

Furthermore, the interaction of the here considered intertidal system with vegetation and salt-marshes deserves extra attention and investigation with coupled model setups. Last but not least, the effects of the presence of multiple sediment fractions on the long-term morphodynamics could be investigated, because a variable bed erodibility might lead to different dominant morphodynamic feedback loops.

REFERENCES

Friedrichs, C.T. (2011), Tidal Flat morphodynamics: A synthesis, In *Treatise on Estuarine and Coastal Science* E. Wolanski and D. McLusky (eds.), Academic Press, Waltham, pp 137-137, ISBN 9780080878850, http://dx.doi.org/10.1016/B978-0-12-374711-2.00307-7.

Friedrichs, C.T. & Aubrey, D.G. (1996), Uniform Bottom Shear Stress and Equilibrium Hyposometry of Intertidal Flats, in *Mixing in Estuaries and Coastal Seas, Coastal and Estuarine Studies*, Vol. 50, edited by C. Pattiaratchi, pp. 405-429, AGU, Washington, D.C., doi:10.1029/CE050p0405

6

AFTERWORD

The defense of my PhD closes a special period of my life. A period in which I experienced what it is like to be a 'professional scientist' (i.e. to earn a living with science). I like the creativity and imagination that you can put in experimental design and drafting theories, or the moments on which everything seem to fall together and you come to an understanding. These are the reasons for me to be a scientist.

However, the difficult and frustrating periods seemed disproportionately long and I started to hesitate about my motivations. Not being able to answer a question that comes back over and over again, can be very frustrating. The apparent slowness of the scientific progress, can make me feel powerless and weak. The many times of re-writing my own work, made me hesitant and tiresome. Could I really be, and did I really want to be, a scientist?

It was inevitable to change my mindset during these periods of struggling and finding answers. Life is too short to spend a lot of time being frustrated, especially if the feelings persist outside the 'working hours'. So, I made rules for myself, like 'not being able to answer a scientific question should not be a reason to doubt your own abilities', and 'be happy with the pursuit of achievement and progress, and do not let your happiness depend on the results you achieve'. These thoughts helped me to focus on *trying* to solve problems and *trying* to finish the PhD and to enjoy the full ride. Ironically, they made me able to really get there in the end.

Many people helped me -in one way or another- in this process and to finish the research project. First of all, I would like to thank my promotors Dr. Bram van Prooijen en Prof. Zheng Bing Wang for their long lasting support. I also like to address Prof. Huib de Vriend, my colleague Stuart Pearson, and the reviewers of my papers, whose comments have lifted the work to a higher level.

In particular, I could never have finished this project without the warm support of my PhD colleagues. Thank you Qin, Zhan, Lodewijk, Marco, Clara, Miguel, Willem, Steven, Nici, Andres, Mohamed, Shahid, Marco, Victor, Maria, Liselot, Irene, Stuart, Gonzalo, Yorick, Merel, Zeinab, Le, Erik, Ana, Jill, Xuexue, Dirk, Pieter, James, Sabine, Melike, Nils, Sotiria, and all the other colleagues with whom I worked over the years. For being such good and open companions and for the enjoyable time we had together during coffee breaks, lunch, or with beers. The good times and solidarity between us makes the difference. I also want to express my admiration to my colleagues from the *Natuurschool*, with whom I started to work a year after my contract with the university ended and I was looking for something else. Working outside in nature with such a close group of motivated people really inspired me.

Last but not least, I am grateful to the people who are closest to me. Thank you Danielle, for still being 'high school friends', while we are both parents now, and Mieke, for motivating each other and training together. Robin, Veronika, Lianne and Niels for sharing nice times and experiences together. Thanks to my parents for always being

6